RESEARCH AND DEVELOPMENT FOR A GROUND-BASED HYDROGEN-MASER SYSTEM

Final Report

Contract NSR 09-015-098

April 1972

Prepared for

National Aeronautics and Space Administration
Washington, D.C. 20546

Smithsonian Institution
Astrophysical Observatory
Cambridge, Massachusetts 02138

RESEARCH AND DEVELOPMENT FOR A GROUND-BASED HYDROGEN-MASER SYSTEM

Final Report

Contract NSR 09-015-098

April 1972

Prepared for

National Aeronautics and Space Administration
Washington, D.C. 20546

Smithsonian Institution
Astrophysical Observatory
Cambridge, Massachusetts 02138

TABLE OF CONTENTS

TABLE OF CONTENTS (Cont.)

RESEARCH AND DEVELOPMENT FOR A GROUND-BASED HYDROGEN-MASER SYSTEM

Final Report

Contract NSR 09-015-098

1. INFORMATION AND BACKGROUND

On July 1, 1969, development of the atomic hydrogen maser conducted by Hewlett Packard (HP) under Contract NASW 1337 was transferred to the Smithsonian Astrophysical Observatory (SAO), Cambridge, Massachusetts, where it continued under Contract NSR 09-015-098. The objective was to continue the development of hydrogen masers and clock systems for terrestrial and satellite use and to perform research on the wall coatings of the maser storage bulb.

The work statement was divided into the following four tasks, which are discussed in subsequent sections:

I. Establish a laboratory to continue hydrogen-maser research and development.

II. Set up and test the existing autotuner.

III. Evaluate the PTFE-coated maser storage bulb and test it for wall-relaxation rate.

IV. Assemble engineering model of the spacecraft maser and perform limited mechanical testing on it.

2. TASK I

Six maser oscillators were transferred to Contract NSR 09-015-098 with SAO on July 1, 1969:

NASA-1	Originally built under Contract NAS 8-2604
NASA-2	Originally built under Contract NAS 8-2604
H-10 #6	Originally built under Contract NAS 8-2604
SR-1 MK II	Spacecraft maser developed under Contract NASW 1337
SM-1	Small-maser system developed under Contract NAS 8-2604
ONR-1	Original prototype maser built in 1960

NASA-1 has been modified under Contract NAS 5-11598 to permit adiabatic fast-passage-state experiments. It has also been equipped with a storage bulb carefully evaluated by the Lyman Laboratories at Harvard University. It serves as the SAO lab reference.

NASA-2 is a source of spare parts and electronics to keep NASA-1 going.

H-10 #6 is used in experiments on wall-shift and wall-relaxation rates.

SR-1 MK II is under continuing development (see Task IV).

SM-1 has been extensively modified at SAO; it serves as a traveling frequency standard.

ONR-1 has been lent to Professor Ramsey at the Lyman Laboratories for flexible-bulb experiments.

Other equipment and supplies were transferred to SAO as part of the contract transfer. New benches, cabinets, hand tools, and wiring supplies were rapidly obtained, and the lab became operational by the middle of July. As plans developed, major capital items were purchased or obtained by transfer from other labs at SAO and from NASA/Marshall

Space Flight Center (MSFC); these items included a bulb-curing oven capable of temperatures to 750°C, a Leeds and Northrup millipoint strip-chart recorder, and amplifiers.

The original lab space of 641 ft^2 was expanded by 434 ft^2 in an adjacent room when the oven and its controlling equipment were obtained.

Requirements for electronic tests have been very nearly met by equipment from NASA/MSFC. Except for a vector voltmeter, an L-band spectrum analyzer, and a low-frequency spectrum analyzer, the requirements for present plans have been met.

The SAO/Harvard College Observatory (HCO) model shop located in the same building has very competently provided services. This shop is well run and has personnel familiar with vacuum requirements and atomic clocks. Glassblowing facilities continue to be provided by the same outside vendor in Cambridge and by the Massachusetts Institute of Technology (MIT) glass shop. High-vacuum welding facilities are available at the nearby Cambridge Electron Accelerator Laboratory.

Because electronic components are readily available from nearby supply houses, it is unnecessary for us to maintain an inventory. The purchasing department at SAO has quickly procured small quantities of electronic components.

Finally, our maser lab and others at SAO, Harvard, and MIT have lent each other equipment very infrequently used, such as a residual-gas analyzer for vacuum studies. This cooperation does much to alleviate budget constraints and often serves to broaden the capabilities and outlook of the people involved.

In contrast to the Varian-HP labs where the maser work was previously carried on, the present setup offers substantially improved capability for research, development, prototype assembly, and testing.

3. TASK II

The existing autotuner, which uses binary logic, has been tested with the SAO lab maser as reference. Its performance has been up to expectation. To test the autotuner-maser combination, we decided to include it with SM-1, which was being compared with the clock ensemble at the National Bureau of Standards (NBS), Boulder, Colorado, to obtain a more definitive hydrogen-cesium frequency relationship. To make the device more compact, the time sequencer was rebuilt.

To the time of writing this report, the performance of the autotuning device combined with the maser has been excellent. Long-term stability (10^4 to 10^5 sec) has been measured at 1.5×10^{-14} in fractional frequency stability.

The results of the experimental redetermination of the hydrogen-cesium hyperfine transition frequency are given in the following paper by Hellwig, Vessot, Levine, Zitzewitz, Allan, and Glaze. These results are related to the wall-shift data taken in Task III.

The performance of the autotuning system is described in the following NASA Tech Brief 70-10616.

4. TASK III

4.1 Introduction

The effect of wall collisions on the phase of the hydrogen atom has long been the cause of inaccuracy in the output frequency of the maser. Further, the relaxation rate of the atom as a result of such collisions, whether due to recombination into molecules (or chemical loss) or to dephasing with the oscillating r.f. field, has been a limitation on the linewidth of the stored aggregate of atoms. These wall processes limit the accuracy of the maser and affect its stability.

The properties of polytetrafluoroethylene (PTFE) films are being studied to determine whether reduced relaxation rates are obtainable and whether it is practical to operate the maser at a temperature where the wall shift can be made small. The H-10 #6 maser has been modified to allow more experimental flexibility and to permit oscillation at temperatures in excess of 100°C.

An important aspect of this work relating to the wall-shift measurements is knowing the unperturbed frequency of the hyperfine separation of hydrogen. This is usually determined by measuring a series of bulbs that have widely differing diameters but are coated in the same manner. Assuming that the wall-collision rate (hence the average phase shift per bounce) is proportional to the reciprocal of the diameter of the bulb, one arrives at a plot whose extrapolation to infinite bulb diameter (zero collision rate) gives the desired hydrogen frequency. The difficulties involved in this technique are due to the variability of the surface texture and the consequent error in the collision rate. The experiments give this value; however, much greater weight to this determination is possible by comparisons with other laboratories where different types of teflon and different coating techniques have been used.

As mentioned in Task II, the small maser has been compared with the clocks of Harvard and NBS to establish the hydrogen frequency and its relation to the best available embodiment of the cesium frequency.

4.2 Wall-Shift Measurements

Wall-shift data as a function of temperature for the 4" and 7" bulbs have been obtained. These bulbs were coated with tetrafluoroethylene (TFE) teflon and cured in a rapid cooling cycle. The data show that the temperature at zero wall shift is much lower than anticipated. The temperature has been determined to be 83° ± 1°C. The 4" bulb gave the same crossover temperature (within 1°C) as did the 7" bulb. With these two bulb diameters, we can extrapolate the wall shift to zero collision rate (infinite bulb diameter). The extrapolation of the frequency-shift plot as a function of $(\text{diameter})^{-1}$ gives a value for the unperturbed atomic hydrogen hyperfine frequency within 2×10^{-3} Hz of the determination made with the clocks of Harvard and NBS and the SM-1. This new value lies within the error limits of the previous experiment.

The wall-shift data have been reduced in terms of phase shift per wall collision. The reduced data points, when plotted against temperature, lie on a straight line with slope 1.31×10^{-7} rad/°C. The intercept of zero phase shift per collision with temperature is, of course, the same as before. It is very interesting to report that the phase shift for collision data for both the 4" and the 7" bulbs lies well within 1×10^{-6} rad over the entire temperature range. This confirms that, at least for these two bulbs, the coatings are similar.

Having successfully obtained the data on the 7" and 4" bulbs coated with PTFE under quenched conditions, we annealed the 4" bulb. This process changes the crystal structure of the PTFE coating and should affect the wall shift and reduce the wall-relaxation rate.

The PTFE we have been using has a very high molecular weight, in the order of 10^6 or greater. This is desirable, since with large molecules it is possible to present a surface with fewer nonfluorine end groups than smaller molecules. There is, however, a difficulty in annealing the polymer of high molecular weight; it is extremely viscous and requires a very long time to cool through the crystallizing range, 340 to 290°C. The rate should be between 0.1 and 0.05°C/min.

A special oven controller with a clock-driven potentiometer was built. This controller was used in place of the set-point adjustment. We provided for a 0.05°C/min rate; roughly 18 hr was required to cool from 340 to 290°C.

The 4" bulb was annealed in this 18-hr cycle. It was then placed in the maser, and wall-shift measurements were made. We found that the bulb showed entirely different properties in its annealed state. The data were discussed in "Studies of Hydrogen Maser Wall Shift for High Molecular Weight Polytetrafluoroethylene," a paper read by Vessot and Levine at the 24th Annual Frequency Control Symposium. A copy of this paper follows.

This work led us to the invention of a method for eliminating the wall shift in the hydrogen maser. The principles of the system are discussed in a paper published in Metrologia and reproduced at the end of this section.

A method for making an automatic temperature-control system to ensure that the bulb is maintained at the temperature of zero wall shift was disclosed to NASA. Subsequently, this disclosure was filed by NASA on behalf of the inventors. The NASA case number for this invention is HQN-10654. A copy of the original disclosure is appended to illustrate the principles of the automatic system.

Measurement of the Unperturbed Hydrogen Hyperfine Transition Frequency

HELMUT HELLWIG, MEMBER, IEEE, ROBERT F. C. VESSOT, MARTIN W. LEVINE, PAUL W. ZITZEWITZ, DAVID W. ALLAN, AND DAVID J. GLAZE

Abstract—The results of a joint experiment aimed primarily at the determination of the frequency of the H^1 hyperfine transition ($F = 1, m_F = 0$) $\leftrightarrow$ ($F = 0, m_F = 0$) is reported. In terms of the frequency of the Cs^{133} hyperfine transition ($F = 4, m_F = 0$) $\leftrightarrow$ ($F = 3, m_F = 0$), defined as 9192 631 770 Hz, for the unperturbed hydrogen transition frequency the value

$$\nu_H = 1420\ 405\ 751.768\ \text{Hz}$$

is obtained. This result is the mean of two independent evaluations against the same cesium reference, which differ by 2×10^{-8} Hz. We estimate the one-sigma uncertainty of the value ν_H also to be 2×10^{-8} Hz. One evaluation is based on wall-shift experiments at Harvard University; the other is a result of a new wall-shift measurement using many storage bulbs of different sizes at the National Bureau of Standards. The experimental procedures and the applied corrections are described. Results for the wall shift and for the frequency of hydrogen are compared with previously published values, and error limits of the experiments are discussed.

I. Introduction

A SERIES of measurements involving hydrogen masers, cesium beam frequency standards, and the NBS clock system was made at the National Bureau of Standards (NBS) in Boulder, Colo., during the period from November 1969 to February 1970. The original purpose of these experiments was an evaluation of the stability performance of the involved systems and devices. A report of these results will be made elsewhere [1].

A unique opportunity thereby existed for a remeasurement of the frequency of the unperturbed hydrogen (H^1) hyperfine transition ($F = 1, m_F = 0$) $\leftrightarrow$ ($F = 0, m_F = 0$) in terms of the cesium (Cs^{133}) hyperfine transition ($F = 4, m_F = 0$) $\leftrightarrow$ ($F = 3, m_F = 0$), defined as 9192 631 770 Hz. This paper reports the results of our frequency measurements.

The hydrogen maser frequency differs from the unperturbed atomic transition frequency because of a variety of effects including cavity pulling, spin exchange, magnetic fields, second-order Doppler (related to the temperature of the storage vessel), and collisions with the walls of the storage vessel. A detailed discussion of these effects is found in [2]. They can be measured and accounted for with fractional uncertainties of less than 10^{-13} with the exception of the wall-collision effect (wall shift). Thus, the measurement of the unperturbed hydrogen transition frequency involves primarily a measurement of the wall shift. We performed two different and independent[1] measurements, which are referred to hereafter as experiment 1 and experiment 2.

Experiment 1 relies on a previous determination of the wall shift at Harvard University [3]: as a result of this wall-shift evaluation the Harvard reference maser has a known wall shift. A comparison between the frequency of this maser and a cesium primary frequency standard[2] (NBS-III), using a different maser as a transfer standard, gave a value for the unperturbed hydrogen hyperfine transition frequency. Experiment 2 is a separate and new measurement of the wall-shift correction with, however, an important difference from any previous wall-shift measurement: the reference oscillator that was used in the measurement of the frequency of the maser equipped with storage bulbs of different sizes was directly related to the frequency of a cesium primary frequency standard (NBS-III). Wall-shift correction and hydrogen–cesium comparison in experiment 2 were thus not separate steps but were integral parts of the same measurement.

The published values of the unperturbed hydrogen hyperfine transition frequency disagree among themselves considerably more than is expected from the published values of the accuracy. In addition, there has been an almost exclusive usage of one particular wall-shift correction in the various publications of the hydrogen frequency. (See Tables I and II.) These were further motivations for our measurements.

The value for the hydrogen hyperfine transition frequency may be written as

$$\nu_H = (1420\ 405\ 751 + \nu_H')\ \text{Hz} \qquad (1)$$

and we shall discuss in the following only ν_H'.

The wall-shift correction may be written as approximately

$$\Delta\nu_W \approx (K/D)[1 + \alpha_1(T - T_1)] \qquad (2)$$

Manuscript received June 5, 1970; revised July 13, 1970. This paper was presented at the 1970 Conference on Precision Electromagnetic Measurements, Boulder, Colo., and the experiments at Harvard University were supported by NASA.

H. Hellwig, D. W. Allan, and D. J. Glaze are with the Atomic Frequency and Time Standards Section, National Bureau of Standards, Boulder, Colo. 80302.

R. F. C. Vessot and M. W. Levine are with the Smithsonian Astrophysical Observatory, Cambridge, Mass. 02138.

P. W. Zitzewitz was with the Lyman Laboratory of Physics, Harvard University, Cambridge, Mass. 02138. He is now with the Department of Physics, University of Western Ontario, London, Ont., Canada.

[1] They are not completely independent in the sense that a common cesium reference (NBS-III) was used.

[2] For our purposes a cesium primary frequency standard is an apparatus that has been experimentally evaluated in relation to all known perturbing effects [4].

TABLE I
WALL-SHIFT RESULTS

Author and Reference	Approximate Year of Measurement	Number of Bulbs	Teflon	$\Delta\nu_W \cdot D$ (mHz·cm)	α (K^{-1})
Crampton *et al.* [5]	1963	2	TFE 852-201 Du Pont	470 ± 47 at 35°C	not measured
Vanier and Vessot [6]	1963–1964	4	FEP-120 Du Pont 1962	528 ± 5 at 40°C	$-(5 \pm 1) \times 10^{-3}$
Mathur *et al.* [7]	1964	4	FEP-120 Blend 33 53.9 percent solids 1964 Du Pont	513 ± 76 at 35°C	not measured
Elkina *et al.* [8]	1968	2	Teflon D	1993 ± 75 (temperature not given)	not measured
Zitzewitz *et al.* [3]	1968–1969	18	FF Bl 5[illegible]olids	386 ± 8 at 40°C	$-(12 \pm 1) \times 10^{-3}$
Menoud and Racine [9], [10]	1968–1969	2	FEP-120 Du Pont	515 ± 28 at 40°C	not measured
Hellwig *et al.* [this paper]	1969–1970	11	TFE Blend 42 34.3 percent solids Du Pont 1969	528 ± 17 at 24°C	not measured

where T_1 is the reference temperature usually chosen at 40°C, T is the operating temperature of the storage bulb, α_1 is the wall-shift temperature coefficient, D is the diameter of the storage bulb, and K is the wall-shift coefficient.

To our knowledge only five independent wall-shift measurements have been published in the past; one reason for this must be sought in the rather tedious and time-consuming experimental effort necessary. The six published results are summarized in Table I together with the results of this paper. Table I gives the author(s) and bibliographic reference, the year(s) of the actual experiment, the number of bulbs different in coating and/or size, the type and year of purchase of the Teflon,[3] and the values $\Delta\nu_W \cdot D$ and α_1 of (2) together with the accuracy claims.

In Table II we list and compare values for ν_H'. Given are the author(s) and published reference, the year(s) of the actual measurement, the Teflon that was used in the storage bulb of the hydrogen maser, the applied wall-shift correction listed by the corresponding author from Table I, the hydrogen maser type that was used, the cesium reference standard, and the value for ν_H'. The values for ν_H' are rounded in the last digit.

A discussion of Tables I and II will be postponed until the end of this paper where we will take a critical look at them in connection with a discussion of our new values.

[3] Trade names and the names of manufacturers are used in this paper for the sole purpose of conveying scientific and technical information, and their citation is not to be construed as an endorsement or approval of commercial products or services by the authors' organizations.

II. MEASUREMENT PROCEDURES

Experiment 1 involved a transportation of the portable hydrogen maser of the Smithsonian Astrophysical Observatory (SAO) first to the Lyman Laboratory of Physics at Harvard University (HU) and then to the Atomic Frequency and Time Standards Section of the National Bureau of Standards (NBS). The SAO maser is described in detail in [20]. At HU its frequency was compared with the HU reference hydrogen maser. The wall shift of the HU maser was known from a previous evaluation [3]. Both masers were tuned and the appropriate bias corrections (see Section III) were applied. From the thus corrected difference frequency of both masers the wall-shift correction of the SAO maser could be inferred as $\Delta\nu_W = +20.19$ mHz. This experiment was done in December 1969. The SAO maser was brought to NBS, where its frequency was referenced to cesium on January 22 and 23, 1970.

Experiment 2 involved the NBS experimental hydrogen maser NBS-H2. Its general configuration is similar to the Varian H-10 hydrogen masers. During the period from November 1969 to January 1970 this maser was successively equipped with bulbs of different sizes ranging from 7.5 to 20 cm in diameter. A total of 15 frequency determinations was made of which 11 were used for the final analysis. Each individual measurement was made with a reference frequency source whose frequency was known in terms of cesium (NBS-III) [19]. Thus the measurement of the wall shift was simultaneously the measurement of the hydrogen–cesium ratio, and the value for zero wall shift was obtained by extrapolating

TABLE II
HYDROGEN–CESIUM MEASUREMENTS
$\nu_H = 1420\,405\,751$ Hz + ν_H'

Author and Reference	Approximate Year of Measurement	Teflon Used	Wall Shift From Reference (See Table I)	Hydrogen Maser	Cesium Reference	ν_H' (mHz)
Crampton *et al.* [5]	1963	← Related → TFE 852-201 Du Pont	Crampton *et al.* (1963)	Harvard laboratory type	NC 2001	800 ± 28
Vanier *et al.* [11]	1963	FEP Du Pont Lot 10144	Vanier–Vessot (1963–1964)	Varian laboratory type	several Cs clocks via Loran C	827 ± 20
Peters *et al.* [12]	1964	FEP Du Pont	Vanier–Vessot (1963–1964)	Varian H-10	HP 5060 A	778 ± 16
Peters and Kartaschoff [13]	1964	FEP Du Pont	Vanier–Vessot (1963–1964)	Varian H-10	LSRH laboratory type	785 ± 16
Johnson and McGunigal [14]	1965	FEP Du Pont	Vanier–Vessot (1963–1964)	Varian H-10	HP 5060 A	781 ± 16
Vessot *et al.* [15]	1965	FEP Du Pont	Vanier–Vessot (1963–1964)	Varian H-10	NBS-III	786 ± 2
Becker and Fischer [16]	1966	TFE 852-201 Du Pont	Vanier–Vessot (1963–1964)	PTB-H2 laboratory type	HP 5060 A	756 ± 3
Becker and Fischer [16]	1967	TFE 852-201 Du Pont	Vanier–Vessot (1963–1964)	PTB-H2 laboratory type	PTB laboratory-type C2 and HP 5061 A	758± 2
Mungall *et al.* [33]	1968	FEP-120 Du Pont Drum 10020	Vanier–Vessot (1963–1964)	NRC laboratory type	NRC laboratory long cesium beam standard	778 (an explicit accuracy claim was not made)
Chi *et al.* [17]	1968	FEP-120 Interchemical vanaflex (1967)	Vanier–Vessot (1963–1964)	NASA-NX-1 laboratory type	4 units HP 5061 A 1 unit HP 5060 A	777 ± 3
Menoud and Racine [9], [10]	1969	← Related → FEP-120 Du Pont	Menoud–Racine (1968–1969)	LSRH-H2 laboratory type	Oscillatom 3 (Ebauches)	778 ± 4
Bangham [18]	1969	PTFE	Vanier–Vessot (1963–1964)	NPL laboratory type	NPL laboratory type	734 ± 25
Hellwig *et al.*, experiment 1 [this paper]	1970	← Related → FEP-120 Blend B-107 Du Pont (1967)	Zitzewitz *et al.* (1968–1969)	portable SAO maser transferred from HU	NBS-III via NBS clock system and NASA-NP3 H-maser	769 ± 2
Hellwig *et al.*, experiment 2 [this paper]	1970	← Related → TFE Blend 42 Du Pont (1969)	this paper (1969–1970)	NBS-H2 laboratory type	NBS-III via NBS clock system and NASA-NP3 H-maser	767 ± 2

the measured data to $1/D = 0$($D \equiv$ bulb diameter).

Fig. 1 shows the measurement system used in both experiments. The receiver for the output frequency ν_M of the hydrogen maser is basically a triple-superheterodyne system. The first intermediate frequency is in the MHz range, the second in the kHz range, and the third is adjusted by means of a synthesizer (output frequency ν_S) to a slow beat frequency ν_B of the order of 1 Hz. If the external reference frequency ν_R is chosen to be nominally 5 MHz we have at the output of the second stage an intermediate frequency of $(\nu_M - 284\nu_R)$ and for the final beat frequency

$$\nu_B = (\nu_M - 284\nu_R) - \nu_S. \tag{3}$$

By comparison with (1) we see that $\nu_S \approx 405$ kHz. The maser frequency ν_M in terms of the reference frequency ν_R can then be calculated from (3). If ν_R is given in terms of the cesium transition frequency the hydrogen–cesium ratio can be computed using the appropriate corrections. A measurement precision of a few parts in 10^{13} was

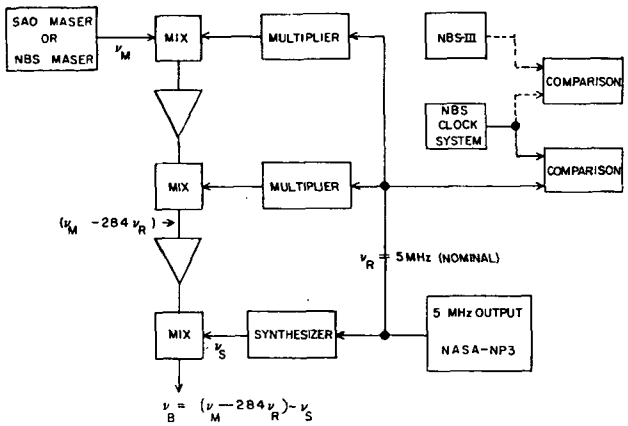

Fig. 1. Measurement system used for determining frequency ratio between two frequency standards.

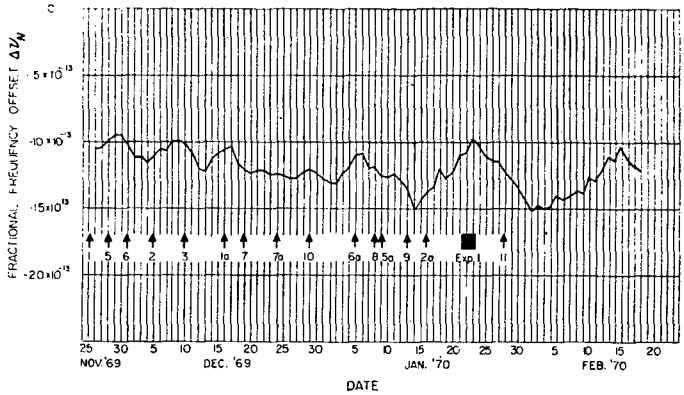

Fig. 2. Fractional frequency offset of NP3 from $\nu_{UTC(NBS)}$. Derived from a 4-day average of the time error of NP3 with respect to UTC(NBS): 6 clocks. Zero on the vertical scale corresponds to $\nu_{UTC(NBS)}$.

desired. To take ν_R directly from the output of a cesium standard would have meant averaging times of many hours to attain this precision. This would have been awkward in experiment 1 and prohibitive for experiment 2 since the NBS-H2 maser had no temperature control, a limitation that necessitated a fast measurement technique (30 minutes maximum duration).

Fortunately we also had available the hydrogen maser standard NP3 of the National Aeronautics and Space Administration (NASA). Its design is described in [21]. The most important features of this maser for the present purpose are its stability and the provision of synthesized standard output frequencies. We used one of its outputs on nominally ν_R = 5 MHz. However, the NASA maser not only served as a highly stable frequency source allowing short- and long-term measurements with a precision of a few parts in 10^{13} but also as a calibrated transfer standard. As indicated in Fig. 1, the frequency of the NASA maser was constantly monitored by the NBS clock ensemble, which consisted of six commercial cesium standards. The clock ensemble generates the atomic time scale AT(NBS) with the frequency $\nu_{AT(NBS)}$; this frequency is set by calibration with the primary frequency standard. The most recent calibration had been made in May 1969 with the NBS-III cesium beam. A coordinated universal time scale is generated from AT(NBS) and is called UTC(NBS) with a frequency of $\nu_{UTC(NBS)} = \nu_{AT(NBS)} + \Delta\nu_{UTC}$. During the course of the measurements we had $\Delta\nu_{UTC} = -299.995 \times 10^{-10}$ $\nu_{AT(NBS)}$. The nominal output of the NASA hydrogen standard NP3 was synthesized to reflect a coordinated universal time scale (UTC) [17]. Fig. 2 shows a plot of the fractional frequency of NP3 referenced to $\nu_{UTC(NBS)}$ (zero on the vertical scale) versus time. From Fig. 2 we can derive the correction $\Delta\nu_N$ as the offset of NP3 from $\nu_{UTC(NBS)}$ evaluated at the nominal hydrogen frequency. Several additional corrections are necessary to relate the frequency of the hydrogen maser to the unperturbed transition frequency in hydrogen. They are summarized in Table III together with those already mentioned.

TABLE III
SUMMARY OF BIAS CORRECTIONS

Offset of $\nu_{UTC(NBS)}$ from $\nu_{AT(NBS)}$	$\Delta\nu_{UTC}$
Offset of NASA-NP3 frequency from $\nu_{UTC(NBS)}$	$\Delta\nu_N$
Wall shift	$\Delta\nu_W$
Second-order Doppler	$\Delta\nu_D$
Thermalization	$\Delta\nu_T$
Magnetic field (Zeeman)	$\Delta\nu_Z$
Spin-exchange collision	$\Delta\nu_{SE}$
Cavity tuning	$\Delta\nu_C$

The wall-shift correction was discussed previously in Section I, and (2), a semiempirical equation, was given. For (2) it is assumed that the wall shift is proportional to the wall-collision rate of the hydrogen atoms, i.e., to the inverse diameter of a spherical storage bulb.

The second-order Doppler effect in the hydrogen maser due to the thermal motion of the atoms necessitates a correction of [15]

$$\Delta\nu_D = C_1 T_S \tag{4}$$

where $C_1 = +1.9557 \times 10^{-4}$ Hz·K^{-1}. We assume here that thermal equilibrium between the kinetic energy of the hydrogen atoms and the walls of the storage bulb is established. T_S is then the temperature of the storage bulb.

If the kinetic energy of the atoms is not fully in equilibrium with the temperature of the storage bulb, we will commit an error in using T_S. We should then introduce a correction $\Delta\nu_T$, which relates to the difference between the bulb temperature and the effective temperature of the stored atoms. Preliminary theoretical calculations of the thermalization process indicate [22] that $\Delta\nu_T$ should be sufficiently small to warrant $\Delta\nu_T = 0$ within our uncertainty limits. Some preliminary experimental results based on velocity selection in an atomic hydrogen beam support this assumption [23].

A magnetic field H causes a Zeeman effect on the energy level structure of hydrogen, and the corresponding frequency correction is given by [15]

$$\Delta\nu_Z = C_2\overline{H^2} \tag{5}$$

where $C_2 = -2750\ \text{Hz}\cdot G^{-2}$, and $\overline{H^2}$ denotes the average of the squared magnetic field over the volume of the bulb. It is possible to measure the average magnetic field $\bar{H}$ by inducing transitions among the magnetic sublevels of the $F = 1$ state and observing a change in the amplitude of the maser signal. This Zeeman frequency is given by [15]

$$f_Z = C_3|\bar{H}| \tag{6}$$

where $C_3 = +1.4 \times 10^6\ \text{Hz}\cdot G^{-1}$. The error that one is forced to commit by substituting $\bar{H}^2$ from (6) for $\overline{H^2}$ in (5) in order to obtain $\Delta\nu_Z$ is negligible because very low and homogeneous magnetic fields ($|H| < 1$ mG) are typically used.

The last two corrections from Table III, $\Delta\nu_{SE}$ and $\Delta\nu_C$, must be discussed together. The effects of spin exchange in combination with cavity tuning have been treated extensively in the literature [24]–[27]. The net result is that spin-exchange frequency shift and cavity pulling have a similar functional relationship to the atomic-resonance linewidth. As a consequence, cavity tuning and spin-exchange shifts cancel each other when the maser is "tuned," or

$$(\Delta\nu_C + \Delta\nu_{SE})_{\text{tuned}} = 0. \tag{7}$$

The "tuned" condition is here defined as a setting of the maser cavity such that the output frequency of the maser ν_M is independent of changes in the hydrogen pressure (beam intensity).

In experiment 1 the SAO maser was tuned in separate runs, both manually and automatically using its own automatic cavity servo, until the output frequency was unaffected by changes in the beam flux. The actual tuning element was a varactor diode mounted inside the cavity. Details of this procedure can be found in [20]. Averaging times of about 10–100 seconds were used to measure ν_B.

In experiment 2 the beat frequency ν_B for the tuned condition was calculated from four measurements of the maser frequency at two cavity settings and two beam intensities using a linear interpolation.[4] The two cavity settings corresponded to maser frequencies that were typically a few parts in 10^{12} above and below ν_M (tuned). In this procedure, the cavity settings did not have to be known in an absolute sense but had to be reproducible to $\Delta\nu_M/\nu_M \approx 10^{-13}$. This was assured in separate experiments. The actual tuning element was also a varactor diode mounted inside the cavity. One complete measurement of ν_B took typically 15 minutes at averaging times of about 10 seconds.

[4] This technique was also used in the comparison between the SAO maser and the HU reference maser.

From Table III and (3)–(7) we are now able to calculate the unperturbed hydrogen transition frequency referenced to NBS-III as

$$\nu_H = 284\nu_R + \nu_S + \nu_B + \Delta\nu_{\text{UTC}} + \Delta\nu_N + \Delta\nu_W + \Delta\nu_D + \Delta\nu_Z, \tag{8}$$

where $284\nu_R = 1420\,000\,000.0000$ Hz with $\nu_R = 5$ MHz. All corrections $\Delta\nu$ are taken at the nominal hydrogen frequency.

III. Experimental Results

We will now discuss the experimental results that we obtained in experiments 1 and 2 together with the uncertainty contributions associated with each of the frequency corrections. We begin with experiment 1; its results are summarized in Table IV.

The synthesizer was set at $\nu_S = 405\,794.4200$ Hz; no uncertainty is associated with this value.

The period of the beat frequency was measured; the beat frequency ν_B is listed in Table IV. In order to obtain this value the maser had to be tuned. This can be done only with a certain precision. From the experimental results we estimate the associated uncertainty as $\pm 3 \times 10^{-13}$.

The fractional frequency offset of UTC(NBS) against AT(NBS) is nominally $\Delta\nu_{\text{UTC}} = -299.995 \times 10^{-10}\ \nu_{\text{AT(NBS)}}$ as listed in Table IV; no uncertainty is involved.

The actual synthesized output frequency of the NASA hydrogen maser standard deviated by a small amount $\Delta\nu_N$ from the frequency $\nu_{\text{UTC(NBS)}}$. For the date of our experiment we can take the corresponding bias correction directly from Fig. 2 and obtain $\Delta\nu_N = -0.0015$ Hz. There is some uncertainty in this value due to the estimate of the accuracy capability of NBS-III ($1\sigma = 5 \times 10^{-13}$ [19]) and due to the frequency dispersion of AT(NBS) since it was calibrated (May 1969). The actual uncertainty (one sigma) during the time of the measurement was $\pm 9 \times 10^{-13}$.[5]

We have already discussed the fact that the wall-shift correction was obtained by a comparison between the portable SAO maser and the HU reference maser. The wall shift of the HU maser was measured in early 1969; a one-sigma confidence interval of ± 0.5 mHz was assigned to this measurement [3]. However, we have to consider the possibility of secular changes of the physical properties of the wall coating since that time. Preliminary measurements at HU indicate that the associated uncertainty could be as large as 2 mHz. A correction of -2 mHz seems most likely [28] and would put the value of experiment 1 very close to that of experiment 2. We are not applying this correction, however, because we do not yet consider this result conclusive. The combination of the original measurement uncertainty and this bulb-aging effect thus leads to a total uncertainty of ± 2 mHz.

[5] This value has been confirmed by comparisons between the rates of AT(NBS) and AT(U.S. Naval Observatory) as well as AT(NRC) over the past year.

TABLE IV
SUMMARY OF RESULTS FROM EXPERIMENT 1

	ν_S	ν_B	$\Delta\nu_{UTC}$	$\Delta\nu_H$	$\Delta\nu_W$	$\Delta\nu_D$	$\Delta\nu_Z$
Observed quantity	synthesizer setting	electronic counter measurement	-299.995×10^{-10}	Fig. 2	beat frequency at HU	T_{bulb} = 47°C (320.15°K)	f_Z = 1020 Hz
Bias corrections (Hz)	+405 794.4200	−0.1193	−42.6115	−0.0015	+0.0202	+0.0627	−0.0015
Bias uncertainties (Hz)	—	±0.0004	—	±0.0013	±0.0020	±0.0001	±0.00002

ν_H = 1420 405 751.7691 ± 0.0024 Hz

The second-order Doppler correction for the SAO maser is calculated from the bulb temperature using (4). The temperature was (47 ± 0.5)°C maintained by the automatic temperature control of the SAO maser. This leads to the values for $\Delta\nu_D$ and its uncertainty in Table IV. The last correction in Table IV is the frequency change due to the Zeeman effect. A Zeeman resonance frequency of 1020 Hz was measured, and $\Delta\nu_Z$ can be calculated from (5) and (6). The Zeeman frequency was typically stable to about ±5 Hz. This leads to a negligible uncertainty.

From (8) and Table IV we can now calculate the result for ν_H, the unperturbed hydrogen hyperfine frequency. Its uncertainty is calculated as the square root of the sum of the squared individual contributions since they are independent of each other. From

Experiment 1:

$$\nu_H = 1420\,405\,751.7691 \pm 0.0024 \text{ Hz}.$$

We now discuss the results of experiment 2. A total of 15 measurements of different coatings and bulb sizes were made. As coating material we used Du Pont's TFE Teflon, Blend 42, Lot 8842, 34.3 percent solids, purchased in 1969.

The actual coating solution consisted of 50 percent Teflon, 40 percent distilled water, and 10 percent Triton X-100 (Rohm and Haas). The bulbs were thoroughly cleaned with diluted sulfuric acid, and the coating solution was applied and then dried by circulating dry nitrogen gas through the bulb. The baking was done at 380°C for one-half hour while oxygen was circulated through the bulb. The bulbs were heated up rapidly in about 15 minutes; the cooling after baking took about 1 hour although the initial drop in temperature to below 300°C occurred rather rapidly within a few minutes. The bulbs were heated up to above 300°C immediately before setting them into the maser. They were put hot into the maser, which was then pumped down immediately. Some bulbs (indicated by a dagger in Table V) received a second Teflon coating on top of their first one. The procedure was identical to the one described previously, including the cleaning of the first coat with acid. No problems were encountered in any of the many coating procedures. All coatings, first and second ones, passed the "water drop test" (tested *after* their use in the maser). The coatings were transparent and appeared only slightly milky. All bulbs, except bulb 1, were new and never coated before.

The first column in Table V gives the identification numbers of the bulbs. The second column lists the dates of their measurements in the hydrogen maser. In the third column we find several remarks; in the fourth, the nominal diameter is given; and in the fifth column we find the accurate inverse diameter that was determined from a volume measurement. The sixth column gives the temperature of the bulb (actually the temperature of the cavity was measured) at the time of the measurement. The NBS-H2 maser used in this experiment had no temperature control of its own. Therefore the temperatures for the various measurements differ slightly. The seventh column lists the Zeeman resonance frequency. The eighth column gives the beat frequency ν_B of the tuned maser. In the ninth column the beat frequency ν_B (corrected) is corrected for the offsets $\Delta\nu_N$ of the NASA hydrogen standard according to Fig. 2. The last column lists the standard deviation of several (more than ten, typically) independent tunings of the maser. A plot of the beat frequency ν_B (without the $\Delta\nu_N$ correction) as a function of the inverse bulb diameter is shown in Fig. 3. No oscillations were possible with bulb no. 4 since this bulb caused a significant reduction of the cavity Q. Bulbs 1*, 5*, 6*, and 10* were excluded from the final analysis (indicated by the asterisk).

They all showed obvious differences from all other bulbs, as we now describe. Bulb 1* was a previously used one, stripped of its old coating with hydrofluoric acid, and recoated. It showed up in the graph with a far too high ν_B, i.e., a larger wall shift than the other bulbs. This may be explained by its surface roughness leading to an effectively larger surface area. A second coating (1†) apparently smoothed out this roughness and brought this bulb in line with the others.

Bulbs 5* and 6* received extremely thin, almost invisible coatings, but they passed the water drop test. They responded with somewhat lower values of ν_B, i.e., less wall shift than the rest of the bulbs. A second coat

TABLE V
DETERMINATION OF THE UNPERTURBED HYDROGEN FREQUENCY
EXPERIMENT 2

Bulb No.	Date of Measurement	Remarks	Nominal Diameter (inch)	Inverse Diameter (cm^{-1})	T (°C)	f_Z (Hz)	ν_B (Hz)	ν_B (Hz) (corrected)	1σ (mHz)
1*	Nov. 25, '69	old bulb, glass etched	6	0.0608	24.0	252	−0.7191	−0.7206	1.4
1†	Dec. 16, '69	old bulb, glass etched	6	0.0608	23.7	256	−0.7094	−0.7107	0.9
2	Dec. 5, '69		6	0.0599	24.1	233	−0.7114	−0.7129	0.9
2†	Jan. 16, '70		6	0.0599	24.1	215	−0.7105	−0.7124	1.0
3	Dec. 10 ,'69		6	0.0597	23.7	271	−0.7095	−0.7109	0.8
4		very heavy bulb	5		no oscillations possible				
5*	Nov. 28, '69	very thin coating	5	0.0786	23.8	255	−0.7172	−0.7186	0.7
5†	Jan. 9, '70		5	0.0786	24.0	262	−0.7210	−0.7228	1.5
6*	Dec. 1, '69	very thin coating	4	0.0975	24.0	265	−0.7226	−0.7241	2.8
6†	Jan. 5, '70		4	0.0975	23.8	277	−0.7313	−0.7328	1.3
7	Dec. 19, '69		4	0.101	24.0	255	−0.7319	−0.7336	1.0
7†	Dec. 24, '69		4	0.101	23.8	250	−0.7299	−0.7316	0.9
8	Jan. 8, '70		4	0.103	24.1	263	−0.7330	−0.7347	0.6
9	Jan. 13, '70		6	0.0655	23.8	252	−0.7106	−0.7125	1.1
10*	Dec. 29, '69	no spin-exchange tuning possible	3	0.134	23.9	248	−0.741	−0.743	7.0
11	Jan. 28, '70		8	0.0504	23.7	244	−0.7052	−0.7069	1.0

* Indicates zero weight given in final analysis.
† Indicates a second Teflon coating.

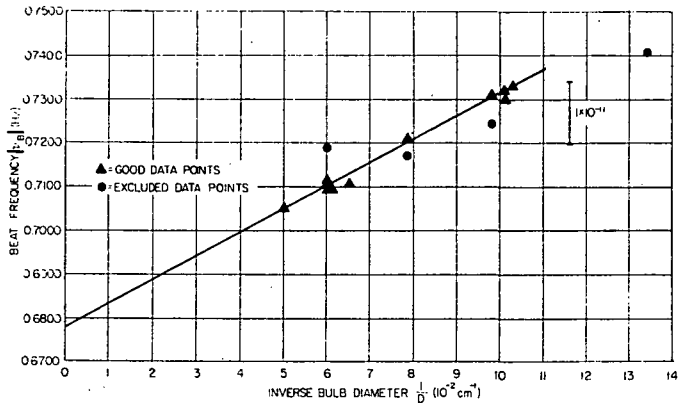

Fig. 3. Wall-shift measurement and hydrogen–cesium comparison from experiment 2 using the NBS-H2 hydrogen maser. As plotted, the beat frequency ν_B does not contain the $\Delta\nu_N$ correction. See Table V for both ν_B and ν_B (corrected). See Fig. 2 for the $\Delta\nu_N$ correction.

(5† and 6†) brought them to values compatible with the majority of the bulbs. We have no good explanation for this effect.

Bulb 10* was so small that oscillations were barely possible. For this reason the spin-exchange tuning procedure, which required a reduction in beam intensity, could not be used. The uncertainty in its ν_B value was therefore prohibitively large for its inclusion in the final analysis.

The "good" bulbs were used in a linear, least-squares fit whereby each measurement point was weighted according to its variance (σ^2 from Table V). The intercept at $1/D = 0$, which corresponds to $\Delta\nu_W = 0$, was obtained as ν_B (corrected) = −0.6798 Hz. The standard deviation of the $n = 11$ points from the straight line was calculated to be $\sigma = 0.00108$ Hz. We can now estimate the confidence interval w of the intercept at $1/D = 0$ from [29],

$$w = \left(\frac{1}{n} + \frac{(x - \bar{x})^2}{\Sigma x^2 - n\bar{x}^2}\right)^{1/2} t_{1-\alpha/2}\sigma \qquad (9)$$

where α is the confidence level, t is the student t, and $x = 1/D$. For one-sigma confidence we calculate w = 0.0012 Hz.

Table VI summarizes this result and all other pertinent data analogously to Table IV. The synthesizer was set at ν_S = 405 795.0000 Hz, and the beat frequency ν_B (corrected) in Table VI is the frequency at the intercept and is thus the frequency for $\Delta\nu_W = 0$. It contains the correction $\Delta\nu_N$ that was already applied in Table V. The uncertainty associated with $\Delta\nu_N$ is the same as in Table IV and was discussed there. For the Doppler correction $\Delta\nu_D$ we use the mean value for the temperatures listed in Table V. The uncertainty of the temperature measurement is again estimated at ±0.5°C, which well includes the systematic differences of the temperatures of the individual measurements. The mean Zeeman frequency of all measurements (Table V) is $f_Z \approx 245$ Hz (175 μG), which leads to a correction of only 0.1 mHz. The individual measurements of f_Z spread around this mean by at most ±30 Hz, which corresponds to a negligible variation of the bias of ±0.02 mHz. This value is listed as bias uncertainty of $\Delta\nu_Z$ in Table VI.

From (8) and Table VI we can now calculate ν_H, the unperturbed hydrogen hyperfine frequency. The uncertainty is the square root of the sum of the squared individual contributions, analogously to experiment 1.

TABLE VI
SUMMARY OF RESULTS FROM EXPERIMENT 2

	ν_S	ν_B (corrected)	$\Delta\nu_{UTC}$	$\Delta\nu_N$	$\Delta\nu_W$	$\Delta\nu_D$	$\Delta\nu_Z$
Observed quantity	synthesizer setting	Fig. 2 and Table V	-299.995×10^{-10}	Fig. 2	Fig. 3	T_{bulb} = 23.9°C (297.05°K)	f_Z = 245 Hz
Bias corrections (Hz)	+405 795.0000	−0.6798	−42.6115	included in ν_B (corrected)	included in ν_B (corrected)	+0.0581	−0.0001
Bias uncertainties (Hz)	—	±0.0012	—	±0.0013	—	±0.0001	±0.00002

ν_H = 1420 405 751.7667 ± 0.0018 Hz

Experiment 2:

$$\nu_H = 1420\ 405\ 751.7667 \pm 0.0018 \text{ Hz}.$$

Fig. 3 and Table V allow a calculation of the wall-shift coefficient K'(at 24°C), where

$$K' = K[1 + \alpha(24 - 40)]. \quad (10)$$

For experiment 2 we find (for TFE-Teflon)

$$K' = +0.528 \text{ Hz}\cdot\text{cm}.$$

From Table I (experiment 1) we calculate for the value of Zitzewitz *et al.* (FEP-Teflon) at the same temperature using $K' = +1.192K$

$$K' = +0.460 \text{ Hz}\cdot\text{cm}.$$

The difference between these values is only about 13 percent despite the fact that two different kinds of Teflon were measured: the homopolymer TFE (tetrafluoroethylene polymer) and the copolymer FEP (TFE plus hexafluoropropylene).

IV. Conclusions

The values for ν_H from experiments 1 and 2 are well within each other's error limits. The uncertainties assigned to the two values are not much different. We therefore take the mean of both as the most probable value of the unperturbed hydrogen transition frequency

$$\nu_H = 1420\ 405\ 751.768 \pm 0.002 \text{ Hz}.$$

This result is based on the two most extensive wall-shift evaluations that have been carried out so far, as evidenced in Table I. Furthermore, the hydrogen–cesium comparison was done while a direct link existed to the wall-shift correction data. In experiment 1 this link was provided by the preservation of the results of the Harvard wall-shift experiment [3] in the HU reference maser, and the calibration of the SAO maser against this reference. In experiment 2 the link was established by the simultaneous, integral wall-shift/hydrogen–cesium comparison experiment. In addition we used one of the best evaluated cesium standards currently in existence as our reference (NBS-III). We feel that our quoted error limits, as documented in this paper, are realistic and meaningful.

The only question not yet completely settled is the problem of thermalization in the bulb. Although there is evidence [22], [23] that a somewhat incomplete thermalization will not cause an observable bias correction today, we encourage experimentation towards clarifying this point in view of the possibility of future, more accurate measurements.

A comparison of our results with those obtained previously is made in Table II. The range of values for ν_H totaling about 6×10^{-11} (90 mHz) far exceeds any quoted uncertainties and therefore requires some critical discussion. We surely can not explain deviations of this magnitude by differences in the cesium reference standards alone. Cesium beam tubes are extensively studied and intercompared devices. The uncertainty to be attributed to the cesium standards that have been used could be as high as 2×10^{-11} (28 mHz) before 1964, 1×10^{-11} in 1964, 3 to 5×10^{-12} (4–7 mHz) between 1965 and 1966, and 1 to 3×10^{-12} (1.4–4 mHz) since then. A larger uncertainty in the wall-shift correction as compared to those quoted in the past is the most likely explanation for most of the discrepancies. It is evident that the wall shift is not a constant of nature, but largely depends on the kind of Teflon (including differences from year to year due to the manufacturing process) and on the many complex parameters involved in the actual coating procedure. This is evidenced in Table I (compare also [3]), in the exclusion of bulbs from the wall-shift evaluation as indicated by the asterisks in Table V, and in [3] where we observed wall shifts that were up to 50 percent different from the wall shifts of "good" bulbs. Two statements can be made in consequence: 1) using only a few bulbs (e.g., two) for a wall-shift measurement can lead to highly erroneous results, and 2) the use of a wall-shift correction not directly related to the hydrogen maser that is used in a ν_H determination may also lead to errors far exceeding those quoted in Table II. If we check the values listed in Table II against the above two state-

ments, we find that the majority of the values do not have the direct experimental link required by statement 2) between the bulb used in the hydrogen maser and the applied wall-shift correction. Furthermore, they are correlated through the almost exclusive use of one particular wall-shift evaluation that we believe to be a valid one at the time of its measurement but that should not be used in the sense of a universal correction (statement 2)). Only the values of Crampton *et al.* and Menoud and Racine are based on a direct relationship between the hydrogen–cesium measurement and a wall-shift determination; unfortunately, however, only two bulbs were used in each case and statement 1) applies. The only values not affected by either statement are those of this paper.

The discussion of discrepancies in past values of ν_H that is given above should not, however, be interpreted to imply that a frequency standard based on hydrogen storage is necessarily inferior to a cesium standard. First, the uncertainties due to the cesium comparison and those due to the wall-shift correction contribute about equally to the uncertainty that we assign to our measurements of ν_H. Furthermore, a more recent measurement of ν_H has been reported [30], which was based on an independent wall-shift evaluation and which was also referenced with transfer standards to the cesium standard NBS-III. This new value of ν_H is almost identical with the results of this paper.

Second, new experimental developments that promise a reduction in the wall-shift limitation have evolved recently. They include the big storage vessel [31], the deformable storage bulb [28], and the operation at elevated bulb temperatures [30], [32]. Thus, hydrogen storage devices should be considered serious competitors for the primary standard of the future, a place now held by the cesium beam standard.

Acknowledgment

The following laboratories with their apparatus participated in these experiments: 1) the Atomic Frequency and Time Standards Section of the National Bureau of Standards with a laboratory-type hydrogen maser, designated NBS-H2, and the NBS clock system that was calibrated by the evaluated cesium primary frequency standard NBS-III, 2) the Smithsonian Astrophysical Observatory with a portable hydrogen maser, and 3) the Lyman Laboratory of Physics of Harvard University with the Harvard reference hydrogen maser. We are grateful for the support received from our respective organizations, which made this joint experiment possible.

We owe special thanks to H. E. Peters and E. H. Johnson for making available their NASA hydrogen maser standard NP3, which greatly facilitated our measurements. The U. S. Army Electronics Command kindly made available several storage bulbs, two of which were used in the experiment. The original design and construction of the NBS-H2 hydrogen maser is the work of Dr. F. R. Petersen. A. S. Risley's and H. E. Bell's help in preparing NBS-H2 for the experiments is gratefully acknowledged.

References

[1] A. S. Risley *et al.*, "Long-term frequency stability of a NASA prototype hydrogen maser," presented at the Conf. on Precision Electromagnetic Measurements, Boulder, Colo., June 1970.
[2] D. Kleppner *et al.*, "Hydrogen maser principles and techniques," *Phys. Rev.*, vol. 138, pp. A972–A983, 1965.
[3] P. W. Zitzewitz, E. E. Uzgiris, and N. F. Ramsey, "Recent results concerning the hydrogen maser wall shift problem," *Rev. Sci. Instr.*, vol. 41, pp. 81–86, 1970.
[4] R. E. Beehler, R. C. Mockler, and J. M. Richardson, "Cesium beam atomic time and frequency standards," *Metrologia*, vol. 1, pp. 114–131, 1965.
[5] S. B. Crampton, D. Kleppner, and N. F. Ramsey, "Hyperfine separation of ground-state atomic hydrogen," *Phys. Rev. Lett.*, vol. 11, pp. 338–340, 1963.
[6] J. Vanier and R. F. C. Vessot, "H-maser wall-shift," *Metrologia*, vol. 6, pp. 52–53, 1970.
[7] B. S. Mathur, S. B. Crampton, D. Kleppner, and R. F. Ramsey, "Hyperfine separation of tritium," *Phys. Rev.*, vol. 158, pp. 14–17, 1967.
[8] L. P. Elkina, G. A. Elkin, and G. M. Strakhovskii, "Measurement of the frequency drift of a hydrogen standard owing to atomic impacts on the flask walls," *Izmeritel'naya Tekh.*, vol. 6, p. 91, 1968; transl. in *Meas. Tech.*, pp. 841–842, 1968.
[9] C. Menoud and J. Racine, "Résultats nouveaux obtenus avec les masers à hydrogène H2 et H3 du LSRH," *Proc. Colloq. Internatl. Chronométrie* (Paris), pp. A8-1–A8-12, September 1969.
[10] ——, "Stabilität und Genauigkeit der Frequenz von Wasserstoff-Masern," *Z. Angew. Math. Phys.*, vol. 20, pp. 578–584, 1969.
[11] J. Vanier, H. E. Peters, and R. F. C. Vessot, "Exchange collisions, wall interactions, and resettability of the hydrogen maser," *IEEE Trans. Instrum. Meas.*, vol. IM-13, pp. 185–188, December 1964.
[12] H. E. Peters, J. Holloway, A. S. Bagley, and L. S. Cutler, "Hydrogen maser and cesium beam tube frequency standard comparison," *Appl. Phys. Lett.*, vol. 6, pp. 34–35, 1965.
[13] H. E. Peters and P. Kartaschoff, "Hydrogen maser frequency comparison with Swiss cesium atomic beam standard," *Appl. Phys. Lett.*, vol. 6, pp. 35–36, 1965.
[14] E. H. Johnson and T. E. McGunigal, "Hydrogen maser frequency comparison with a cesium standard," NASA, Tech. Note TND-3292, April 1966.
[15] R. Vessot, H. Peters, J. Vanier, R. Beehler, D. Halford, R. Harrach, D. Allan, D. Glaze, C. Snider, J. Barnes, L. Cutler, and L. Bodily, "An intercomparison of hydrogen and cesium frequency standards," *IEEE Trans. Instrum. Meas.*, vol. IM-15, pp. 165–176, December 1966.
[16] G. Becker and B. Fischer, "Beitrag zum internationalen Wasserstoffmaser Vergleich mit transportabler Atomuhr," *PTB—Mitt.*, vol. 78, pp. 177–183, 1968.
[17] A. R. Chi, F. G. Major, and J. E. Lavery, "Frequency comparison of five commercial cesium standards with a NASA experimental hydrogen maser," *Proc. IEEE* (Letters), vol. 58, pp. 142–143, January 1970; also *Proc. 24th Ann. Symp. on Frequency Control* (Fort Monmouth, N. J.), 1970 (to be published).
[18] M. Bangham, "Hydrogen maser work at the National Physical Laboratory," *Proc. Colloq. Internatl. Chronométrie* (Paris), pp. A7-1–A7-13, 1969.
[19] D. J. Glaze, "Improvements in atomic cesium beam-frequency standards at the National Bureau of Standards," *Proc. XVI General Assembly of URSI: Progress in Radio Science, 1966–1969* (Ottawa, Canada), August 1969 (to be published); also *IEEE Trans. Instrum. Meas.*, vol. IM-19, pp. 156–160, August 1970.
[20] R. Vessot, M. Levine, L. Cutler, M. Baker, and L. Mueller, "Progress in the development of hydrogen masers," *Proc. 22nd Ann. Symp. on Frequency Control* (Fort Monmouth, N. J.), pp. 605–620, 1968.
[21] H. E. Peters, T. E. McGunigal, and E. H. Johnson, "Atomic hydrogen standards for NASA tracking stations," *Proc. 23rd Ann. Symp. on Frequency Control* (Fort Monmouth, N. J.), pp. 297–304, 1969.
[22] P. W. Zitzewitz, "Surface collision frequency shifts in the

atomic hydrogen maser," Ph.D. dissertation, Harvard University, Cambridge, Mass., 1970.
[23] H. E. Peters, private communication.
[24] N. F. Ramsey, "The atomic hydrogen maser," *Metrologia*, vol. 1, pp. 7–15, 1965.
[25] S. B. Crampton, "Spin exchange shifts in the hydrogen maser," *Phys. Rev.*, vol. 158, pp. 57–61, 1967.
[26] J. Vanier and R. F. C. Vessot, "Cavity tuning and pressure dependence of frequency in the hydrogen maser," *Appl. Phys. Lett.*, vol. 4, pp. 122–123, 1964.
[27] H. Hellwig, "Hydrogen spin exchange frequency shifts," NBS, Boulder, Colo., Tech. Note 387, 1970.
[28] P. Débely, "Hydrogen maser with deformable storage bulb," *Proc. 24th Ann. Symp. on Frequency Control* (Fort Monmouth, N. J.), 1970 (to be published).
[29] M. G. Natrella, "Experimental statistics," NBS, Washington, D. C., Handbook 91, pp. 5–18, 1963.
[30] R. F. C. Vessot and M. W. Levine, "Studies of hydrogen maser wall shift and relaxation rates for high molecular weight polytetrafluoroethylene," *Proc. 24th Ann. Symp. on Frequency Control* (Fort Monmouth, N. J.), 1970 (to be published).
[31] E. E. Uzgiris and N. F. Ramsey, "Multiple region hydrogen maser with reduced wall shift," *Phys. Rev. A*, vol. 1, pp. 424–446, 1970.
[32] P. W. Zitzewitz, "Surface collision frequency shifts in the atomic hydrogen maser," *Proc. 24th Ann. Symp. on Frequency Control* (Fort Monmouth, N. J.), 1970 (to be published).
[33] A. G. Mungall, D. Morris, H. Daams, and R. Bailey, "Atomic hydrogen maser development at the National Research Council of Canada," *Metrologia*, vol. 4, pp. 87–94, 1968.

November 1970 Brief 70-10616

NASA TECH BRIEF

System Automatically Tunes Hydrogen Masers

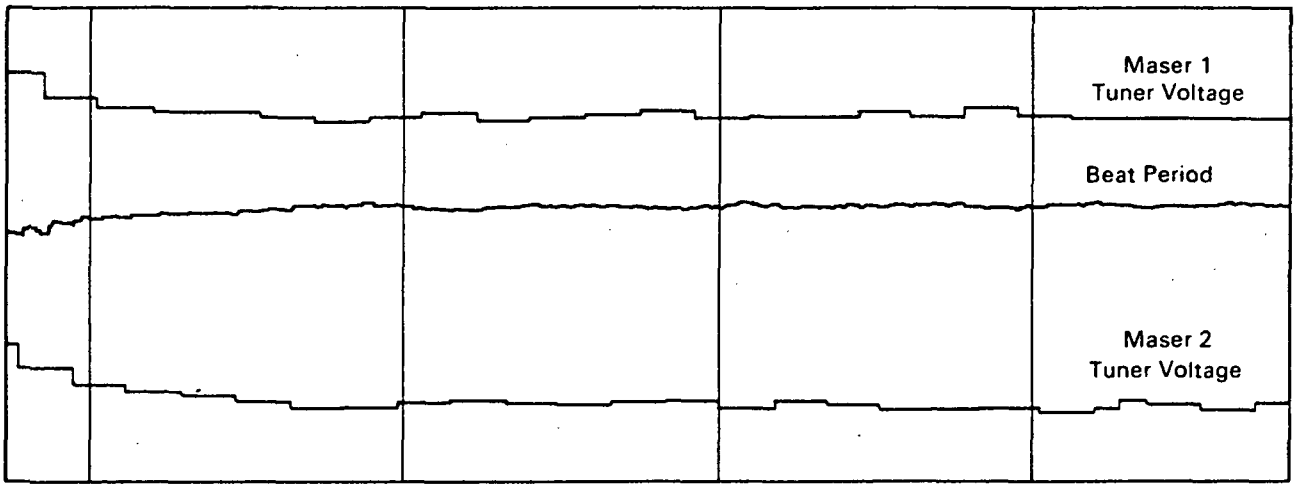

An automatic tuning system has been developed that permits frequency synchronization between two hydrogen masers. Although the system was originally designed to match a space-borne clock performance with that of a ground-based clock to test the so-called "red shift" (or effect of gravity on time predicted in Einstein's general theory of relativity), it should be of interest to organizations concerned with industrial and educational research programs. Additionally, this system, used in conjunction with radio astronomy for long-baseline interferometer experiments, should interest the astrophysical community as a new tool for investigation of distant phenomena in the universe.

A typical tuning run is illustrated in the figure. The tuning varactor voltage for maser 1 is recorded on the upper track of a strip chart recorder, and that for maser 2 on the lower track. Full scale for both tracks is 2.0 V and each major time increment in the time axis is 10 minutes. The center track displays an analog record of a digital measurement of the beat frequency between the two masers with a full-scale range of 2.5×10^{-11}. Synthesizers in phase-lock loops in system electronics are offset by 0.6 Hz and 100-period averages are taken to provide an observation time for each measurement of 166 seconds. Maser 1 is deliberately detuned by arbitrarily setting the tuning diode voltage to 5.0 V. The corresponding initial frequency error was about 3.8×10^{-12}. Similarly, maser 2 was offset about 5.5×10^{-12} by setting its tuning diode voltage to an arbitrary 4.0 V.

The loop gain on each tuner is deliberately reduced to effectively demonstrate the tuning operation. The correction process operates smoothly, as shown by the recording, alternating from maser 1 to maser 2. After 150 minutes, the initial total error of 8×10^{-12} is reduced to less than 5×10^{-13}. Of particular interest are the fluctuations in the beat period, due to pressure changes, which can be seen clearly for the first

(continued overleaf)

60 minutes of the recording. These fluctuations damp out rapidly, as expected, when proper tuning is approached.

Note:

The following documentation may be obtained from:

Clearinghouse for Federal Scientific
and Technical Information
Springfield, Virginia 22151
Single document price $3.00
(or microfiche $0.65)

Reference:
NASA-CR-94937 (N68-25901), Atomic Hydrogen Maser for Space Vehicle Application

Patent status:

No patent action is contemplated by NASA.

Source: R. F. C. Vessot and M. W. Levine of
Hewlett-Packard Co.
under contract to
NASA Headquarters
(HQN-10502)

STUDIES OF HYDROGEN MASER WALL SHIFT FOR HIGH MOLECULAR WEIGHT POLYTETRAFLUOROETHYLENE*

R.F.C. Vessot and M.W. Levine
Smithsonian Astrophysical Observatory
Harvard College Observatory
Cambridge, Massachusetts

Summary

The use of high molecular weight Polytetrafluoroethylene (PTFE) as a wall coating for the atomic hydrogen maser appears to offer some real advantages. By operating the maser bulb at a temperature where the wall shift is zero the effects of bulb size, shape and the surface texture of the coating can be eliminated. Coatings of PTFE can be applied in two quite distinguishable conditions; quenched and annealed. It is believed that the quenched coatings offer good reproductivity of the zero wall shift temperature. The annealed coating has a higher zero wall shift temperature and appears to offer somewhat lower relaxation rate than the quenched coating.

The results from some initial experiments are presented to support these contentions. Further work on wall coatings is in progress.

Introduction

Recent studies[1] of the temperature dependence of the wall shift in the atomic hydrogen maser have shown that the average phase shift per collision can be made positive or negative with respect to the phase of the free hydrogen oscillating dipole moment. We expect that the temperature at which a zero average phase shift per collision occurs is a property of the chemical nature of the walls and not of the mechanical surface conditions. By operating at this temperature, masers with bulbs of any size and surface condition should oscillate at the same frequency, provided that their surfaces are of the same type of material and free of contamination. The surface conditions will affect the relaxation rate and for this reason the wall collision rate should be kept as small as possible.

High molecular weight Polytetrafluoroethylene (PTFE) films cast from water dispersed resin are of particular interest since these materials have, on the average, about ten times the molecular weight of the tetrafluoroethylene (FEP) copolymer most often used as a wall coating material. The PTFE material should have fewer end groups exposed to the atomic hydrogen in the bulb. The end groups, chiefly CF_2H can contribute a significant area of sites containing bound hydrogen that result in larger negative values of phase shift per collision than the fluorine sites and can also contribute substantially to recombination processes (and consequently to relaxation) since the end-group hydrogen atom is much less energetically bound than the fluorine atoms. The tetrafluoroethylene homopolymer can be almost completely crystallized by the very careful and slow annealing through the range 340°C - 295° C. This should result in a 30-fold reduction in porosity to gases and the possibility of much reduced hydrogen collision rates.

Studies of PTFE[2] have shown that the change in the ordering of the amorphous PTFE teflon known as the alpha transition is at a higher temperature than the temperature for zero wall shift making this temperature a viable operating point.

Experimental Techniques

The Reference Oscillator

A reference standard was used to obtain the wall shift data and relate the data taken over a time interval of several months. The reference oscillator used to provide the frequency datum was compared with the Harvard reference maser and with the N.B.S. Maser using a traveling maser frequency standard. This measurement is described by Hellwig et al (1970)[3] and is part of an experiment to determine the unperturbed Hydrogen Hyperfine Transition Frequency. The wall shift of the reference oscillator was determined to be $-.022 \pm .002$ Hz at 319°K. This value has been used in all the measurements.

Working Maser

The working maser used for measuring the effect of temperature on wall shift is a modified Varian H-10 series maser. The r.f. power supply to the dissociator discharge was made to be controllable so as to permit variation of the

* This work is supported by NASA under Contract NSR-09-015-098.

dissociator efficiency and consequently the flux rate of atoms into the bulb. By using automatic cavity tuning techniques[4] much of the effort required to tune the maser has been avoided.

Serious problems with magnetic quenching were encountered at high cavity and bell jar temperature due to thermal gradients across junctions where different metals came into contact. All the oven cylinders, the solenoid and the bell jar components were electrically insulated from each other. The problem has been almost completely eliminated and it is possible to operate over a range of magnetic fields from 0.7 to 100 millioersteds with very little variation of signal amplitude when the maser is oscillating near threshold. For wall relaxation measurements the residual magnetic quenching is still not entirely negligible.

The maser bulb and cavity were both enclosed in the maser vacuum system. The bulb temperature was measured by measuring the cavity temperature by means of a thermocouple after allowing a 4-day period for thermal equilibrium of the bulb-cavity-bell jar assembly.

Maser Bulbs

Bulbs of 7" and 4" diameter were used for taking wall shift data as a function of temperature.

These bulbs were equipped with integral collimators that were coated with the bulbs in order to be assured that hydrogen atoms would encounter only one kind of teflon surface. Figure 1 shows a bulb of 4" diameter with integral collimator.

Coating Procedures

The bulbs were chemically cleaned by using a water solution of nitric acid and rinsed with several changes of hot distilled water. No attempt was made to roughen the interior surface of the bulbs.

The coating material consisting of a mixture of 10% Triton X-100, 50% Teflon 42 (duPont), and 40% distilled water was carefully poured into the bulb to be coated, swirled around to cover all the interior surface and drained out. The wet bulb was then placed on a rack with a small diameter tube extending upwards into the collimator. A flow of approximately 1 cm3/minute of dry nitrogen, at room temperature was allowed to flow into the bulb to dry the coating.

The bulb was then cured in a horizontal air flow oven for 20 minutes at 360°C. A very small flow of oxygen was piped into the bulb during the curing cycle. The oxygen was of high purity and was passed through a cold trap at -78.5°C (dry-ice) prior to entering the bulb. At the end of the 20 minute curing cycle the bulb was quickly removed from the oven and cooled by a draft of room temperature air. In this condition, the bulb is considered to be quenched.

The subsequent annealing cycle that is required for crystallizing the PTFE coating consists of placing the bulb in a specially controlled oven with the same oxygen flow and cooling the oven, in a steady rate, from 340°C to 290°C. The bulb was removed from the oven at 290°C and cooled in air to room temperature.

Experimental Data

Relation of Wall Shift to Phase Shift per Collision

The quantity of interest is the average phase shift per collision.

This quantity is related to the wall shift by the following expression:

$$\bar{\phi}(T) = \frac{2\pi \Delta\nu_w(T)}{\nu_c} \qquad \text{where}$$

$\Delta\nu_w$ is the wall shift and ν_c is the wall collision rate. The collision rate, ν_c is related to $\bar{v}$, the average velocity and the mean free distance λ by

$$\nu_c = \frac{\bar{v}}{\lambda}$$

For a sphere $\lambda = \frac{4}{3}R$ and $\bar{v} = \left(\frac{8kT}{\pi m}\right)^{1/2}$ The resulting expression relating average phase shift with bulb radius, wall shift and temperature is

$$\bar{\phi}(T) = 5.78 \times 10^{-4} \frac{R}{T^{1/2}} \Delta\nu_w$$

The data are plotted in figure 2 in terms of average phase shift per wall collision. It is seen that the 4" and 7" quenched bulb data lie very nearly on the same straight line. The least squares fit on each set of points is as follows:

7" bulb.

$$\bar{\phi}_7(T) = -53.36 \pm 1.37 + (0.1503 \pm .004)T$$
$$= 0 \text{ at } 355°K$$

4" bulb

$$\bar{\phi}_4(T) = -56.53 \pm 1.5 + (0.159 \pm .005)T$$
$$= 0 \text{ at } 355.1°K.$$

The same 4" bulb was then annealed and data on it are shown in the same figure. Since we wanted to get data in time for the conference we did not have time to allow the bulb and cavity to come to thermal equilibrium and consequently the scatter is larger than for the previous data. We have for the 4" annealed bulb

$$\bar{\phi}_4(T) = -39.09 \pm 3.67 + (.0903 \pm .011)$$
$$= 0 \text{ at } 432.9°K.$$

In both cases the data excluded the 5 circled points in figure 2.

Summary of Data

Table 1 is a summary of these preliminary data and a comparison with other data.

It should be noted here that the Teflon 42 used in all the data shown in this table is from the same sample of Teflon 42 obtained by the Smithsonian Astrophysical Observatory from E.I. duPont de Nemours and Company on July 29, 1969. This sample, which was donated to SAO by duPont, is identified as Blend #8892, % solids 34.3. It should further be noted that the coating procedure used by Hellwig[3] was similar to the quenched procedure described above except for the very rapid cooling employed in the present experiment.

It is possible to extrapolate to zero wall shift from data shown in the "quenched" plot of Figure 2. By using the least square fit to a straight line for the 4" and 7" bulbs quenched data, recalculating the wall shift at 4 temperatures and plotting the results vs. the reciprocal of the bulb diameter one obtains the plot shown in Figure 3.

Figure 3 illustrates an interesting point and leads us to a new method of determining the wall shift. This figure is, in fact, a plot of wall shift versus collision rate. Collision rate depends on the bulb geometry and on the collimator geometry; the effect of the latter is still not well understood.

In making wall shift vs collision rate plots using several bulbs we make the following two assumptions:

1. That the walls of the two bulbs are exactly the same;

2. That we know the collision rate of the hydrogen atoms in each bulb.

The plot of wall shift vs 1/D at different temperatures shows us that the convergence point is not at 1/D = 0 but somewhere near 1/D = .008. Here the convergence is good and lies within 2 mHz of our calibration. Judging from the data it appears that we are making a consistent error in the prediction of the collision rate. However, if we use our knowledge of the temperature at which the observed wall shifts are equal we have no longer to depend on our knowledge of the collision rate. We depend only on the similarity of the teflon used in the two bulbs. The data is in the form

$$\nu(T) = \Delta\nu_e + \Delta\nu_w$$
$$= \Delta\nu_e + \left(\frac{2kT}{\pi^2 m}\right)^{1/2} \frac{\bar{\phi}(T)}{\lambda}$$

where $\Delta\nu_e$ is an unknown offset error and $\Delta\nu_\omega$ is the wall shift. λ is mean free path of atoms in the bulb and collimator. By changing λ, either by changing bulbs (or by using a deformable bulb as suggested by Brenner[5]) we see that the only condition making $\nu(T)$ the same for the two values of λ is to make $\bar{\phi}(T) = 0$.

To illustrate this technique we have reduced the data discussed earlier in a different way.

We find that

$$\frac{\nu(T)}{T^{1/2}} = \frac{\Delta\nu_e}{T^{1/2}} + \left(\frac{2k}{\pi^3 m}\right)^{1/2} \frac{\bar{\phi}(T)}{\lambda}$$

is quite linear with temperature when $\Delta\nu_e$ is small. For the two quenched PTFE bulbs, we have that

$$\frac{\nu_7(T)}{T^{1/2}} = \frac{\Delta\nu_e}{T^{1/2}} + \left(\frac{2k}{\pi^3 m}\right)^{1/2} \frac{\bar{\phi}_7(T)}{\lambda_7} = C_1 + \alpha_1 T \quad (1)$$

$$\frac{\nu_4(T)}{T^{1/2}} = \frac{\Delta\nu_e}{T^{1/2}} + \left(\frac{2k}{\pi^3 m}\right)^{1/2} \frac{\bar{\phi}_4(T)}{\lambda_4} = C_2 + \alpha_2 T \quad (2)$$

Under the assumption that $\Delta\nu_e$ is the same for both (1) and (2) and that

$$\bar{\phi}_7(T) = \bar{\phi}_4(T).$$

Crossover occurs where $\bar{\phi}(T) = 0$ at a temperature $T_0 = C_2 - C_1/\alpha_1 - \alpha_2$.

Recalculating the calibration error, we have

$$\Delta\nu_e = T_0^{1/2}(C_1 + \alpha_1 T_0)$$

From the same data used to plot Figure 2, we obtain a temperature of intercept of 355.3°K and a $\Delta\nu_e$(error) = 0.2 x 10^{-3} Hz.

Wall Relaxation

So far, we have made wall relaxation measurements only using 4" bulbs. Our results confirm the data obtained by Zitzewitz for PTFE. At temperatures up to 100°C we see no increase in wall relaxation rate. Relaxation rate measure-

ments are being continued at the Smithsonian Astrophysical Observatory using larger bulbs with very long bulb storage time.

Conclusions

(1) From the data taken so far we conclude that it is possible to operate a maser with its bulb at 355°K (82°C) and substantially reduce the wall shift and its contribution to the uncertainty of the maser output frequency.

(2) It is possible to eliminate the uncertainty due to collision rate in the determination of wall shift by measuring wall shift as a function of bulb temperature using several bulbs of different sizes.

References

(1) "Preliminary Report on the Temperature Dependence of the Wall Shift of the Hydrogen Maser for FEP and TFE-Teflon." Paul Zitzewitz, Harvard University, October 2. 1969.

(2) "Fluorine-Containing Polymers. II. Polytetrafluoroethylene." C.A. Sperati and H.W. Starkweather, Jr. Advances in Polymer Science, Springer-Verlag, Berlin 1961.

(3) "Measurement of the Unperturbed Hydrogen Hyperfine Transition Frequency." H. Hellwig, R. Vessot, M. Levine, P. Zitzewitz, H. Peters, D. Allan, D. Glaze. Conference on Precision Electromagnetic Measurements, Boulder, Colorado, June 1970.

(4) "The Design of an Atomic Hydrogen Maser System for Satellite Experiments." R. Vessot, M. Levine, L. Mueller and M. Baker. Proceedings of the 21st Annual Symposium on Frequency Control. U.S.A.E.C.O.M. Ft. Monmouth, N.J., April 1967.

(5) "Flexible Bulb Method of Measuring Wall Shift of the Hydrogen Maser." D. Brenner, Bull. Am. Phys. Soc. 14, 943 (1969).

Table I

Parameter	Present Data	Previous Data
		Zitzewitz 1964
Average phase shift Temperature	0.15 ± .004 Rad/°K P.T.F.E. quenched	0.1294
		0.1248
	0.09 ± .011 Rad/°K P.T.F.E. annealed	
Zero phase shift Temperature	355°K quenched	375°K
	433°K annealed	369°K
Wall Shift, K mHz Cm at 297°K	522 Hz-Cm	630.6 Hz-Cm
		640.7
		570.9
		544.8
		Hellwig 1970 528 Hz-Cm

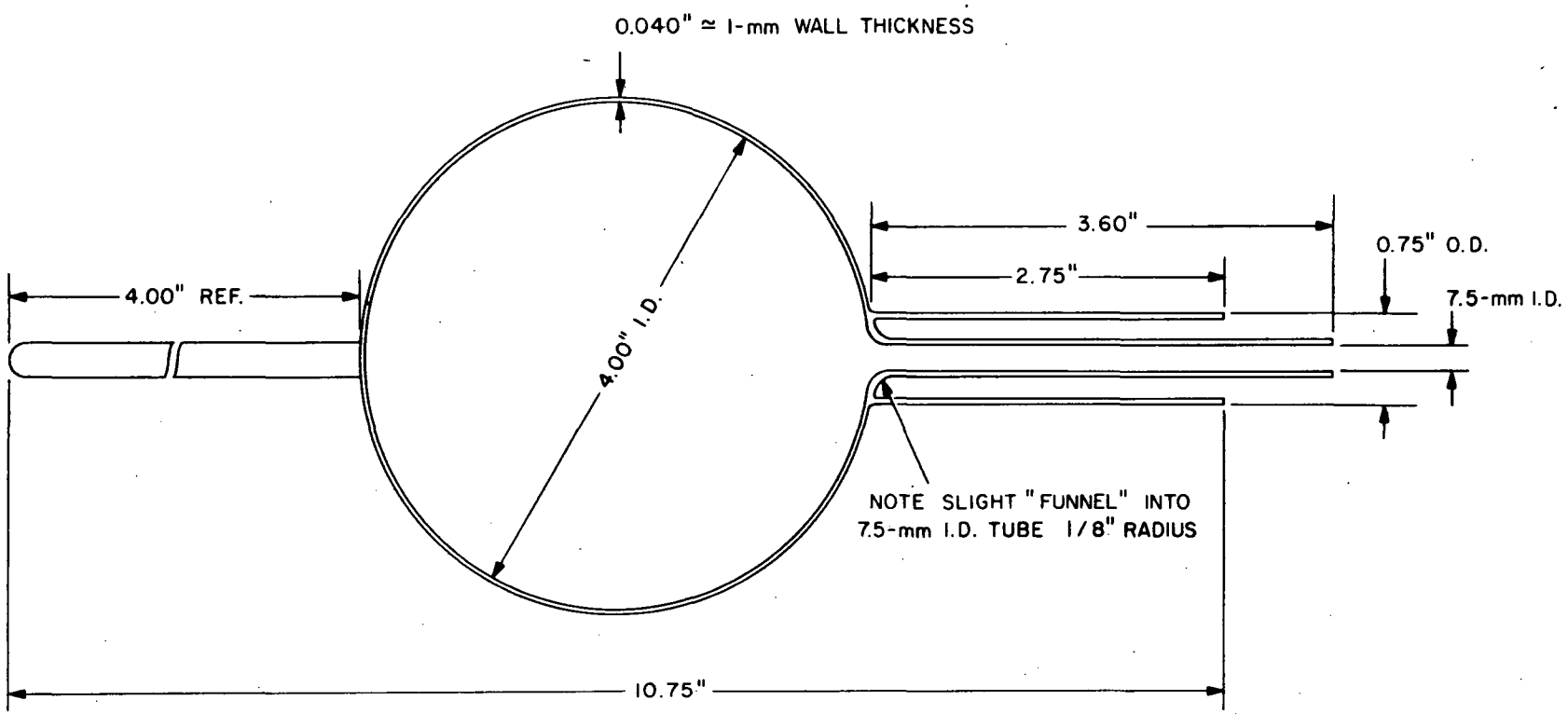

Figure 1 Four-in.-diameter fused silica storage bulb for wall-shift experiments.

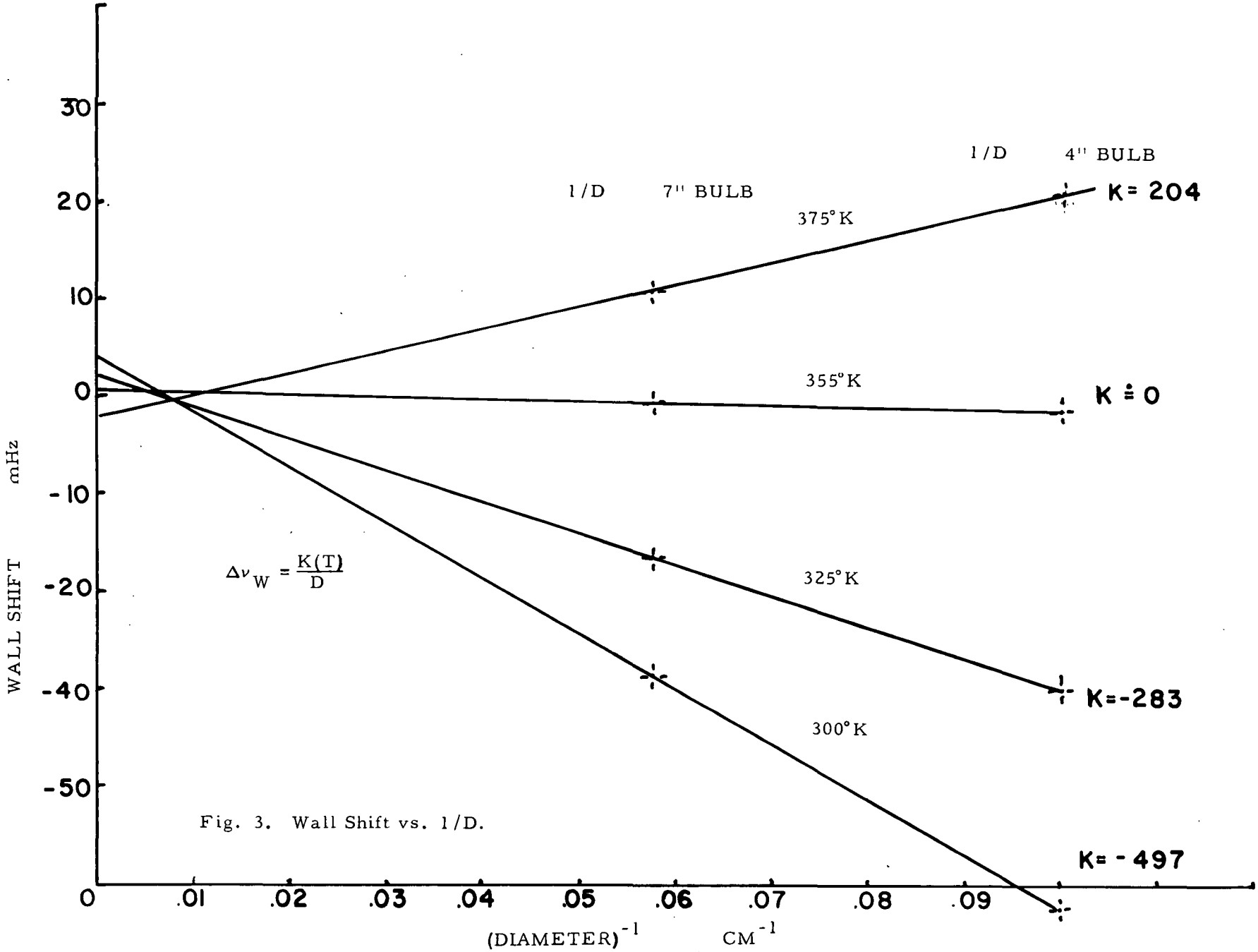

Fig. 3. Wall Shift vs. 1/D.

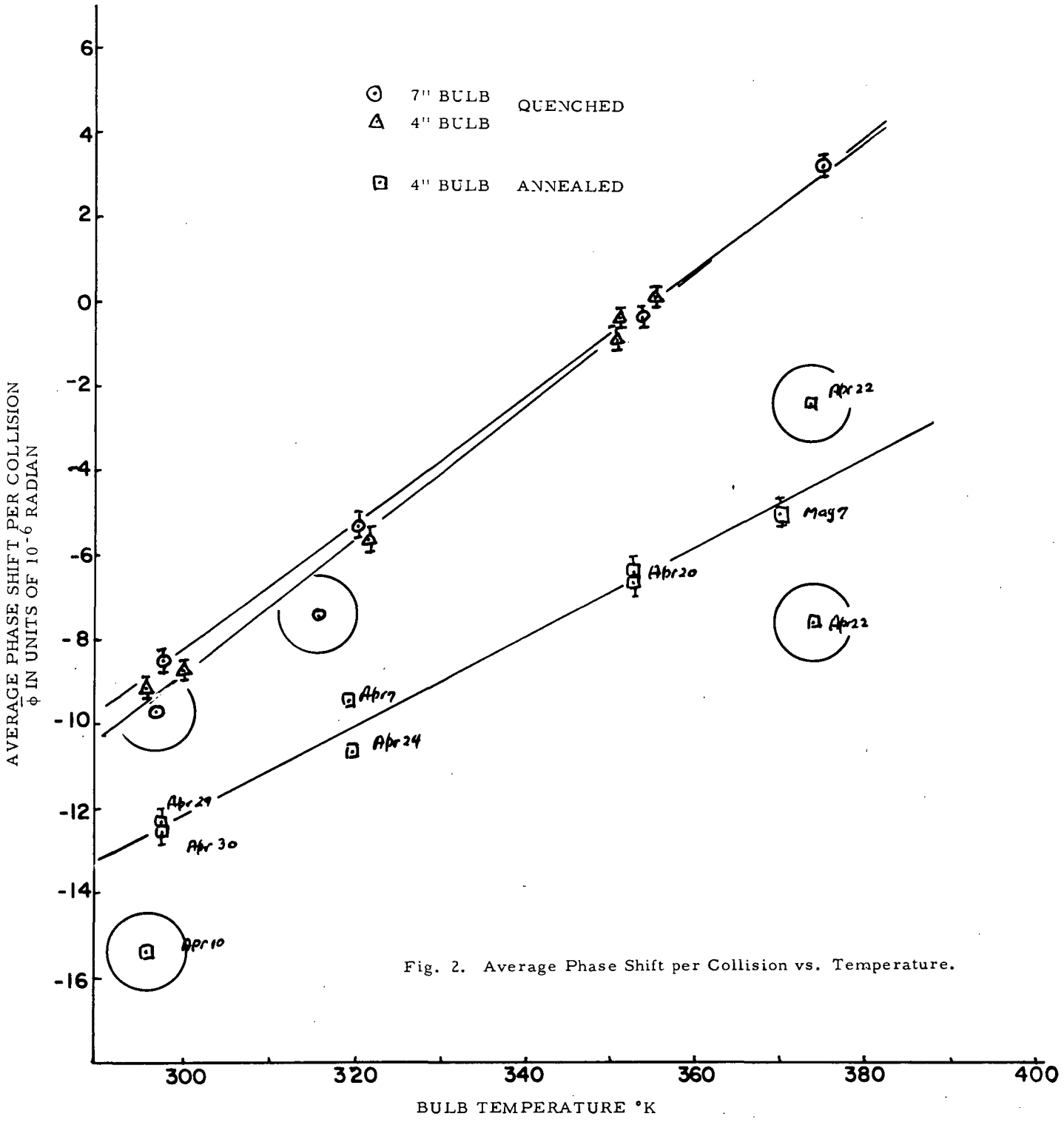

Fig. 2. Average Phase Shift per Collision vs. Temperature.

Offprint from "Metrologia"
Journal International de Métrologie scientifique — International Journal of Scientific Metrology
Internationale Zeitschrift für wissenschaftliche Metrologie. Vol. 6, No. 4, October 1970, Pages 116—117

A Method for Eliminating the Wall Shift in the Atomic Hydrogen Maser*

R. F. C. Vessot and M. W. Levine

Harvard College Observatory
and
Smithsonian Astrophysical Observatory,
Cambridge, Mass. USA

Abstract

The wall shift of the hydrogen maser depends on the collision rate and the average phase shift per collision of the atoms in the storage bulb. By operating at the temperature where the average phase shift per collision is zero it is possible to remove the wall shift. The determination of this temperature is made by measuring the wall shift as a function of temperature for two similarly coated bulbs offering different collision rates to the stored atoms. The intercept of the wall shift vs. temperature curve for the two bulbs occurs at the zero phase shift per collision temperature. To eliminate the possible differences in wall coatings the use of a flexible storage bulb is recommended.

An experimental example of the technique is given using two separate bulbs. The data is in good agreement with a previous measurement of the unperturbed hydrogen hyperfine frequency by H. Hellwig *et al.*

One of the most vexing problems affecting the accuracy of the output frequency of the atomic hydrogen maser is the shift in frequency due to collisions of the hydrogen atoms with the storage bulb walls (wall shift). This shift results from the deformation of the electron cloud of the hydrogen atom during the collision process and can be represented as an average advance or retard per collision of the phase of the oscillating magnetic dipole moment of the atom with respect to the phase of the r.f. magnetic field in the maser cavity.

The usual method of measuring wall shift [1] has been to coat a number of spherical storage bulbs of different diameters with the wall coating material and to measure the maser output frequency associated with each bulb.

Plotting the output frequency as a function of collision rate (inversely proportional to bulb diameter for spherical bulbs) and extrapolating to zero collision rate gives the zero wall shift output frequency of the maser.

The chief difficulties and uncertainties in making these measurements lie (1) in estimating the collision rate of the atoms in the bulb and (2) in the assumption that all the bulbs are similarly coated. Since the microscopic texture of the wall coating can affect the collision rate, these two uncertainties are not always independent. Furthermore, the effect of the bulb collimator on the collision rate is still not well understood.

Recent studies of wall shift versus temperature by Zitzewitz [2] and Vessot and Levine [3] have shown that there is a temperature dependence in the average phase shift per collision that goes from negative to positive values. In particular, there is a temperature at which the effect is zero. For polytetrafluoroethylene (PTFE, Du Pont Teflon 42) applied by rapid sintering and quenching, we have found that this temperature is about 82 °C.

We wish to report the following procedure for determining the zero wall shift frequency which eliminates the error due to the uncertainty in the collision rate.

The output frequency of the maser is measured over a range of temperatures usually from 23 °C to 150 °C using two bulbs providing substantially different collision rates that are coated in the same manner with the same material. (A better method might be to use a single bulb having a flexible wall allowing a change in volume without a change in surface, as suggested by Brenner [4]. This has the advantage of removing the uncertainty associated with the chemistry of the wall surfaces of two separate bulbs.)

The wall shift, $\Delta \nu_w (T)$ is given by $\Delta \nu_w (T) = \frac{\nu_c}{2\pi} \bar{\phi} (T)$ where ν_c is the collision rate and $\bar{\phi} (T)$ is the average phase shift per collision. In the case of spherical bulb, one can replace ν_c by $\frac{3\bar{v}}{4R}$ where $\bar{v} = \left(\frac{8kT}{\pi m}\right)^{1/2}$ is the average velocity of the atom, R is the bulb radius, k is the Boltzmann constant, m is the atomic mass, and T is the absolute temperature.

The only way that the output frequency of the maser can be made independent of collision rate is to make $\bar{\phi} (T)$ zero. If the output frequency of the maser is plotted against temperature under two (or more) different bulb diameters, or two different configurations of a flexible bulb, the intercept of the two plots will be at the zero wall shift maser output frequency.

We offer the following example of this technique applying it to two bulbs coated with PTFE, and quenched rapidly after sintering the coating. The wall shift data are taken in the form: $\nu (T) = \Delta \nu_c + \Delta \nu_w (T)$ where $\Delta \nu_c$ is the frequency difference between the two masers after application of the magnetic field, and second order Doppler corrections to both masers and a wall shift correction to the reference maser. $\Delta \nu_c$ is the residual offset of the reference oscillator, and $\Delta \nu_w (T)$ is the temperature dependent wall shift. Since the effect of the second order Doppler effect in the temperature varying maser has been accounted for, $\Delta \nu_c$ is a constant. When $\Delta \nu_c$ is small we find that

$$\frac{\nu (T)}{T^{1/2}} = \frac{\Delta \nu_c}{T^{1/2}} + \left(\frac{2kT}{\pi^3 m}\right)^{1/2} \frac{1}{T^{1/2}} \frac{\bar{\phi} (T)}{\lambda}$$

* This work is supported by the National Aeronautics and Space Administration under contract NSR-09-015-098.

where λ is the mean free path between collisions. The expression $\frac{\nu(T)}{T^{1/2}}$ varies approximately linearly with T, and thus calculation of the intercept is readily accomplished.

We have that for two different bulbs 1 and 2,

$$\frac{\nu_1(T)}{T^{1/2}} = \frac{\Delta\nu_e}{T^{1/2}} + \left(\frac{2k}{\pi^3 m}\right)^{1/2} \frac{\bar{\phi}_1(T)}{\lambda_1} = C_1 + \alpha_1 T \qquad (1)$$

and

$$\frac{\nu_2(T)}{T^{1/2}} = \frac{\Delta\nu_e}{T^{1/2}} + \left(\frac{2k}{\pi^3 m}\right)^{1/2} \frac{\bar{\phi}_2(T)}{\lambda_2} = C_2 + \alpha_2 T\,. \qquad (2)$$

If we assume that $\Delta\nu_e$ is the same for (1) and (2) and that $\bar{\phi}_1(T) = \bar{\phi}_2(T)$, cross-over occurs where $\bar{\phi}(T) = 0$, at a temperature $T_0 = \frac{C_2 - C_1}{\alpha_1 - \alpha_2}$.

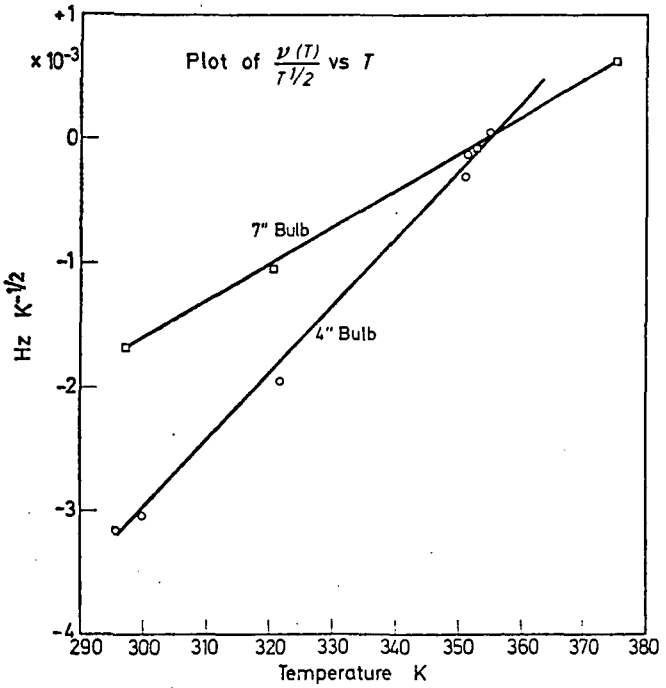

Fig. 1

We can thus determine the offset $\Delta\nu_e$,

$$\Delta\nu_e = T_0^{1/2}(C_1 + \alpha T_0)\,.$$

Fig. 1 shows the values of $\frac{\nu(T)}{T^{1/2}}$ plotted as a function of T for two bulbs of 18 and 10 cm diameter. The lines drawn are the least squares fit to the data. The temperature at which the lines cross is 355.28 ± 0.2 K and the value of $\nu(T)$ at the crossing point is $(0.2 \pm 1.1) \times 10^{-3}$ Hz.

The quantity $\nu(T)$ had been corrected for the following offsets in frequency:

1. Magnetic field effect for each maser.
2. The second 1 order Doppler effect for each maser.
3. The wall shift of the reference maser.

The first two corrections are well known functions of temperature and magnetic field [6]. However, considerable pains were taken to calibrate the wall shift of the reference maser. This work involved making direct frequency comparisons with wall shift determined at Harvard by Zitzewitz and at NBS by Hellwig by using a traveling maser frequency standard. From this determination the wall shift of the SAO reference was determined to be $-.0222 \pm .002$ Hz. (This maser is equipped with a 16.36 cm spherical bulb coated with DuPont FEP-120 teflon and operates at 45.5 °C.)

The value of ν_e derived from the crossing point of the lines in Fig. 1 is less than 0.2×10^{-3} Hz and provides a further, independent, confirmation for the value of the unperturbed hydrogen hyperfine frequency given in reference 1 as 1420405751.768 ± .003 Hz, with respect to the NBS III cesium standard.

Using our knowledge of the radius of the 18 and 10 cm bulbs and calculating the average phase shift per collision we obtain the following equations based on least squares fits to a straight line.

For the 18 cm bulb

$$\bar{\phi}_1(T) = -53.36 \pm 1.37 + (0.1503 \pm .004)\,T\,.$$

For the 10 cm bulb

$$\bar{\phi}_2(T) = -56.53 \pm 1.5 + (0.159 \pm .005)\,T\,.$$

The similarity of these two temperature functions gives us a measure of the similarity of the wall coatings in the two bulbs and allows us to make a measurement of the wall shift parameter $K(T)$ which is defined here as

$$\Delta\nu_w = \frac{K(T)}{D}\,.$$

At 297 K we obtain $K(T) = 522$ Hz · cm. Hellwig [1] obtains a value $K(T) = 528$ Hz · cm for the same PTFE Teflon and finds it to be consistent for a large number of bulbs. Note that a limitation on the measurement of K is due to the uncertainty in the effective diameter, D.

From these data we conclude the following:

1. That we can operate a maser with very small wall shift.

2. The zero wall shift temperature can be determined as the temperature at which variations in collision rate have no effect on the output frequency. A flexible bulb maser is ideal for this determination since the question of the similarity of the chemical nature of the walls of two or more separate bulbs is eliminated.

3. High molecular weight polytetrafluoroethylene homopolymer (PTFE) may be a more reproducible wall coating material than the tetrafluoroethylene-hexafluoropropylene co-polymer (FEP) that is most often used as a maser wall coating material.

4. The present data confirm the unperturbed hydrogen hyperfine frequency given in reference [1] by Hellwig *et al.*

References

1. Hellwig, H., Vessot, R. F. C., Levine, M. W., Zitzewitz, P. W., Allan, D. W., Glaze, D. J.: IEEE Trans. Instr. Meas., (in press).
2. Zitzewitz, P. W., Uzgiris, E. E., Ramsey, N. F.: Rev. Sci. Instr. **41** (1970).
3. Vessot, R. F. C., Levine, M. W.: Proc. 24th Annual Symposium on Frequency Control, U.S. Army Electronics Command, Ft. Monmouth, N.J.
4. Brenner, D.: Bull. Am. Phys. Soc. **14**, 943 (1969).
5. Kleppner, D., Berg, H. C., Crampton, S. B., Ramsey, N. F., Vessot, R., Peters, H. E., Vanier, J.: Phys. Rev. **138**, A 972 (1965).
6. Vessot, R., Peters, H., Vanier, J., Beehler, R., Halford, D., Harrach, R., Allan, D., Glaze, D., Snyder, C., Barnes, J., Cutler, L., Bodily, L.: IEEE Trans. Instr. Meas. **IM-15**, 165 (1966).

INVENTION DISCLOSURE

To the attention of the NASA Patent Department:

The herein described invention is submitted in pursuance of Contract NSR 09-015-098.

The invention relates to the Atomic Hydrogen Maser Frequency Standard.

The purpose of the invention is to remove the effect of the shift in the maser output frequency resulting from the collisions of the hydrogen atoms with the storage bulb walls.

Brief Description

Recent work on bulb coatings by Zitzewitz at Harvard and by Vessot & Levine at Smithsonian Astrophysical Observatory have shown that there is a temperature at which the wall shift crosses through zero from negative values to positive values as temperature is increased. More recently (see appended preprint of paper to be published in the Proceedings of the 24th Annual Symposium on Frequency Control, USAECOM, Fort Monmouth, N. J.). Vessot & Levine show that there is a lower temperature zero wall shift point than that found by Zitzewitz and they prove that this zero wall shift point is independent of the collision rate of the atoms in the bulb.

This forms the basis for the invention when combined with D. Brenner's idea (see reference in appended preprint) of using a flexible bulb. A servo system is used to keep the temperature of the maser bulb at a value where no change in frequency is observed or changing the collision rate by flexing the bulb so as to change its surface to volume ratio.

The diagram shown as fig. (1) describes the servo system. The cycling timer moves the bulb's flexible end in and out, say, every 5 minutes. The frequency of the maser output is measured when the bulb is at low volume and compared automatically with the frequency obtained when the bulb is at high volume. The frequency difference is used to control the temperature of the bulb. If the bulb is too cold the frequency difference Δf (high vol.-low vol.) is positive. If the bulb is too hot the frequency difference is negative. Figure (2) shows the wall shift vs. temperature as a function of the bulb in its two positions.

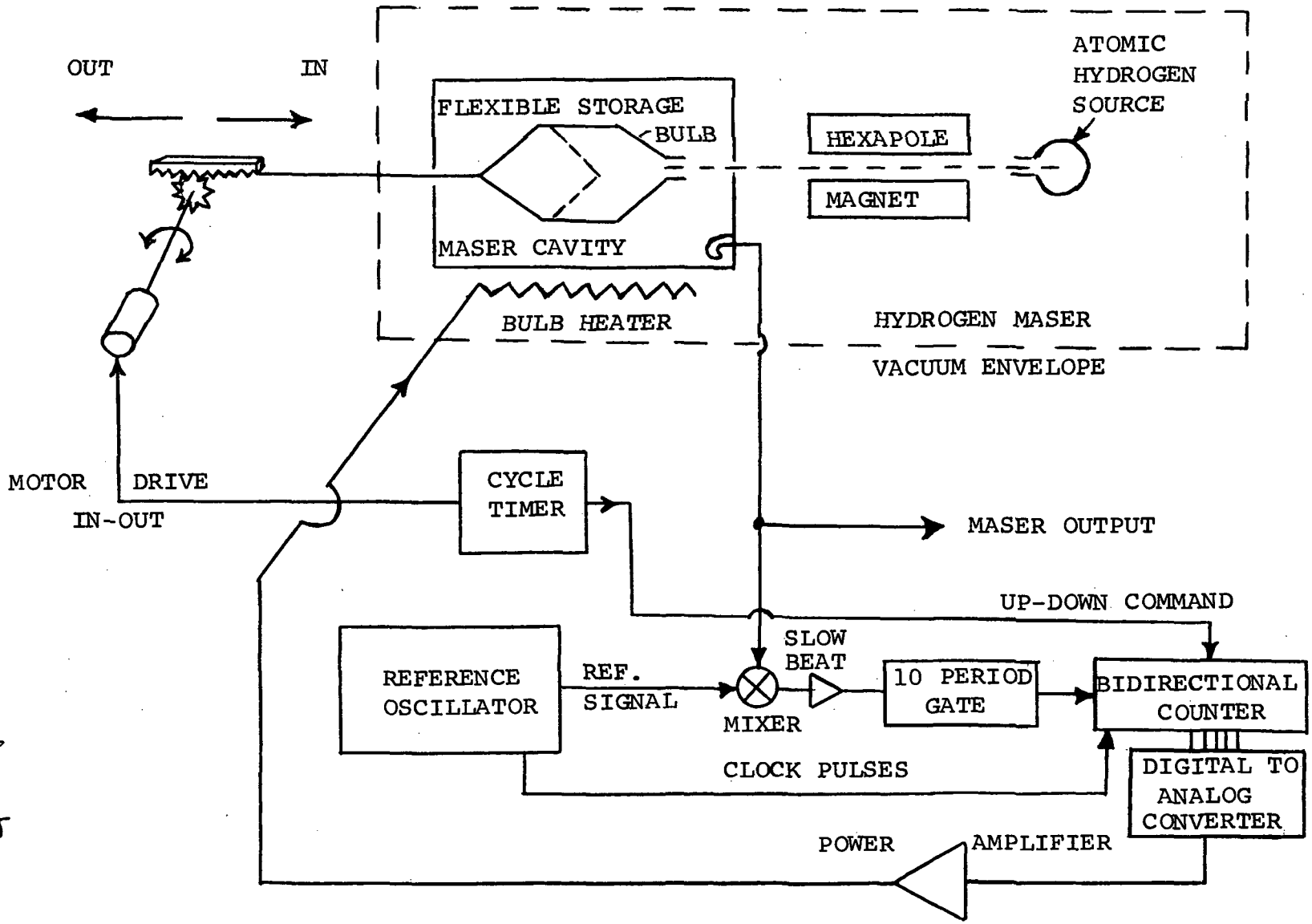
OUT
IN
FLEXIBLE STORAGE BULB
ATOMIC HYDROGEN SOURCE
HEXAPOLE
MAGNET
MASER CAVITY
BULB HEATER
HYDROGEN MASER VACUUM ENVELOPE
MOTOR DRIVE IN-OUT
CYCLE TIMER
MASER OUTPUT
UP-DOWN COMMAND
REFERENCE OSCILLATOR
REF. SIGNAL
SLOW BEAT
MIXER
10 PERIOD GATE
BIDIRECTIONAL COUNTER
CLOCK PULSES
DIGITAL TO ANALOG CONVERTER
POWER AMPLIFIER

FIGURE 1

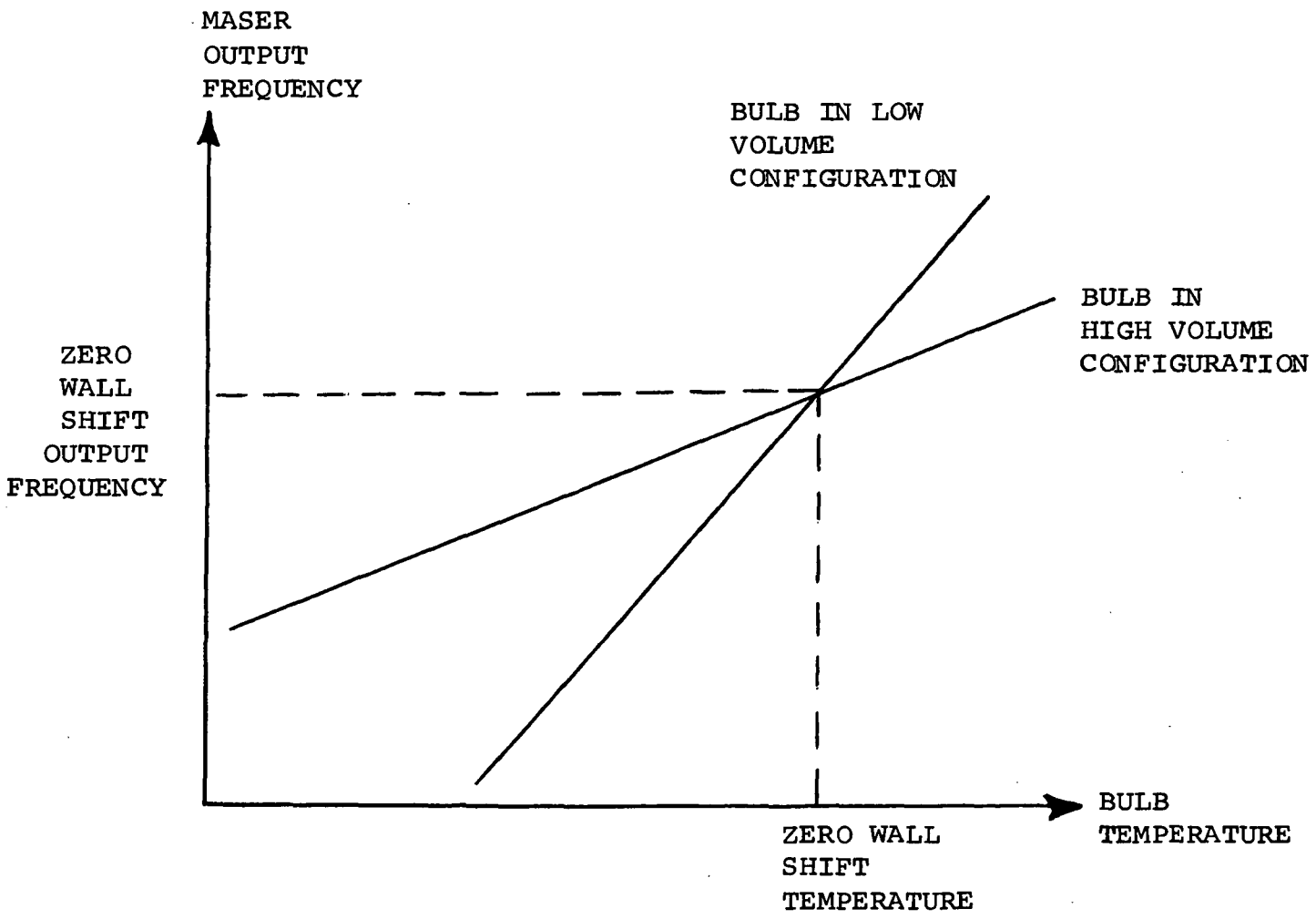

FIGURE 2

R Verrot
June 1, 1970

A good way to implement this servo technique is by using a bidirectional counter to measure the period of a fixed number, (say 10), of cycles of the slow heat between the maser and the tuning reference. The beat signal operates a gate that allows a number of steady "clock" pulses to be counted by the bidirectional counter. The number of these pulses will depend on the frequency of the beat signal. When the bulb is in its low volume configuration the bidirectional counter will count "up" when the gate is open during 10 cycles of the beat. The bulb is then changed to high volume and the pulses are again gated for 10 cycles, this time the counter counts "down". The residue in the counter is a measure of the frequency shift between the high and low bulb volume configuration and can be used to operate a digital-to-analog device controlling the bulb temperature.

In this system the motion of the bulb will affect the tuning of the maser cavity "pulling" the frequency of the maser. This effect will be taken out by the use of the automatic cavity tuning servo system invented by Vessot & Levine ("Automatic Tuning of Hydrogen Masers" - NASA Tech Brief 69-10452). The cavity mistuning due to the bulb motion can be programmed out by using pre-set tuning points at the two bulb positions.

By the use of the temperature tuning servo the effect of the frequency shift due to wall collisions can be eliminated.

This invention was conceived on April 20, 1970. First entry and sketches were made on May 27, 1970, in notebook of R.F.C. Vessot, Smithsonian Astrophysical Observatory - Used from October 20, 1969.

This disclosure is written June 1, 1970.

R. Vessot
334 Ocean Avenue, Marblehead, Mass.

M. Levine
Big Rock Road, Manchester, Mass.

This invention was explained by the above identified inventors to me and understood on June 1, 1970.

Signature of Witness

Date of Signature

5. TASK IV

5.1 Pump and Dissociator Assembly

With parts transferred to Contract NSR 09-015-098 from the original NASA Contract NASW 1337 with Varian Associates, the small-maser pump section, including the r.f. dissociator hexapole state selector and the gas-handling system, was assembled and tested under simulated operating conditions; a copper oxide target at the position of the bulb collimator verified the alignment of the atomic hydrogen beam. The lightweight pump with its reduced magnetic field operated successfully; the target showed clearly that the alignment of the magnet and its stopping disk is satisfactory.

5.2 CER-VIT Cavity Design

A significant innovation in this task was a new design of the CER-VIT cavity resonator for the maser. The original resonator was constructed of five pieces of CER-VIT clamped together with sufficient force to withstand the "g" loading effected by launching the maser into a 24-hr orbit with a Titan 3C booster. Although this design survived sine-sweep testing on three axes at the levels prescribed by NASA, the cavity was difficult to tune and delicate to assemble. A new design simpler in concept was deemed necessary.

An invention disclosure, which has subsequently been written up as a patent application, has been filed by NASA. It describes in detail the cavity and its mounting system and is reproduced at the end of this section.

5.3 Assembly of Maser Oscillator

The maser was completely assembled, as shown in Figure 1. Before assembly, the r.f. cavity-bulb subassembly was cold-tested and checked for tuning, with a helium-filled enclosure to simulate the dielectric qualities of vacuum. Tests were conducted of the r.f. system by means of the 0.070" coaxial r.f. lines to be used in

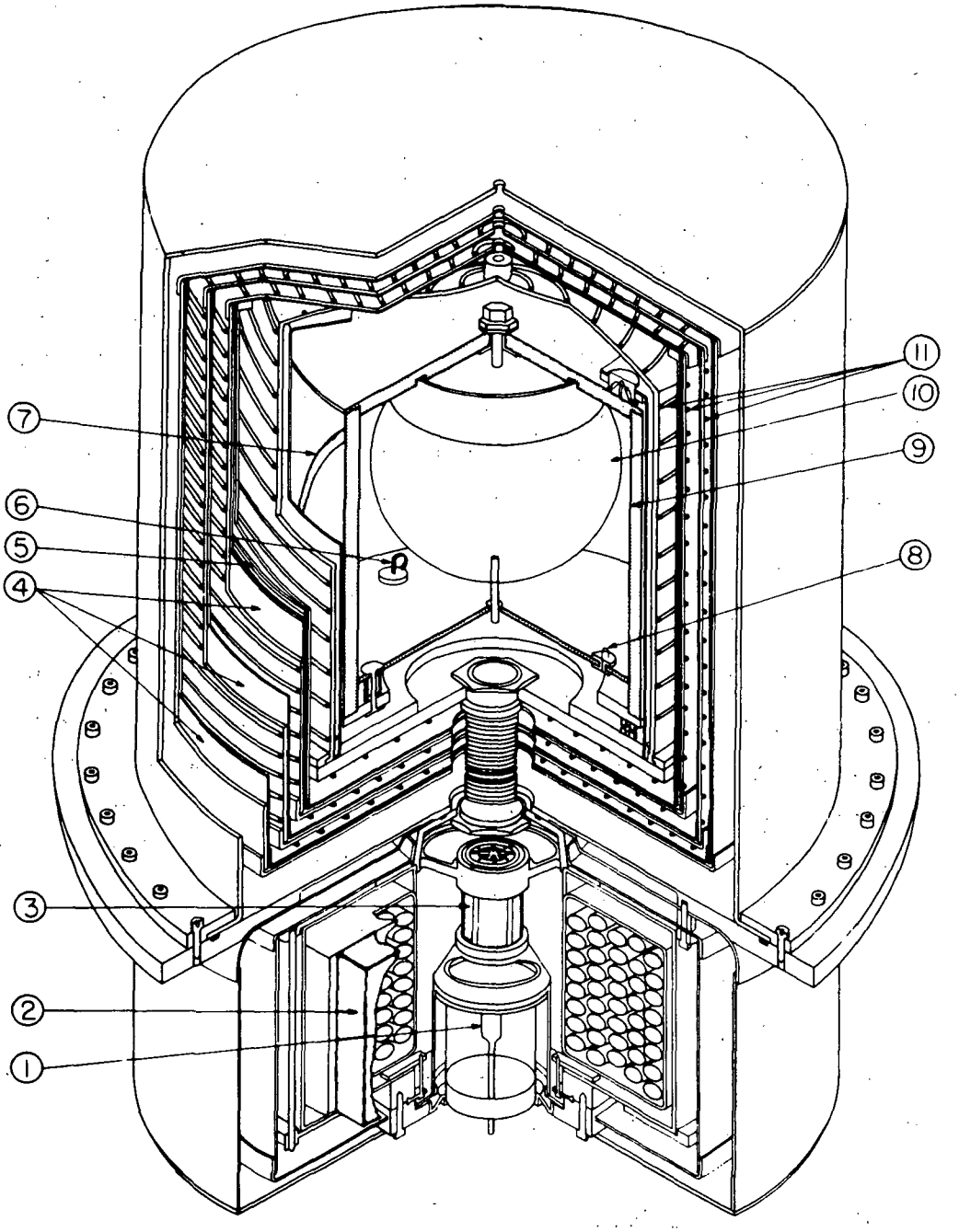

Figure 1. Hydrogen maser. Item 1, r.f. discharge tube; item 2, ion pump; item 3, hexapole magnet; item 4, magnetic shield; item 5, solenoid; item 6, tuning loop; item 7, low-frequency transition coil; item 8, output coupling loop; item 9, cavity structure; item 10, quartz storage bulb; item 11, oven heaters.

the maser. The cavity was then placed on the bell-jar base and fastened with 90 lb of preload from three springs at the top of a canister that enclosed the cavity and connected it in compression to the bell-jar base.

Three 0.070" copper coaxial lines, one each leading to the coupling loop, the tuning diode, and the transverse r.f. coil (Zeeman coil), were fastened in good thermal contact with (but electrically insulated from) the neck heat station. This heat station lies midway between the pump and the bell-jar base, which are connected with phosphorus bronze bellows. The heat station is equipped with two thermistor sensors, one thermocouple, and, of course, a heater winding. A second heat station was installed at the end of the pump nearest the neck; it consists of a heater, a thermocouple, and a thermistor. We believe that, with the thermal control on the jar and with a single oven surrounding the jar, plus the two-stage control on the neck, the temperature of the cavity system can be controlled with a stability of $\pm 0.01°C$ over changes in ambient temperature of $\pm 10°C$. With the present fused-silica cavity, the frequency change resulting from a temperature variation of $0.01°C$ is about ± 5 Hz. The resultant pulling of the output frequency, assuming a ratio of cavity Q to line Q of 2×10^{-5}, is about 7 parts in 10^{14}.

The atomic hydrogen source, hexapole magnet, and beam stop were separately assembled to test the alignment of the beam. The cavity bell-jar base and neck assembly were joined to the bell-jar assembly, which had been previously made into a single potted unit including all the oven solenoids and magnetic shields. The oven and shield canisters were closed layer by layer over the bell-jar base. Each oven and shield canister in the potted assembly was insulated electrically to prevent thermoelectric currents that would cause magnetic-field gradients. The final end cap enclosing the nested assembly consists of a layer of moly-permalloy to ensure that the magnetic fields from the pump and hexapole magnet are well isolated from the three-layer magnetic shield enclosing the cavity. The wires leading to the solenoid, three ovens, and neck were all brought out together near, but not touching, the neck and led to a groove in the main mounting plate to which the cavity-oven-shield assembly is bolted.

This plate, with the maser neck protruding through, was then mounted. Again, all cables were led to the same location on the mounting plate. The neck vacuum joint was secured to the pump, and the hexapole atom-source assembly was placed in the pump.

The main vacuum flange serves as an aligning jig for the hexapole magnet. When secured, it provides about 100-lb pressure on the stacked array by deforming a large Beleville spring. The maser r.f. discharge electronics were then installed, along with the newly designed pressure-control system. Finally, the magnetic-shield caps were installed, thus completely enclosing the pump.

The redesigned gas-handling system includes a gas cylinder, a pressure gauge, and a valve; it is mounted to the main vacuum flange. Hydrogen at 1000 psi is led to the palladium valve. The cylinder and gas-handling system extends 2" from the main vacuum flange and remains within the diameter of the outer pump magnetic shield.

5.4 Electronics

The thermal controllers differ from previous practice in three respects:

A. Standardized thermistors are used as oven sensors, eliminating the need for adjustment potentiometers for setting the oven temperatures. The thermistor R-T curves are predictable to within $\pm 0.5°C$, so that the bridge resistors can be preselected for a given oven temperature. Since no temperature trimming is required, the reference resistors can be mounted inside the thermally controlled enclosure. This technique eliminates the resistor temperature coefficients and thermal EMF as a source of thermal drift.

B. Very low-drift operational amplifiers are used to sense the resistance changes of the oven thermistors. The amplifier circuitry is designed to reduce the temperature variations associated with input-voltage offset to insignificant proportions, so that temperature control of the electronic environment is not necessary. One oven and its associated electronics and power supplies are eliminated, and the mechanical layout and the accessibility for maintenance of the electronics are greatly simplified.

C. Pulse-duration controllers are used on the outer ovens to increase overall efficiency and reduce power dissipation in the output transistors. The pulse-duration controller can supply up to 50 w to the outer oven, with a maximum transistor dissipation of 2.5 w. This very low-power dissipation permits the use of ordinary techniques for mounting printed-circuit boards, without any necessity for massive heat sinks.

The pressure controller is a distinct departure from past practices in that temperature-compensation techniques will be used to eliminate the Pirani block oven. Two carefully matched thermistors, one exposed to hydrogen flow and the other in vacuum, will be used in a special self-balancing bridge configuration to minimize the effect of ambient temperature changes on the pressure sensor.

The magnetic-field controllers for the masers are factory-assembled digital Kelvin-Varley voltage dividers. The overall voltage-temperature coefficient of this circuitry is sufficiently low that temperature stabilization is not necessary.

A high-efficiency switching controller supplies 15 w to the bell-jar heater, with a total power dissipation of approximately 2 w. No heat sinks are required, and all controller components are located on the same chassis; thus, many of the interconnecting cables formerly required are now eliminated. The thermistor resistance changes are sensed by very low-drift operational amplifiers, which require no ambient temperature control over the normal variations of room temperature (± 10°C). Figure 2 is a circuit diagram of the switching controller.

The pressure controller is an extremely stable, temperature-compensated Pirani gauge. One thermistor senses the hydrogen gas flow; a second is pumped directly by the ion pump but is in thermal equilibrium with the gas sensor. The second thermistor controls the "automatic vacuum zero" circuit shown in Figure 3. The new pressure control does not require a temperature-controlled environment and has been operating with good stability over normal room-temperature fluctuations.

The maser is connected to all its controllers – thermal, pressure, field, source, and varactor – through a single connector. The cabling has been designed for simplicity and ease of maintenance; a complete wiring diagram for the thermal control assembly is shown in Figure 4.

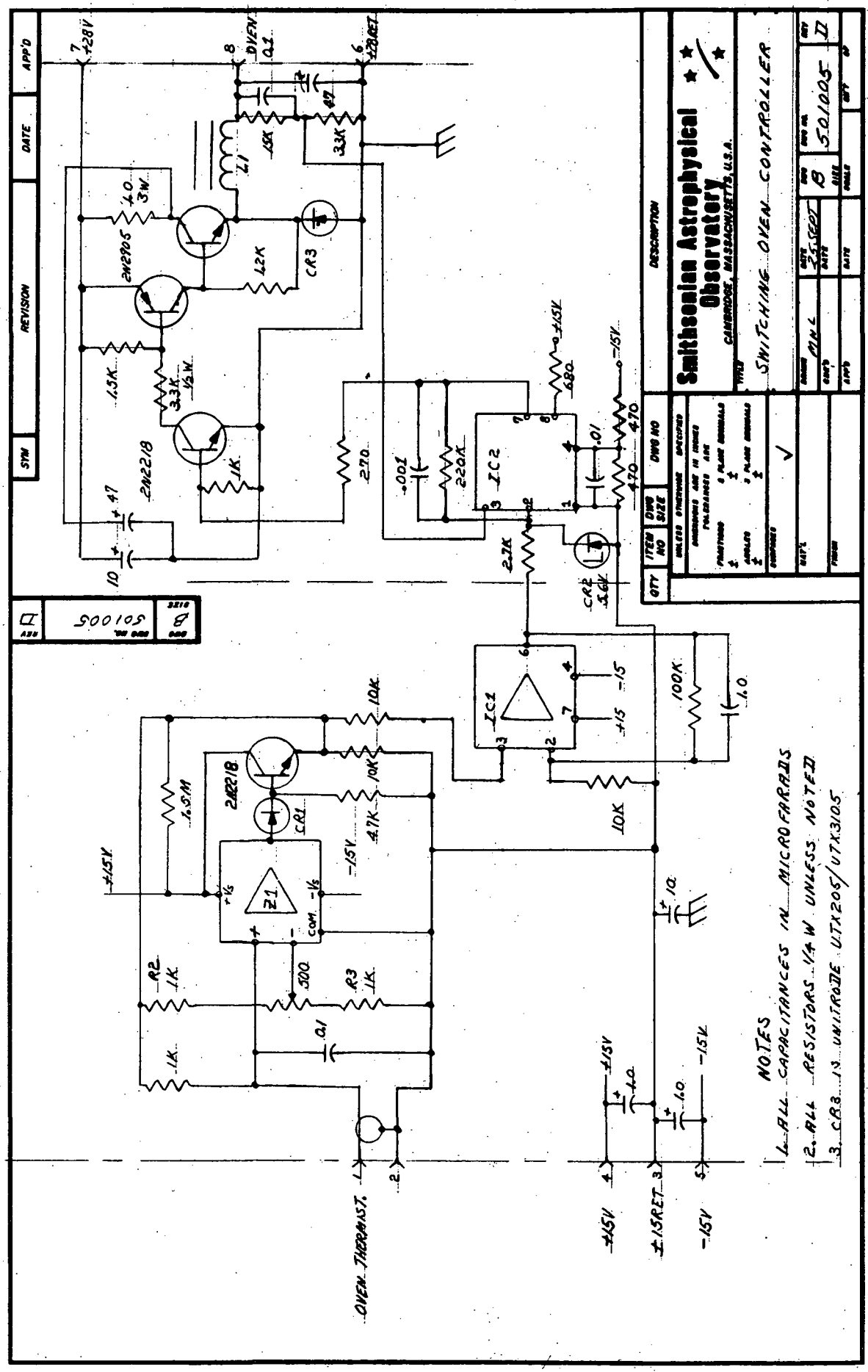

Figure 2. Switching oven controller.

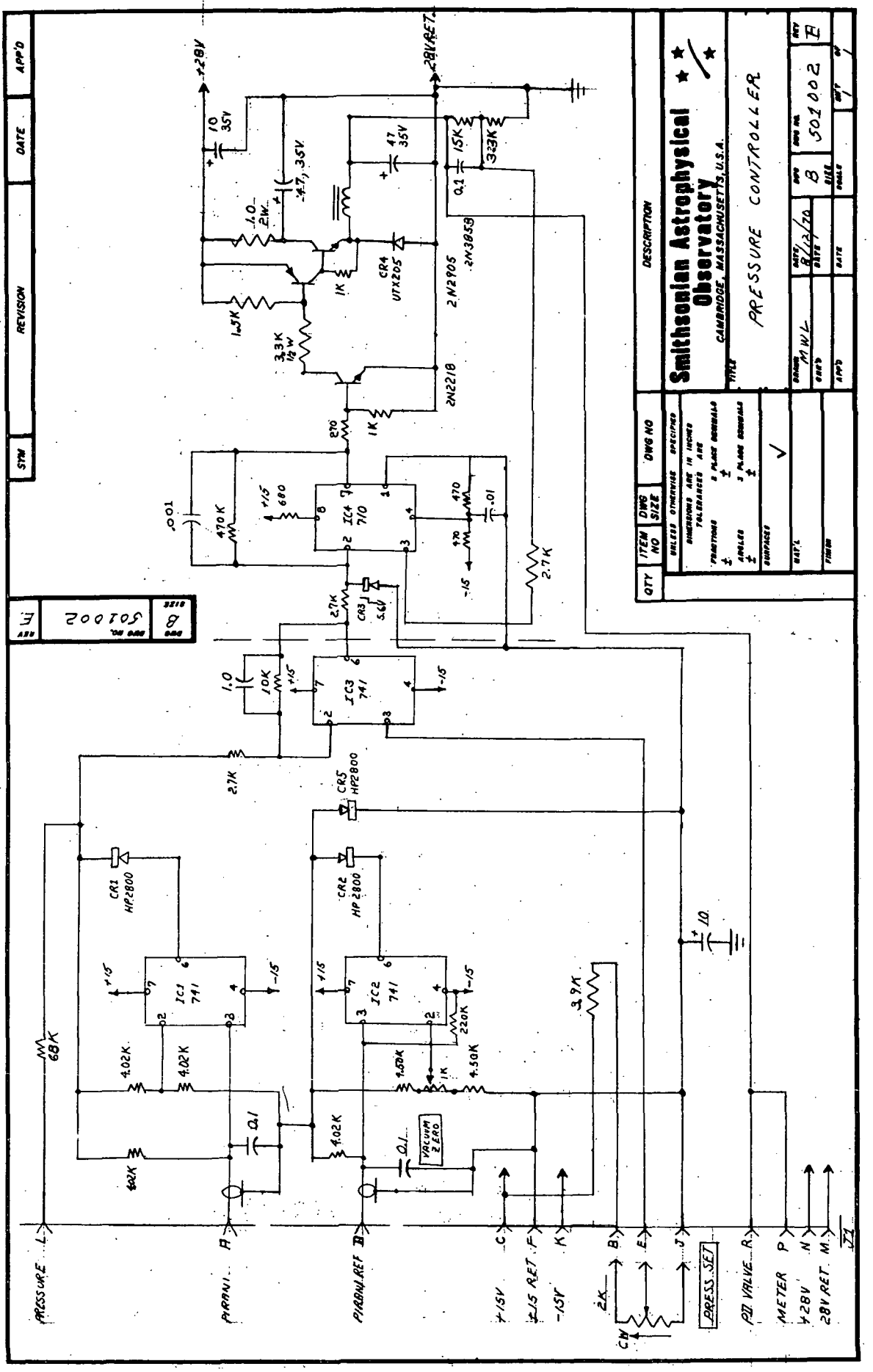

Figure 3. Pressure controller.

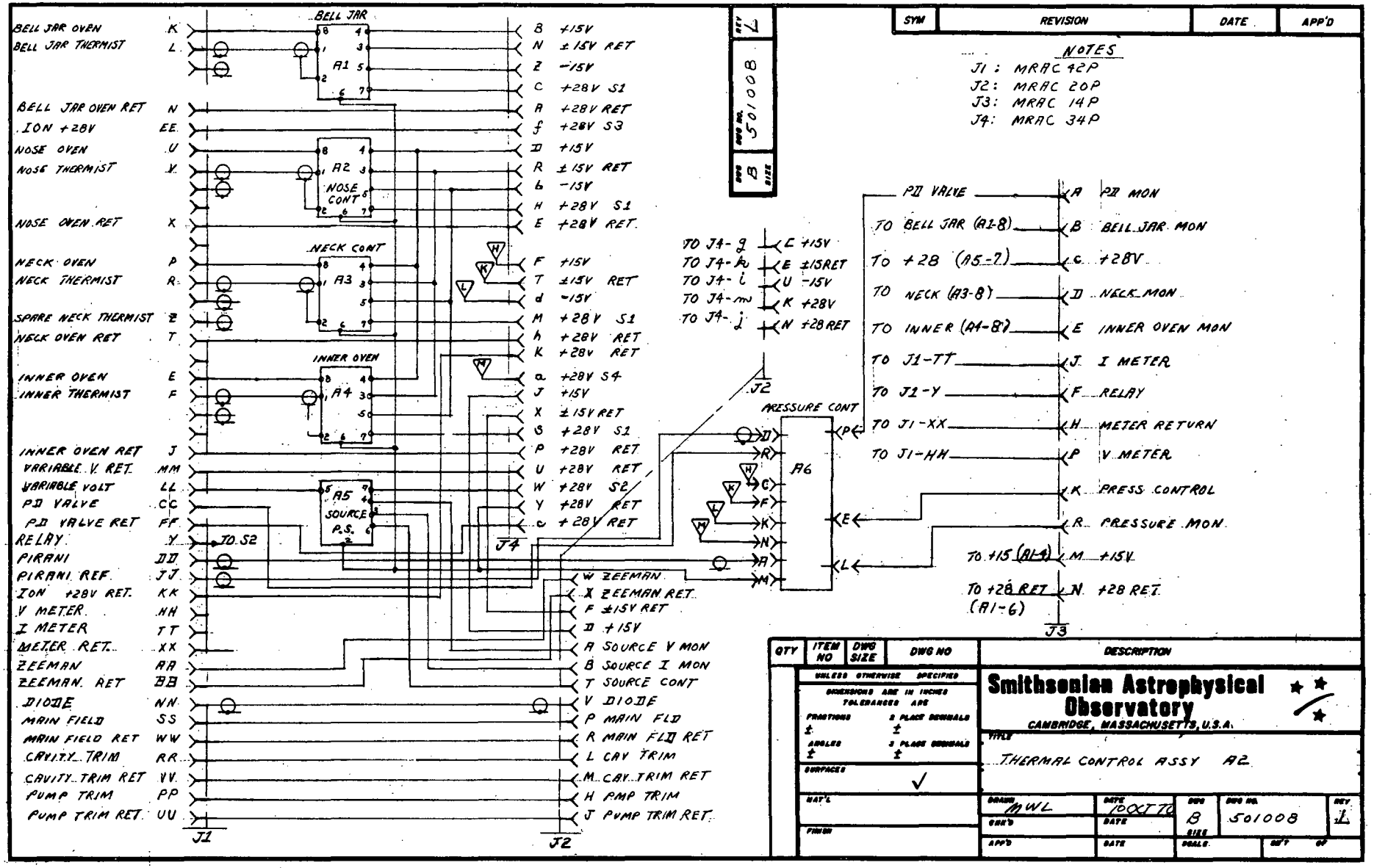

Figure 4. Thermal and pressure control assembly.

5.5 Tests of Frequency Stability

Results of the short-term frequency stability between the new maser package and the small maser formerly built for NASA under Contract NAS 8-2604 are shown in Figure 5. These data were obtained by locking a 5-MHz oscillator to the NAS 8-2604 maser by means of a conventional receiver system consisting of a multiplier to 1400 MHz and a double heterodyne first to 20.405 MHz and then to 0.405 MHz. The final phase-detection and phase-correction signal to the crystal oscillator was obtained by phase comparison with a digital synthesizer at 405794.3 Hz. This puts the maser time scale very close to universal time (UT).

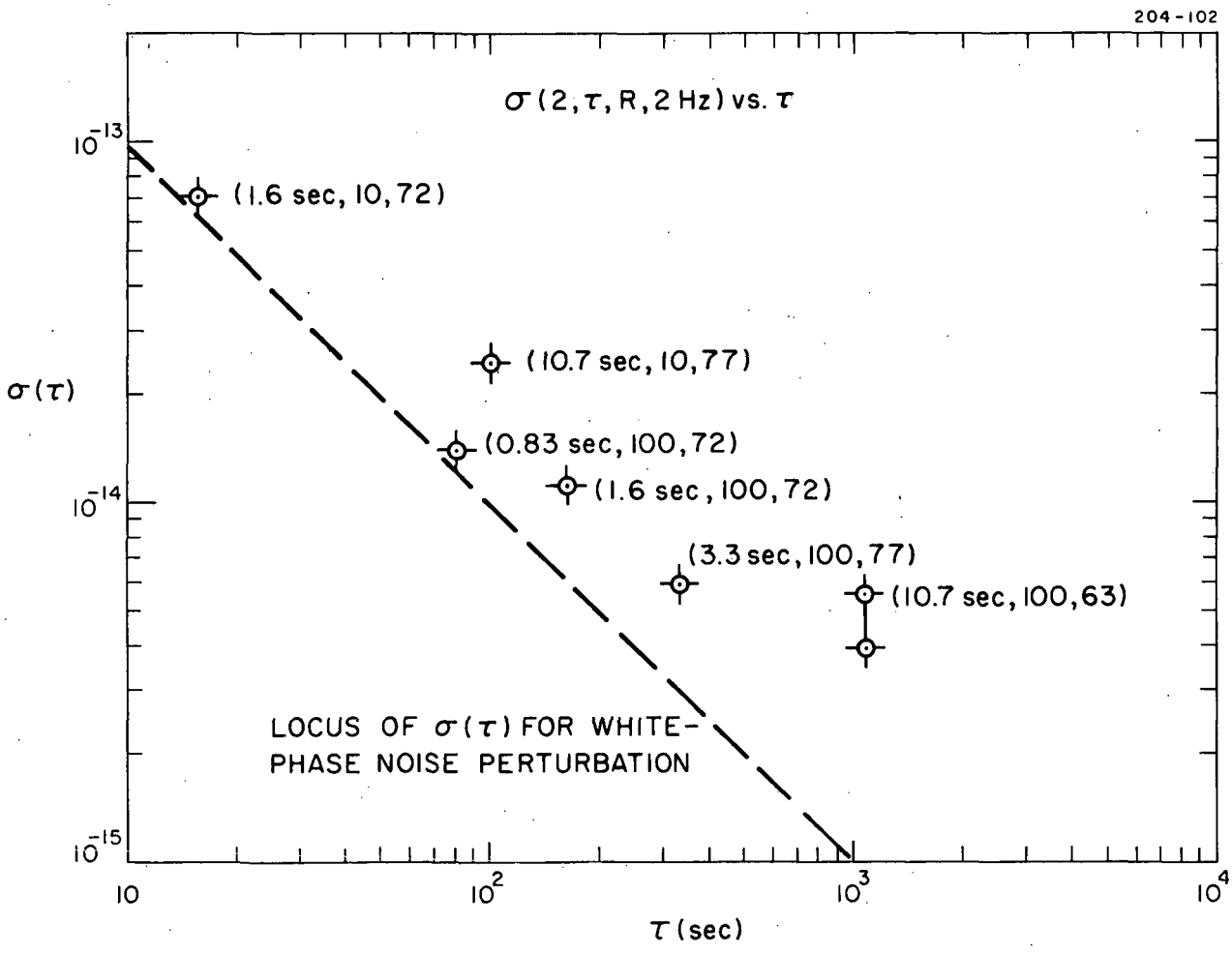

Figure 5. Stability (two-sample variance) versus averaging time τ of new NASA maser system. The data have been normalized to one system. The data points show the beat period, the number of beat periods per reading, and the number of readings required to estimate σ.

The 5-MHz signal is then led to the new receiver, which employs a different system to obtain a 1400-MHz local-oscillator signal.

The primary power for the maser is +28 v DC to permit operation on standby battery supplies. Two DC-DC converters are required for this mode of operation. The first, to supply ±15 v, will be purchased from Arnold Magnetics. The second converter is to provide 2500 v for the ion pump.

A converter to supply 2500 v for the ion pumps has been constructed. At the normal maser operating pressure, the converter requires 28-v output at 0.8 Å, so that a standby battery can be used to provide pump power in the event of AC power failure. The converter is extremely compact; all the circuitry is enclosed in a shielded housing 7" × 4" × 2".

5.6 Phase-Lock Receiver

Figure 6 is a block diagram of the receiver, showing all major subassemblies. This receiver differs from earlier designs in that the source for the 1400-MHz first local oscillator is a transistor oscillator phase-locked to the 5-MHz precision quartz-crystal oscillator. The previous receiver designs used frequency multipliers to generate 1400 MHz from 5 MHz; these multipliers have been shown to be a source of phase noise and phase drift. The subsystems, less the crystal oscillator and synthesizer, are housed in a shielded aluminum box 12" × 17" × 4", which can be installed within the maser cabinet.

To make the maser comparison and to evaluate the new receiver, the maser phase-lock loop was opened (see "tune" position in Figure 6). The digital synthesizer was offset to produce a beat signal, which was fed to a counter and printer. Several combinations of frequency offset and averaging times were used; the data points in Figure 5 show the beat period, the number of periods per reading, and the number of readings used for the statistics. The data to 300 sec roughly follow a $1/\tau$ behavior, indicating, as expected, that the dominating noise process is additive white-phase noise. Some indication of flattening out is observed at 1000 sec; this is due to systematic effects.

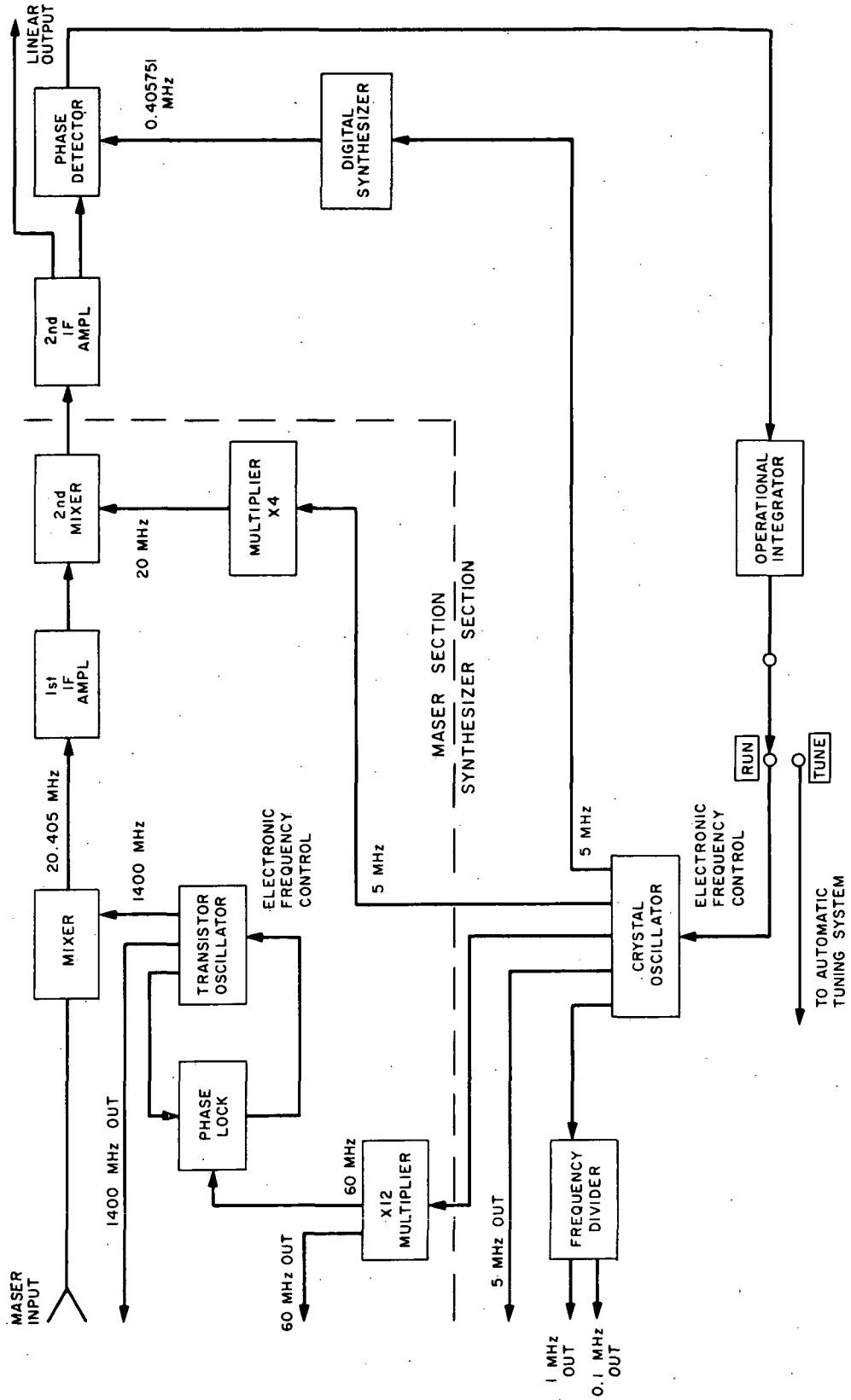

Figure 6. Phase-lock receiver.

The data are remarkably good and show that the receiver-synthesizer is at least as good as any other system yet tried. Two such receiver systems will be required to obtain more definitive data. Considering that there are two multiplier chains from 5 to 1400 MHz and two digital synthesizers in the system, we can only conclude that for averaging times to 1000 sec, this system is at least comparable in stability to the existing NAS 8-2604 maser system. We believe that the data point (taken twice) at 1000 sec may be a new low bound for instability measurements between masers.

In testing the maser, we found some real weaknesses in the magnetic shields. These shields are 6 years old and have been reused many times in different configurations of the maser. No doubt they have suffered work-hardening and should be reannealed or replaced. This problem is not apparent in the SM-1 maser, which has not been disassembled dozens of times, as has the present one.

The maser is still equipped with a fused-silica cavity. Since the new CER-VIT cavity was not obtained in time for assembly in this maser, it will be tested in a subsequent contract.

The packaging of the maser into a single cabinet is shown in Figures 7a, b, and c. Additional space in the cabinet is available for a digital synthesizer and a 5-MHz oscillator. The base of the cabinet has room for a battery supply that could operate the maser for about 4 hr. With the addition of the digital synthesizer, oscillator, and batteries, this maser system can be a completely self-contained source of highly stable signals at 5, 60, and 1400 MHz.

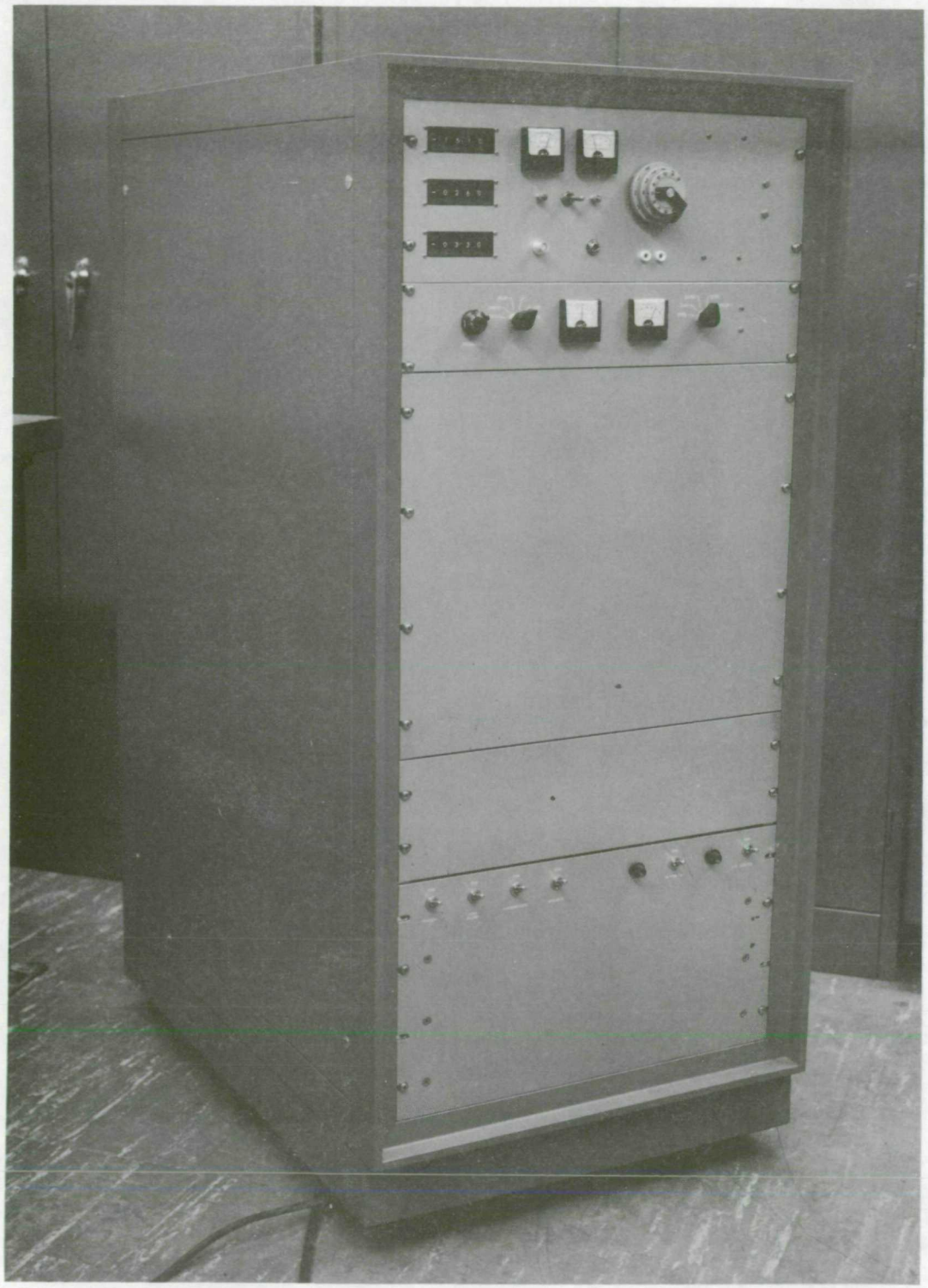

Figure 7a. Packaged maser.

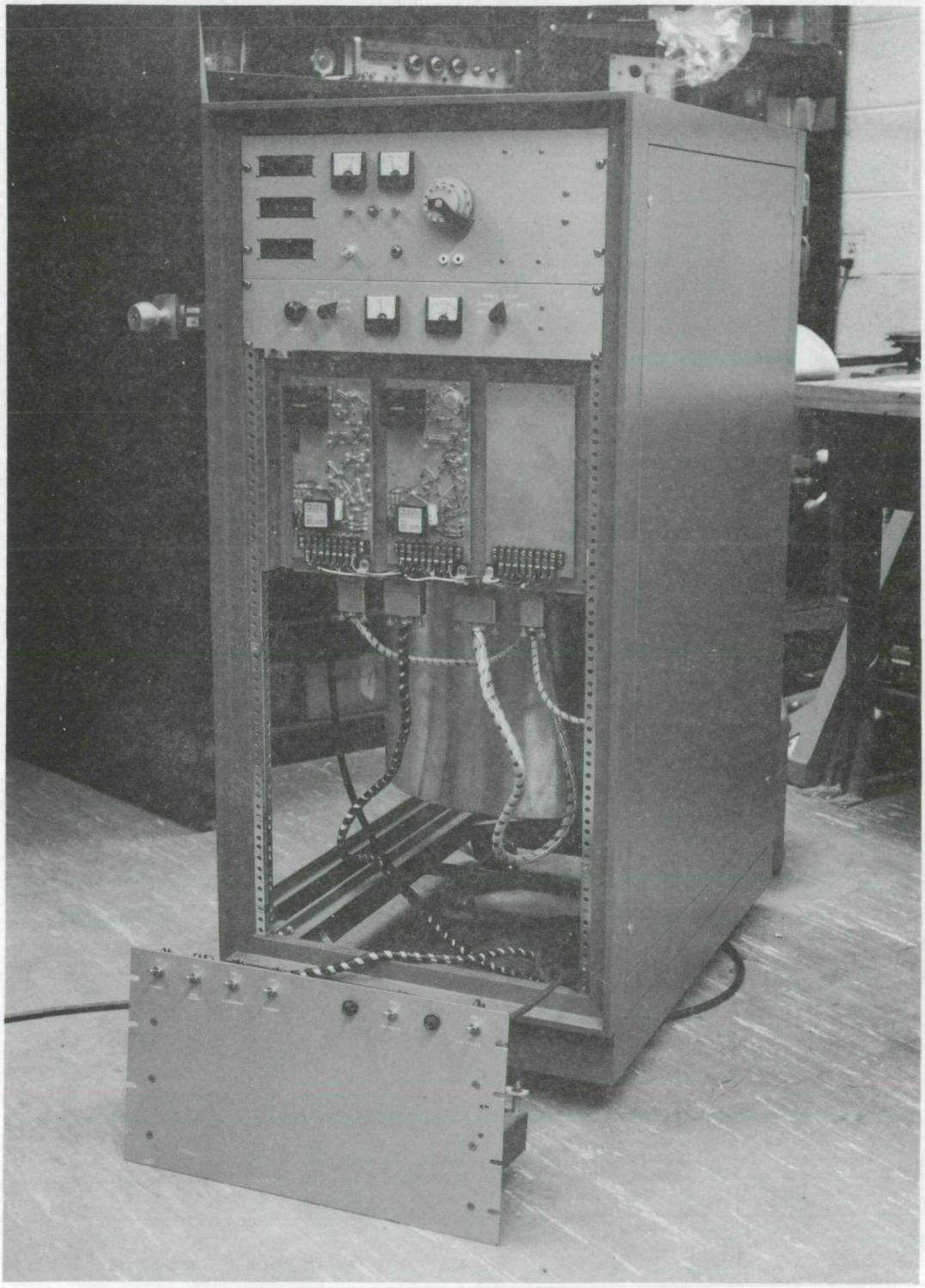

Figure 7b. Packaged maser with power supply and front panel removed.

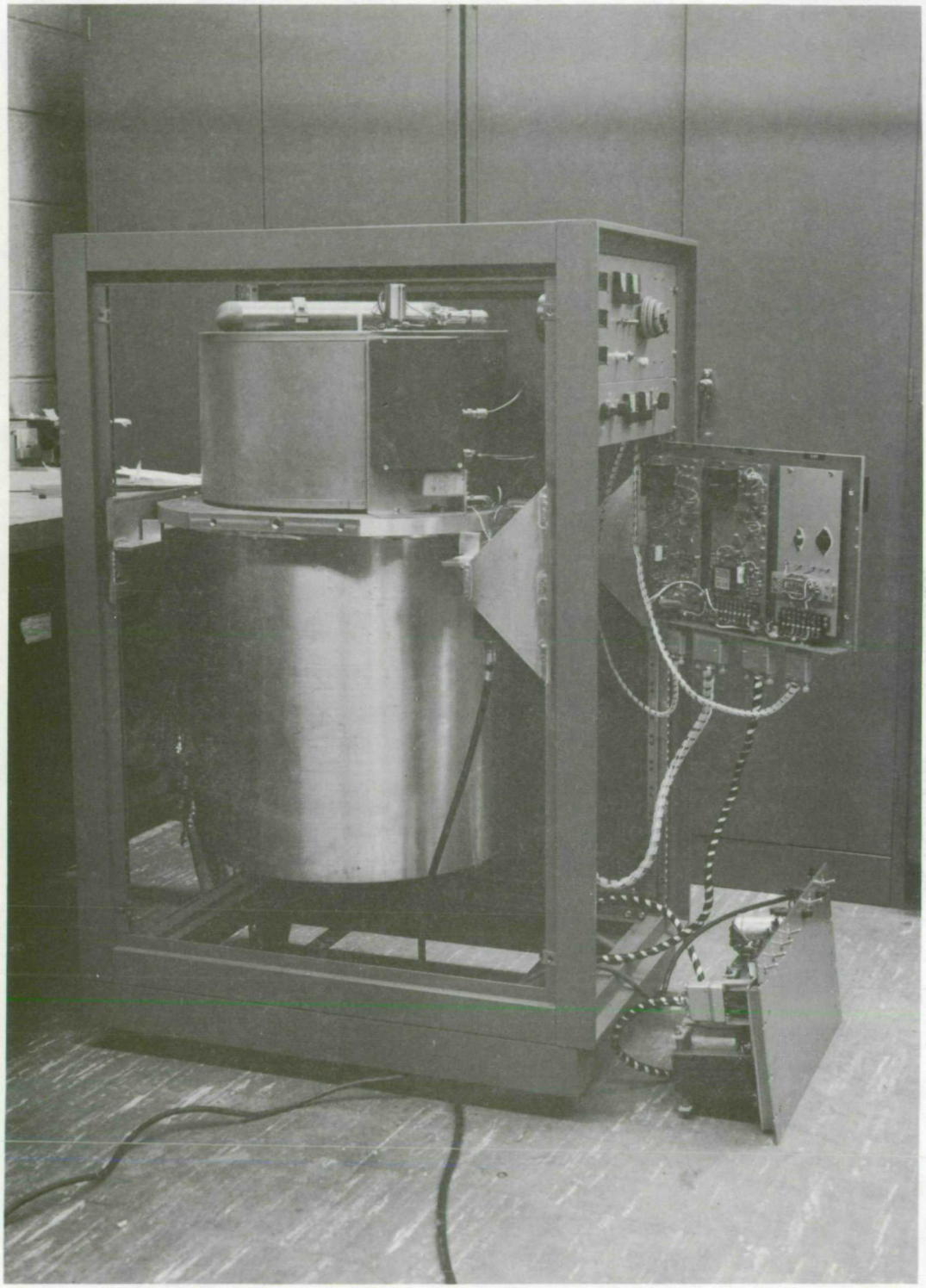

Figure 7c. Packaged maser with side panel removed.

INVENTION DISCLOSURE

To the attention of the NASA Patent Department:

The herein described invention is submitted in pursuance of Contract NSR-09-015-098.

The invention relates to the Atomic Hydrogen Maser Frequency Standard.

The purpose of the invention is to provide a new type of cavity resonator for the maser. This cavity is made of three pieces of CER-VIT ®(a glass-ceramic material having an extremely low thermal coefficient of expansion) and is made tuneable in an extremely stable mechanical manner.

Brief Description

Cavity resonator mistuning causes a shift in the output frequency of the Hydrogen Maser proportional to the extent of the mistuning times the ratio of the cavity Q to the line Q. Normally this ratio is about 10^{-5} so that a 10 HZ shift causes a 10^{-4} HZ shift (or 7 parts in 10^{14}) in the output frequency. Hence the mechanical and thermal stability of the cavity are of great importance to the overall stability of the maser. An extremely low thermal expansion material called CER-VIT having thermal expansion coefficient $\alpha < |0.5 \times 10^{-7}|$ and having excellent mechanical properties is extremely suitable for the cavity. Heretofore this material has been used for the top and bottom plates and for the cylinder of an earlier cavity. The adjustment of frequency was done by inserting metallic parts and problems of their mechanical stability in view of the desired micro-inch positional tolerances contributed to the instability of the cavity in both a thermal and mechanical manner.

A new type of maser cavity has been designed and constructed using only three CER-VIT components. Figure 1 shows the cavity assembly that includes 1) a top plate with three integral stiffening webs, 2) a cylinder with a three-fold interrupted helical ramp or thread at its bottom, and 3) the base which also contains the bottom plate. The cavity is shown resting on an aluminum disc. Three inclined ramp lugs on the base engage the cylinder interrupted thread. The cavity is tuned by rotating the cylinder and thereby raising or lowering it on the base. Figure 2 shows the cylinder and top plate up-ended. The web structure of the base can be seen through the transluscent CER-VIT. Note that the base legs are rigidly connected to the bottom plate. Figure 3 shows the maser bulb assembly fastened to the top plate.

® T.M. Owens-Illinois

The assembly shown in Figure 1 is secured by means of a hold-down cylinder that is fastened to the aluminum disc as the base of the cavity. A Belville spring assembly is used to provide uniform downward pressure at the outer circumference of the top plate. The tension of the spring is set so that thermal movement of the aluminum hold-down cylinder relative to the CER-VIT does not cause an appreciable change in the compressive force on the cavity. Figure 4 is a sketch of the hold-down assembly.

This new concept of an adjustable all CER-VIT cavity was conceived November 17th. First drawings were made by Thomas E. Hoffman on November 23, 1970. The cavity was built by Owens-Illinois and delivered June 17, 1971. We silvered the cavity and tested its electromagnetic properties July 14-15, 1971.

This disclosure was first written June 1, 1971.

R Vessot

by R. Vessot
334 Ocean Ave. Marblehead, Mass.

T. E. Hoffman

T. E. Hoffman
18 Franklin St., Marblehead, Mass

M. W. Levine

M. W. Levine
Big Rock Rd., Manchester, Mass.

This invention was explained to me by the above-identified inventor on 12 August, 1971.

R. F. Jendrock
Signature of Witness

August 12, 1971
Date of Signature

FIGURE 1

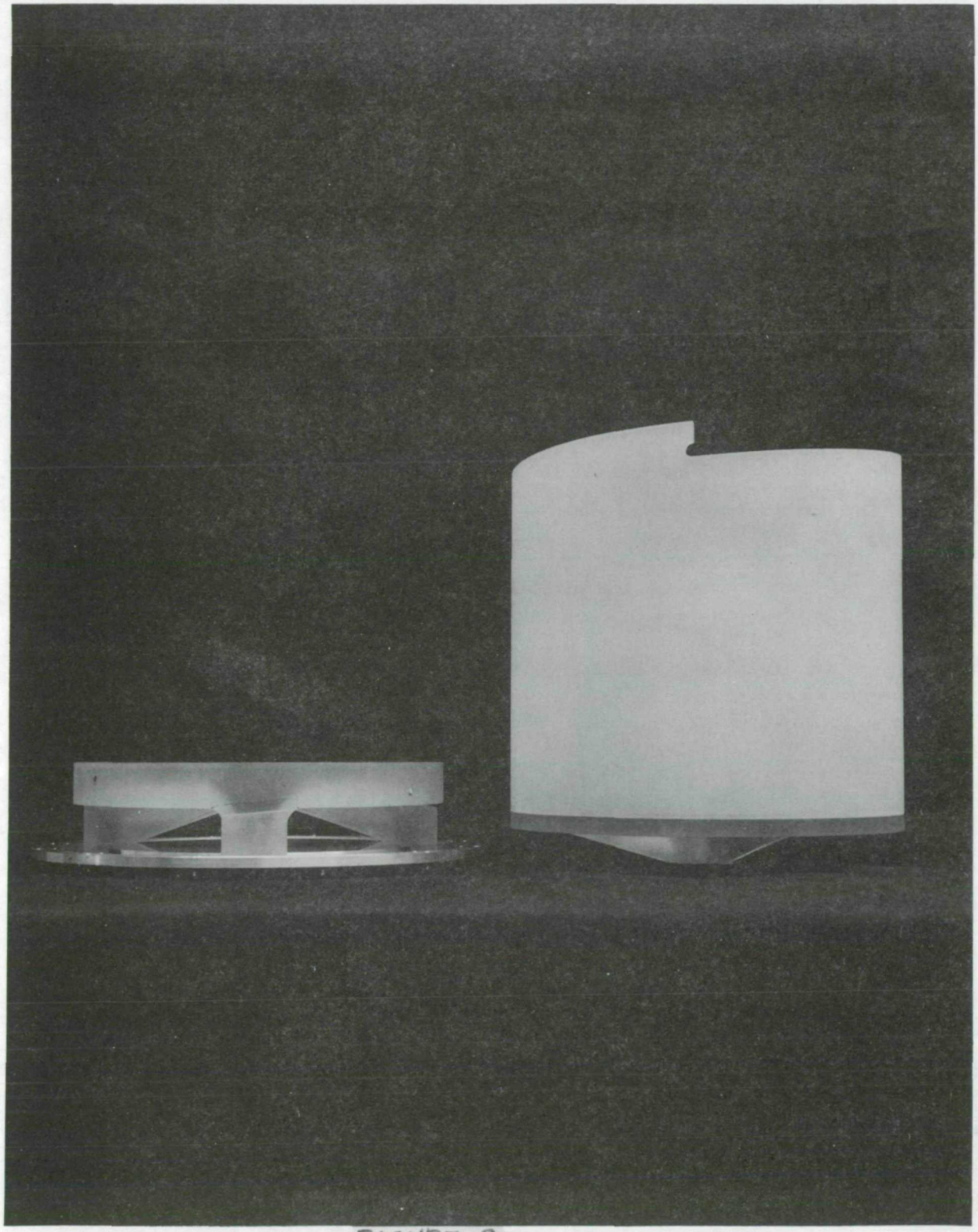

FIGURE 2

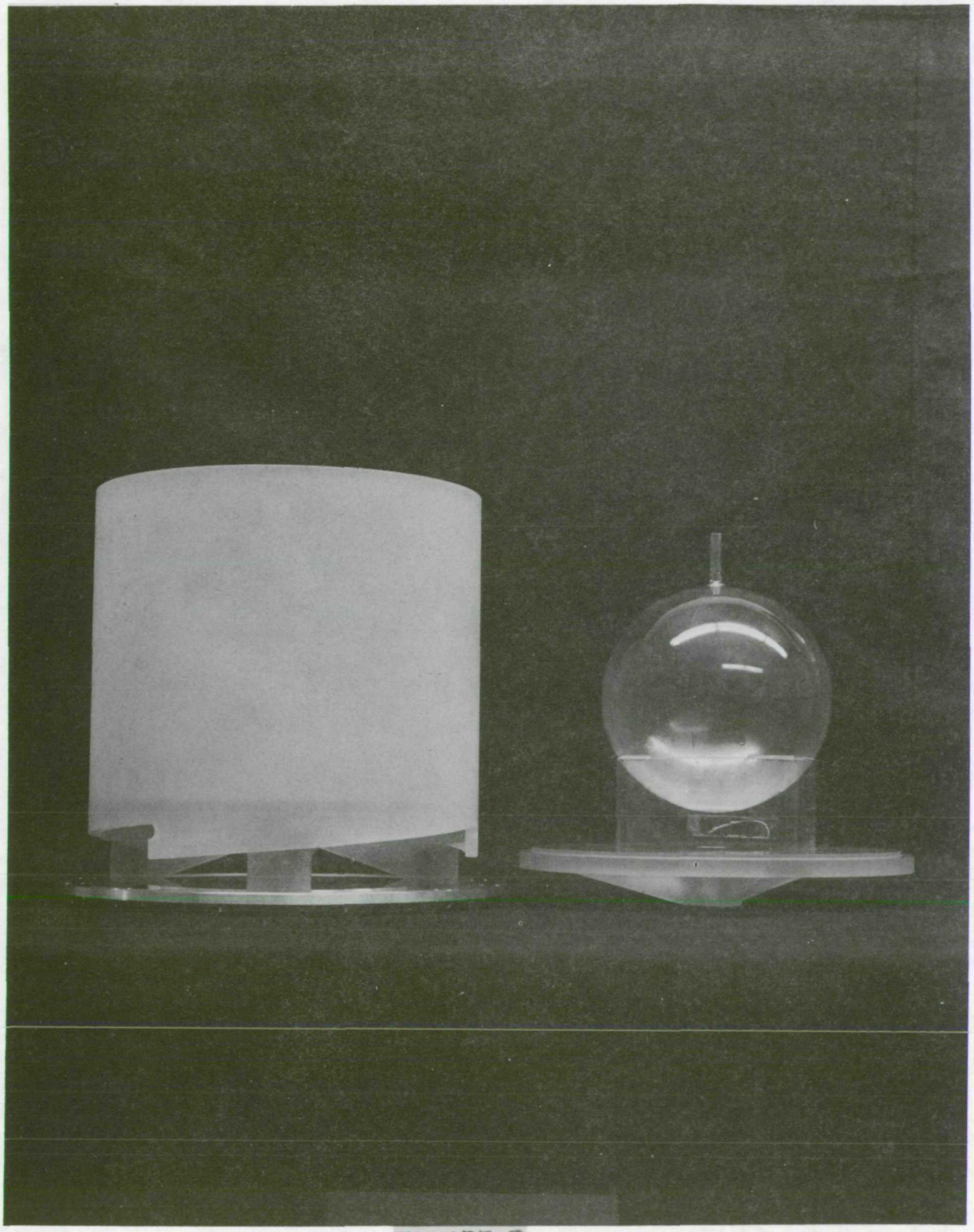

FIGURE 3

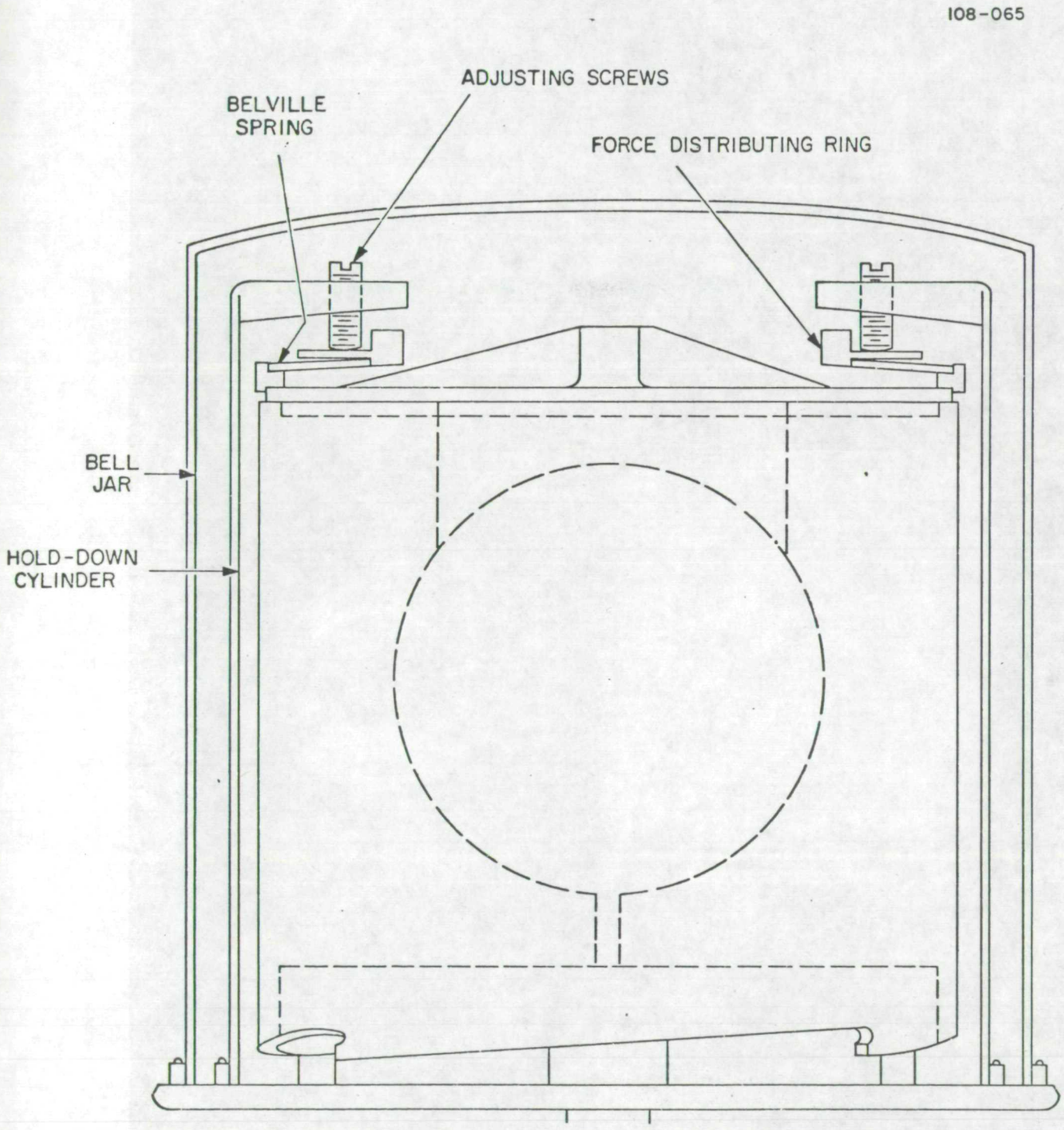

CAVITY HOLDING SYSTEM

Figure 4

R Vesnit
July 29 '41

6. OTHER ACTIVITIES AND PUBLICATIONS BEYOND THE SCOPE OF THIS CONTRACT

Concurrent with work directly related to the contract were other activities closely connected with application of the maser to very long-baseline interferometry and to measurement of the gravitational redshift by means of a direct maser clock in a satellite.

A. The small maser originally built for NASA under Contract NAS 8-2604 was refurbished and extensively tested. With NASA's permission, the maser has been used in very long-baseline interferometry experiments at the following sites:

Agassiz Observatory, Harvard, Mass.
Haystack Observatory, Westford, Mass.
Naval Research Laboratory, Maryland Point, Md. (two trips)
National Radio Astronomy Observatory, Greenbank, W. Va.
Jet Propulsion Laboratory Deep-Space Station DSS-62, Robledo, Spain

The methods employed to adapt existing stations to use the maser are described in a reprint from Radio Science at the end of this section.

B. The continuing interest of the principal investigator and coinvestigator associated with the present NASA contract, as well as the interest of NASA's Physics and Astronomy Department, has led to further study in the feasibility of testing the Einstein equivalence principle by measuring the gravitational redshift of the earth. This experiment would make use of the extraordinary frequency stability of the hydrogen maser in a vehicle that moves upward and downward by being either in a highly eccentric orbit or, as suggested by Dr. Nancy Roman of NASA, in a rocket probe where the clock is launched vertically to about 10,000 n.mi. and allowed to impact into the ocean.

Vessot and Levine presented "Measurement of the Gravitational Redshift Using a Clock in an Orbiting Satellite" at the conference on Experimental Tests of Gravitation Theories at the California Institute of Technology on November 11, 1970. This was subsequently published in the proceedings of that conference and forms part of the present report.

C. Further activity by the principal investigator and coinvestigator in the field of frequency standards has resulted in the following papers, which are also appended as part of this report:

Recent Developments Affecting the Hydrogen Maser as a Frequency Standard, published in NBS Special Publication 343 Precision Measurement and Fundamental Constants, edited by D. N. Langenberg and B. N. Taylor, August 1971.

Characterization of Frequency Stability, published in IEEE Transactions on Instrumentation and Measurement, Vol. IM-20, No. 2, May 1971; also as NBS Technical Note 394, issued October 1970.

7. CONCLUSION

The contract has been very productive, and we have achieved the objectives set forth in the original work statement. The establishment of a laboratory at SAO to continue the research and development of hydrogen masers for space and ground applications has ensured that activities begun in 1960 at Varian Associates would be continued in an unbroken manner. SAO's affiliation with Harvard University and the fact that the Principal Investigator and Coinvestigator are Associates of HCO have led to stimulative interactions with the Physics and Applied Science departments of Harvard University. In particular, we have enjoyed a productive and interesting liaison with Professor Ramsey and his graduate students; we have given several informal seminars to this group and have coauthored articles with them.

In addition to the interaction of ideas, there has been interaction at the hardware level. Two surplus hydrogen masers in very decrepit condition have been loaned by SAO to the Maser Lab at Harvard, where they have been rebuilt and put into service as frequency references. One of these was used in the flexible-bulb experiments. We have freely borrowed equipment and components, saving both time and money. During these years of stringent support for research, this interaction has been of great value to the programs both at SAO and at Harvard.

SAO and HCO have an ongoing need for maser frequency standards to conduct Very Long-Baseline Interferometry (VLBI) experiments. This has led us to become involved with the reality of making the masers work in the field and in applications where the stability and high spectral purity of the maser signal are pressed to their limits.

The small maser, developed under contract NAS 8-2604, has been the workhorse VLBI instrument. It has also served as a lab standard and as a transfer standard to bring together the Harvard, SAO, and NBS (hydrogen) masers for comparison with the NBS embodiment of the cesium frequency. Much has been learned about making a useful instrument, and this knowledge has led us to the redesign of a ground-based maser that incorporates many of the improvements developed or discovered in the

contract now completed. The redesign has been done under contract with a consortium of five separate organizations, NRL (A), NRL (B), National Radio Astronomy Observatory (NRAO), MIT, and the Swedish National Science Foundation. For the redshift experiment mentioned below, two additional masers will be required for NASA.

Our facilities at SAO have been expanded to meet the demands of these contracts. The new package is a completely self-contained frequency standard requiring input power at 110 v AC and 28 v DC.

During the course of our contract, we have been called on to refurbish or rebuild masers at MIT, NRAO, NRL, and the U.S. Naval Observatory. This work, performed under other contracts, has resulted in keeping a number of badly needed instruments operational so that VLBI and other experiments could be conducted. The experience gained in such field activity has been valuable, since we can review after many years the design faults of masers put into the field as long as 7 years ago.

We have now begun a redirection of our efforts (under NASA Contract NAS 8-27969) toward the goal of performing an experiment of potentially great significance to physics and astronomy. We plan to apply the hydrogen maser technology to measure the gravitational redshift due to the earth's mass and to test by direct measurement the equivalence principle.

We are grateful to the National Aeronautics and Space Administration for the support during the last 3 years that has allowed us to continue our work on masers at SAO. We look forward to a continuing successful involvement with NASA as we proceed toward our new objectives.

Radio Science, Volume 5, Number 10, pages 1287–1292, October 1970

Hydrogen-maser time and frequency standard at Agassiz Observatory

Martin W. Levine and Robert F. C. Vessot

Smithsonian Institution, Astrophysical Observatory, Cambridge, Massachusetts 02138

(Received July 1, 1970.)

A hydrogen maser was installed at the Harvard College Observatory-Smithsonian 84-foot radio telescope in Harvard, Massachusetts, for very long baseline interferometry (VLBI) experiments in October, November, and December of 1969. The maser is a compact unit (42 by 22 by 22 inches) of relatively low power consumption, designed specifically for field use; it is readily transportable. A precision 5-MHz crystal oscillator that is phase locked to the maser provides all frequency and time references for the VLBI receivers, recorders, and clocks. The maser was tuned against a rubidium standard by a rapid flux-switching technique; maser frequency resettability was estimated to be approximately $\pm 3 \times 10^{-13}$ with an over-all accuracy of approximately $\pm 1 \times 10^{-12}$. Loran-C was continuously monitored during the VLBI experiments, and the results of the Loran-C maser comparisons are included.

INTRODUCTION

The hydrogen maser is generally regarded as the ideal time and frequency standard for VLBI; it has a unique combination of superior short-term phase stability and freedom from drift. Further, the maser is a primary standard with unsurpassed resettability of frequency. In the past, the size, weight, and general awkwardness of the equipment have limited the use of the hydrogen maser to fixed installations. For observatories with only periodic or infrequent need for the phase stability of the maser standard, the investment required for the maser and its supporting electronics could not be justified.

The Smithsonian Astrophysical Observatory (SAO) hydrogen maser described in this paper was designed to be easily transportable and rugged enough to withstand the normal rigors of being moved from one station to another. It was transported by truck from Cambridge to Agassiz Station, Harvard, Massachusetts, for use during two VLBI experiments from October 14 to 15 and November 22 to December 14, 1969. The maser was installed at Agassiz, tuned against a rubidium-cell reference, and operated as the master time and frequency standard for the observatory for the duration of the observations. At the completion of the experiment, the maser was returned to Cambridge for use in other experiments.

HYDROGEN-MASER OSCILLATOR

The SAO hydrogen maser originated from a program to develop a clock for orbital applications for a precise test of the principle of equivalence [*Kleppner et al.*, 1970]. A second program was funded for construction of a small ground hydrogen maser incorporating the advanced technology of the space maser.

The design features of the SAO hydrogen maser are described in detail in an earlier paper [*Vessot et al.*, 1968]. Figure 1 is a diagram of the major assemblies of the maser. It should be noted that the design philosophy of this maser emphasizes good long-term frequency stability without the necessity for continuous automatic tuning. The cavity resonator is silver-coated Cer-Vit (Owens-Illinois trade name for a low-expansion coefficient partly vitrified glass) thermally compensated and enclosed in a two-stage oven. Provisions have been made for manual or automatic tuning that would use only a stable external reference oscillator and a digital-period counter. The tuning procedure, usually required only when the maser is moved to a new location, is given in detail in a later section.

The short-term performance of the SAO hydrogen maser is summarized in Figure 2, which is a conventional $\sigma(\tau)$ plot. The rms frequency stability as a function of averaging time is shown for quartz-crystal oscillators, rubidium and cesium standards, and the maser. The same data are shown in Figure 3 in a form that might be more useful for VLBI experimenters. The rms phase deviation as a function of observation time (normalized at 1 GHz) is shown for the four types of frequency standards.

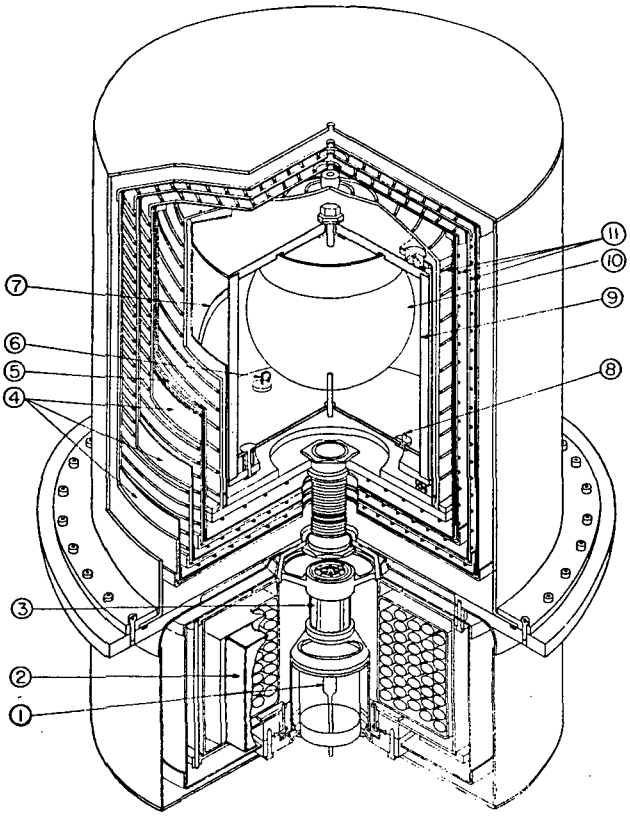

Fig. 1. A cut away section of the SAO hydrogen maser showing: 1, R F discharge tube; 2, ion pump; 3, hexapole magnet; 4, magnetic shield; 5, solenoid; 6, tuning loop; 7, low frequency transition coil; 8, output coupling loop; 9, cavity structure; 10, quartz storage bulb; and 11, oven heaters. This unit, which constitutes the maser oscillator, is mounted with the electronic support systems in a steel cabinet 42 × 22 × 22 inches.

MASER CLOCK SYSTEM

The hydrogen maser is an active oscillator with an output of approximately −95 dbm at 1420 MHz. A 5-MHz crystal oscillator is phase locked to the maser signal to provide standard frequencies at levels useful to the clock system. A simple dual-conversion receiver is used to generate the phase locking signals; a synthesizer is also used to set the time scale.

The entire maser clock system is shown in block diagram in Figure 4. The maser output at 1420·405 MHz is fed to a balanced crystal diode mixer where it is hetrodyned with the 1400-MHz output of a 5- to 1400-MHz (or ×280) multiplier. The first IF signal at 20.405 MHz is amplified by 40 db and then heterodyned with the 20-MHz output of the ×4 multiplier. The first IF signal at 20.405 MHz is amplified by 40 db and then heterodyned with the 20-MHz output of the ×4 multiplier. The second IF signal, at 405 kHz, is amplified by approximately 50 db and fed to one input of a balanced phase detector. The reference signal for the phase detector is supplied by a Hewlett-Packard 5102A digital synthesizer. The synthesizer is usually set at 405,794.3 Hz to approximate the UTC time scale. The output of the phase detector is used to phase lock a precision 5-MHz quartz-crystal oscillator through a very high-gain operational integrator. Double integration is incorporated into the phase-locked loop so that the phase tracking error (or velocity error) is very nearly zero. The time constant of the integrator is selected so that the closed loop response is critically damped and the closed loop bandwidth is approximately 10 Hz. The output of the phase-locked 5-MHz oscillator is used to drive the ×280 and ×4 multipliers and the digital synthesizer so that the entire maser clock system is phase coherent. A 1-MHz signal, derived from internal dividers in the crystal oscillator, is used to drive the VLBI timing system.

The Agassiz VLBI installation includes a Hewlett-Packard 5065A rubidium standard. This instrument provides the 5-MHz quartz-crystal oscillator used in the hydrogen maser clock system. The rubidium-cell reference loop in the 5065A is usually disabled and, as shown in Figure 4, the quartz oscillator is slaved to the maser. Using the rubidium standard in this fashion has a number of advantages. The cost of an additional quartz oscillator is eliminated, a stable backup standard is always available on-line, and the tuning of the maser is simplified. The change from hydrogen maser operation to the rubidium standard requires only the turn of a switch to transfer the electronic-frequency control of the quartz oscillator from the external maser circuitry to the internal rubidium cell. The amplitude of the clock signals at 5 MHz, 1 MHz, and 100 kHz is not affected by the changes in the phase lock circuitry, nor are any interconnection changes required.

TUNING THE HYDROGEN MASER

The oscillation frequency of a hydrogen maser is 'pulled' by the maser cavity resonator. The amount of pulling is a function of cavity detuning and the line width [*Vanier and Vessot,* 1964] of the atomic resonance:

$$\nu = \nu_H + \left(\frac{\nu_c - \nu_H}{\nu_c} Q - \frac{0.29 \nu a_0^2 \hbar V_c}{Q \mu_0^2 \eta V_b}\right) \Delta\nu_l \qquad (1)$$

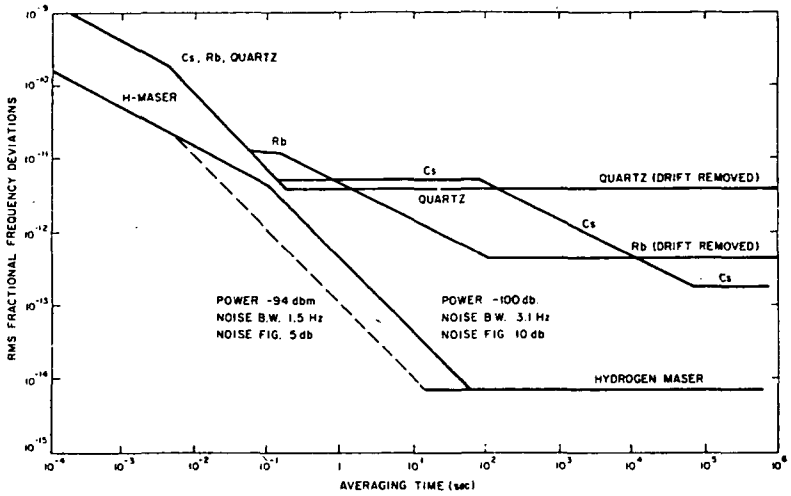

Fig. 2. The rms frequency stability of the hydrogen maser as a function of observation time. The characteristics of typical quartz-crystal, rubidium, and cesium standards are shown for comparison.

where

- ν is maser oscillation frequency.
- ν_H is center frequency of the atomic resonance line.
- ν_c is center frequency of the cavity resonance.
- Q is quality factor of the cavity.
- $\mathbf{v}$ is mean velocity of the hydrogen atoms.
- a_0 is first Bohr orbit radius.
- $\hbar$ is Planck's constant divided by 2π.
- μ_0 is Bohr magneton.
- V_c is volume of the cavity.
- V_b is volume of the storage bulb.
- η is ratio of average electromagnetic field energy density in the storage bulb to average energy density over the entire cavity.
- $\Delta\nu_l$ is atomic resonance line width.

If the cavity is tuned to a frequency ν_{c0} such that

$$\nu_{c0} = \nu_H\{1 - [0.29\mathbf{v}a_0^2\hbar V_c/Q^2\mu_0^2\eta V_b]\}^{-1} \quad (2)$$

then the term in brackets in equation 1 vanishes and

$$\nu = \nu_H \quad (3)$$

The maser oscillates at the center of the atomic resonance line.

The cavity is tuned to ν_{c0} by modulating the flux of atoms entering the storage bulb. It can be shown that the spin-exchange contribution to the line width is directly proportional to the flux, and (referring to equation 1), when the cavity is at the tuning point ν_{c0}, then ν is independent of line width and therefore also independent of the total hydrogen flux.

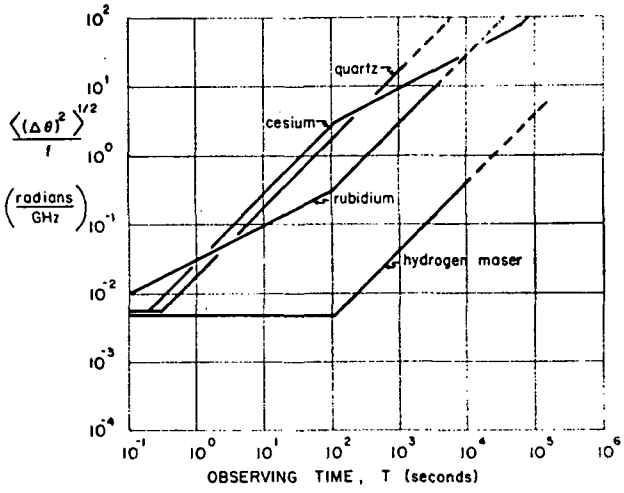

Fig. 3. The data of Figure 2 are replotted to express directly the phase stability of the four types of frequency standards as a function of observation time. All the data have been normalized to 1 GHz [from *Cutler and Vessot, 1968*].

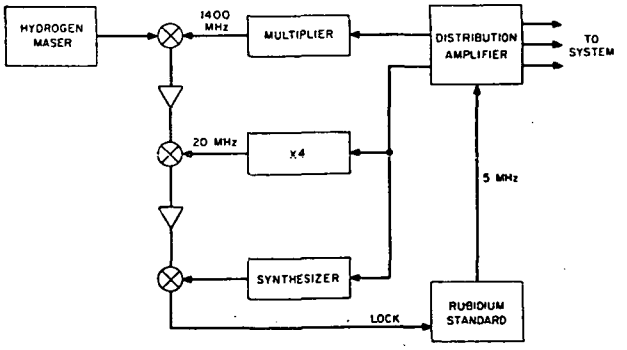

Fig. 4. The maser clock system in block diagram form. The rubidium cell in the Hewlett-Packard 5065A is disabled, and only the internal quartz-crystal oscillator is used.

The maser can be tuned by using a frequency reference much less stable than that of the maser itself. The technique used is switching of the hydrogen flux periodically from a very low level, near threshold, to a very high level and looking for corresponding changes in the oscillator frequency of the maser. The flux level must be modulated as rapidly as possible to minimize the phase-noise contribution from the reference oscillator. The phase-noise power spectral density of quartz-crystal oscillators, rubidium standards, and cesium standards decreases as the offset from the carrier frequency is increased.

The effect of linear frequency drift in the reference standard can be eliminated by using an algorithm devised by L. C. Cutler (private communication, 1968). The period of the beat between the maser and the reference oscillator is measured an odd number of times, alternately at low and at high flux. The measurements at low flux are assigned a negative sign and the measurements taken at high flux are assigned a positive sign. The first and last measurements are divided by two, and all the measurements are then summed algebraically. This residue,

$$N_R = \frac{-(a_1 + a_n)}{2} + \sum_{k=2}^{n-1} (-1)^k a_k \qquad (4)$$

is a measure of the cavity detuning. It can be readily shown that the value of the residue is unaffected by linear frequency drift of the reference.

The maser at Agassiz was tuned against the HP 5065A rubidium standard by the procedure outlined in the previous paragraph. Control of the atomic hydrogen flux into the maser storage bulb is achieved by varying the RF power level in the hydrogen dissociator. The power level can be switched between two preset values by a manual control on the front panel or by a logic signal from an external controller. The output of the phase detector (Figure 4) was disconnected from the 5065A rubidium standard and temporarily connected to a digital frequency counter set to read 10-period averages. The 5065A was slaved to its internal rubidium-cell reference to provide maximum stability. The frequency of the digital synthesizer was offset by 1.2 Hz to yield a beat period of 0.833 sec at the phase-detector output for a 10-period measurement interval of 8.333 sec.

Figure 5 shows the results of a tuning run at Agassiz taken just before the VLBI observations. The flux switching was done manually with the front-panel control on the maser. The data, eleven 8.3-sec measurements for each point on the curve, were recorded by a digital printer. A desk calculator was then used to calculate N_R from equation 4. (The entire process has since been automated by the addition of an index register and a reversible counter.)

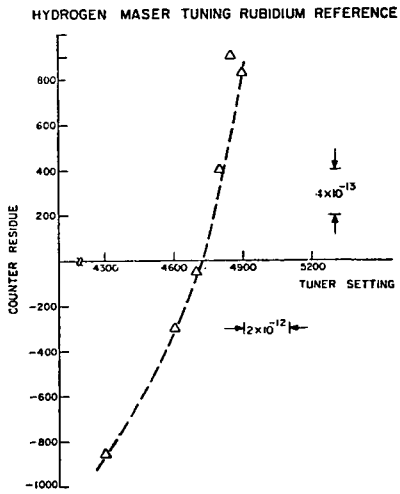

Fig. 5. Data from a tuning run of the hydrogen maser using the rubidium standard as a reference.

The precision of this tuning procedure is estimated to be approximately $\pm 7 \times 10^{-13}$. That is, the maser can be reset to the same oscillation frequency with a standard deviation of about one millihertz. The actual oscillation frequency, the mean of a large number of such measurements, is a function of the bulb wall shift, the second-order Doppler shift in the bulb, and the magnetic field. These effects can be measured or calculated; they are discussed in the next section.

MASER ACCURACY AND LORAN-C

The wall shift of the SAO hydrogen maser has been directly measured against the Harvard University reference maser, the SAO reference maser, and a maser at the National Bureau of Standards. The second-order Doppler was calculated for the known temperature of the storage bulb, and the magnetic field was estimated from the measured frequency of the Zeeman transition. The oscillation frequency of the maser [*Hellwig et al.*, 1970] is determined as follows:

Unperturbed hydrogen frequency in terms of the cesium second	1, 420, 405, 751. 768 Hz ± 0.003
Conversion for A1 to UTC	42.612
Second-order Doppler	−0.063
Measured wall shift	−0.020
Magnetic field shift	+0.001
Total (ν_H in UTC)	1, 420, 405, 794. 298 Hz ± 0.003

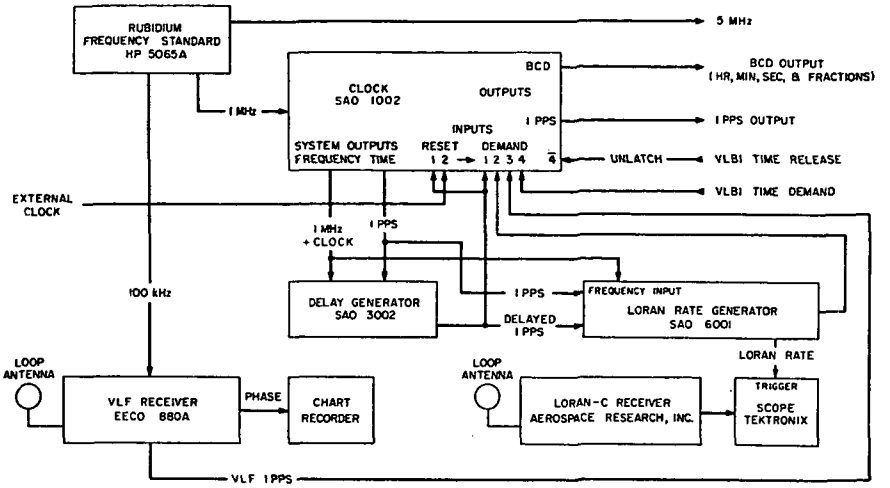

Fig. 6. The VLBI timing system shown controlled by the hydrogen-maser clock system. The Loran-C capability permits continuous monitoring of the epoch.

The digital-synthesizer resolution was limited to 0.1 Hz; therefore, the closest synthesizer setting was 405,794.3 Hz. We thus introduced a known 'error' of −0.002 Hz; the VLBI timing-system clocks should have run 1.4 parts in 10^{-12} fast with respect to Loran-C.

Loran-C timing pulses were continuously monitored at Agassiz from November 24 to December 15, 1969. The Agassiz VLBI timing system gained 6 μsec with respect to Loran-C, whereas the United States Naval Observatory (USNO) daily phase values predict a gain of 1.6 μsec. The difference of 4.4 μsec for a 21-day period corresponds to a local clock 2.42 $\times$ 10^{-12} high in frequency. Since it is known that the Agassiz clock was 1.4 $\times$ 10^{-12} low, owing to the granularity of the synthesizer, the total average discrepancy between the maser and Loran-C was

$$2.42 \times 10^{-12} + 1.4 \times 10^{-12}, \text{ or } 3.8 \times 10^{-12}$$

The Loran-C transmissions are monitored and steered by the USNO, which establishes and maintains a coordinated time scale based on the average of a large number of clock systems in this country and abroad. The unperturbed hydrogen frequency shown in an earlier paragraph was measured against the ensemble of cesium clocks at the National Bureau of Standards (NBS) in Boulder, Colorado. The discrepancy of 3.8 parts in 10^{-12} observed in this experiment lies well within the combined error limits of the Loran-C time scale and the precision of the hydrogen-cesium intercomparison at NBS, Boulder.

VLBI TIMING SYSTEM

The hydrogen maser clock provides the 1-MHz signal that drives the VLBI timing system shown in Figure 6. The SAO digital clock accumulates and displays the time of day with a resolution of 1 μsec. The digital clock also generates a 1-pps signal for the SAO digital delay generator. The delay generator is used to preset the Loran-C propagation delay and to determine the time differential between a portable clock and the system clock.

Time of day is set into the VLBI timing system by means of either a portable quartz-crystal clock or Loran-C transmissions. The digital clock is designed so that it can be directly reset to the 1-pps portable-clock signal. Setting the digital clock to the Loran-C epoch is accomplished visually by means of an oscilloscope triggered by the Loran rate generator.

The 'demand' inputs of the timing system freeze the clock display at the time of a demand input pulse. The Loran rate generator, the delayed 1 pps, a VLF 1-pps signal, and the VLBI event encoder can be used to 'demand' the clock. (The complete VLBI timing system is described in the article by R. D. Michelini in this issue.)

CONCLUSION

For VLBI observations of more than a few minutes or at wavelengths less than 5 cm, the hydrogen maser is the only satisfactory frequency standard. The SAO hydrogen maser has demonstrated that it can be used routinely and reliably for VLBI. The ease with which the maser can be transported makes feasible the fabri-

cation of complete traveling back ends for radio telescopes so that maximum utilization of existing observatories and baselines can be achieved.

Acknowledgments. The SAO hydrogen maser originated from a program sponsored by NASA Headquarters under contract NASW-1337; work continues under NASA contract NSR 09-015-098. A second program, to build a small ground hydrogen maser, was funded by Marshall Space Flight Center of NASA under contract NAS 8-2604.

REFERENCES

Cutler, L. S., and R. Vessot (1968), Present status of clocks and frequency standards, *Northeast Electronics Research and Engineering Meeting Record*, 68–69.

Hellwig, H., R. Vessot, M. Levine, P. Zitzefitz, and H. Peters (1970), Determination of the unperturbed hydrogen hyperfine transition frequency with the hydrogen maser, *IEEE Trans. Instrum. Meas., 19*.

Kleppner, D., R. Vessot, and N. Ramsey (1970), An orbiting clock experiment to determine the gravitational red shift, in *Astrophysics and Space Science*, vol. 6, pp. 13–32, D. Reidel, Dordrecht, Holland.

Vanier, J., and R. Vessot (1964), Cavity tuning and pressure dependence of frequency in the hydrogen maser, *Appl. Phys. Lett., 4*, 123–124.

Vessot, R., M. Levine, L. Cutler, M. Baker, and M. Mueller (1968), Progress in the development of hydrogen masers, in *Proceedings, Twenty-Second Annual Symposium on Frequency Control, Atlantic City, New Jersey*.

Measurement of the Gravitational Redshift Using a Clock in an Orbiting Satellite*

R. F. C. Vessot and M. W. Levine
Smithsonian Astrophysical Observatory
and
Harvard College Observatory

I. Introduction

The proposed experiment uses a hydrogen-maser clock in a satellite to measure the gravitational effect on time scales with an accuracy substantially higher than has ever been used before. This is a test of the principle of equivalence, which asserts that there is no way of distinguishing locally between a gravitational acceleration and an oppositely directed mechanical acceleration. This principle, first stated by Einstein (Ref. 1) as a generalization of the observed proportionality between gravitational mass and inertial mass, can be justified only by experiments. Experiments were carried out by Isaac Newton using pendula of various materials; more recently, the proportionality has been tested to a few parts in 10^{11} by Roll, et al. (Ref. 2) using a highly refined Eötvös balance.

The principle of equivalence affects radiation and manifests itself in the gravitational redshift, where a source radiating in a gravitational field will appear to be shifted in frequency by a fractional amount:

$$\frac{\Delta f}{f} = \frac{\Delta \phi}{c^2}$$

where $\Delta\phi$ is the gravitational potential difference between the source and the observer.

A number of proposals have been made to test the equivalence principle for clocks (Refs. 3-7). Pound and Rebka (Ref. 8) and Pound and Snider (Ref. 9) used the extremely narrow linewidth of Fe^{57} radiation and absorption due to the Mössbauer effect in a series of experiments over a 75-ft (approximately 23-m) vertical distance. Their results confirmed the prediction of the equivalence principle to 1 part in 100.

The advances in space-flight technology over the last decade and the availability of atomic oscillators with frequency stabilities better than 1 part in 10^{14} make possible a much more sensitive test of the principle of equivalence applied to clocks. The experiment we propose is a direct test of the relation with an accuracy of 1 part in 10^5 between the rates of proper clocks located at substantially different gravitational potentials.

A discussion of this experiment has been reported recently by Kleppner, Vessot, and Ramsey (Ref. 10).

The expression describing the fractional shift in frequency of a satellite-borne oscillator observed from the earth is given by

*This work was supported in part by contract NSR 09-015-098 from the National Aeronautics and Space Administration.

$$S = \frac{f_s - f_e}{f_c} = \frac{1}{c^2}(\phi_s - \phi_e)$$

$$- \frac{1}{2c^2}\left(v_s^2 - v_e^2\right) \qquad (1)$$

where the velocity is measured in terms of an inertial frame whose origin is at the center of the earth and whose axes are aimed at the "fixed" stars, and where $(\phi_s - \phi_e)$ is the gravitational potential difference between the satellite and the earth's surface. If we neglect the effect of the earth's rotation (or locate our ground station at the north or south pole) and if we consider the earth to be spherical, we obtain the time average of the redshift:

$$\langle S_0 \rangle = \left\langle \frac{GM_e}{c^2 R_e}\left(1 - \frac{3R_e}{2a}\right)\right\rangle \qquad (2)$$

where a is the semimajor axis of the orbit, and $GM_e/c^2 R_e = 6.94 \times 10^{-10}$ is the total redshift that would result if the satellite were at rest at a very large distance from the earth. The value of $\langle S_0 \rangle$ is shown plotted in terms of orbital radius in Fig. 1. It is seen that with a 24-h orbit, we obtain 77% of the total effect due to the earth's gravity. The value of $\langle S_0 \rangle$ for these orbits is 5.37×10^{-10}.

If the orbit is eccentric, S will vary periodically, and we can describe the variations as a gravity-induced frequency modulation of the oscillator in the satellite. We can use two separate properties of the oscillator – the precision* and its stability† – by means of an eccentric orbit.

Assuming a spherical earth and no other perturbations, the time average value of S is independent of eccentricity and depends only on the orbital period. The average frequency of the satellite oscillator can be related to its previously determined value on the ground with an accuracy that is limited by the precision of the oscillator. On the other hand, the extent of modulation of the oscillator frequency due to excursions back and forth in the earth's gravitational potential can be determined with an accuracy that depends on the oscillator's stability. This stability, as will be seen later, depends on the averaging time. The applicable averaging time will depend on the period of the modulation. As in other modulated systems, the accuracy of the determination can be improved by repeating the measurement over many cycles.

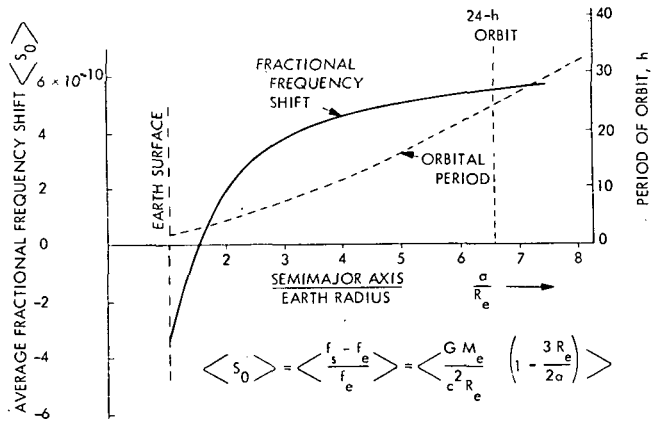

Fig. 1. Redshift and orbital period plotted versus semimajor axis in units of the earth radii

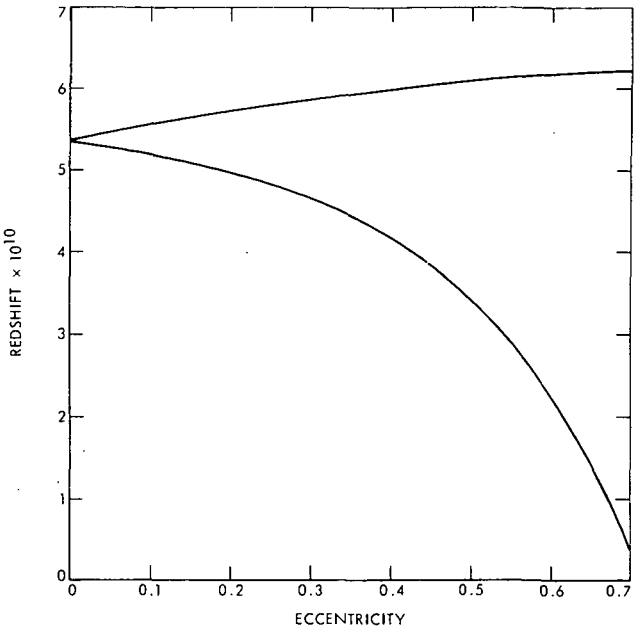

Fig. 2. Extremes of redshift versus eccentricity (The upper and lower branches give the redshift at apogee and perigee, respectively.)

For a 24-h orbit, the extremes in the value of S are plotted in Fig. 2 as a function of orbital eccentricity.

There are limits imposed on the eccentricity of the orbit by the desirability of keeping the satellite constantly in view of the ground station so that the telemetry system will operate with no interruption of carrier phase. In Fig. 3 (from Ref. 10), we show the minimum angle of elevation h_{min} as a function of eccentricity of the orbit for a 24-h orbit with inclination 28.5°. The value of h_{min} observed from earth stations at the equator and at latitude 20° are shown. On the same figure, the value of the diurnal variation is plotted versus eccentricity. Since it is desirable to keep the minimum elevation angle more than 15° above the horizon, we will look into the characteristics of

*By precision, we mean the ability of the oscillator to be independently restarted to oscillate at a previously determined frequency.

†The stability is defined here as the two-sample variance or the Allan variance (see Ref. 17).

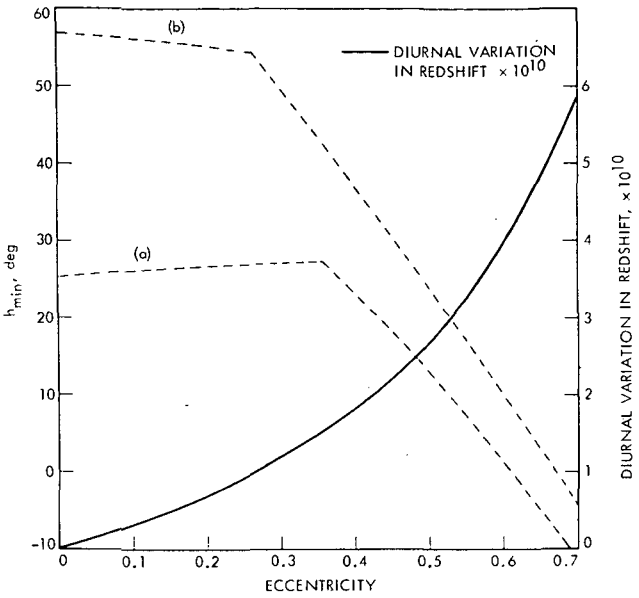

Fig. 3. Variation in redshift and minimum angle of elevation for 24-h orbit inclined at 28.5° as seen from an earth station: (a) 20° (b) 0°

an experiment performed with a 24-h orbit with eccentricity 0.52 and a ground station at latitude 20°. Under these conditions, we can expect the shift to vary from 3.09×10^{-10} to 6.08×10^{-10} with a 24-h period. The behavior with time of the redshift is plotted in Fig. 4 (from Ref. 10). Shown in the same figure as a first-order doppler effect for a carrier frequency of 2.5 GHz.

II. The Telemetry System

From Fig. 4, we see that the frequency shift we want to measure is very small compared to the doppler shift of the telemetry carrier. However, by use of a phase-coherent system, it is possible

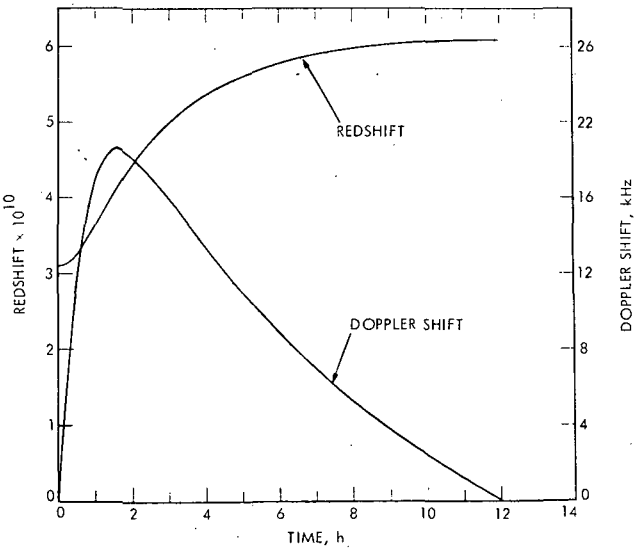

Fig. 4. Redshift and doppler shift versus time for a 24-h orbit with eccentricity 0.52 and inclination 28.5° (obtained from an earth station at 20° latitude using a 2.5-GHz carrier)

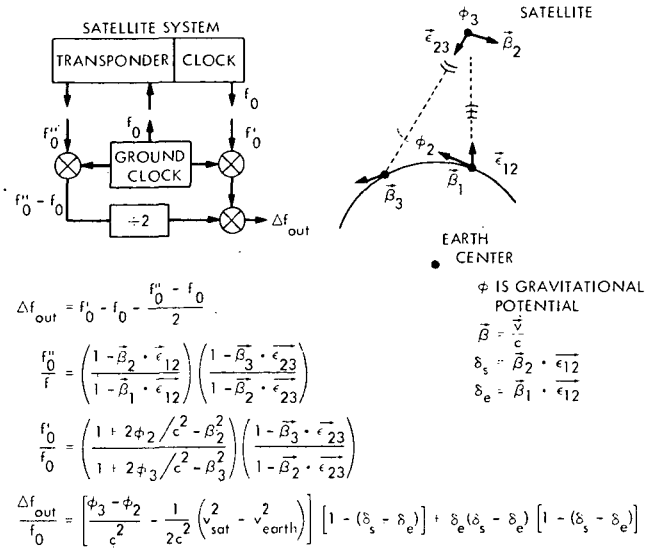

$$\Delta f_{out} = f'_0 - f_0 - \frac{f''_0 - f_0}{2}$$

$$\frac{f''_0}{f} = \left(\frac{1 - \vec{\beta}_2 \cdot \vec{\epsilon}_{12}}{1 - \vec{\beta}_1 \cdot \vec{\epsilon}_{12}}\right)\left(\frac{1 - \vec{\beta}_3 \cdot \vec{\epsilon}_{23}}{1 - \vec{\beta}_2 \cdot \vec{\epsilon}_{23}}\right)$$

$$\frac{f'_0}{f_0} = \left(\frac{1 + 2\phi_2/c^2 - \beta_2^2}{1 + 2\phi_3/c^2 - \beta_3^2}\right)\left(\frac{1 - \vec{\beta}_3 \cdot \vec{\epsilon}_{23}}{1 - \vec{\beta}_2 \cdot \vec{\epsilon}_{23}}\right)$$

$$\frac{\Delta f_{out}}{f_0} = \left[\frac{\phi_3 - \phi_2}{c^2} - \frac{1}{2c^2}\left(v_{sat}^2 - v_{earth}^2\right)\right]\left[1 - (\delta_s - \delta_e)\right] + \delta_e(\delta_s - \delta_e)\left[1 - (\delta_s - \delta_e)\right]$$

$\vec{\beta} = \frac{\vec{v}}{c}$

$\delta_s = \vec{\beta}_2 \cdot \vec{\epsilon}_{12}$

$\delta_e = \vec{\beta}_1 \cdot \vec{\epsilon}_{12}$

Fig. 5. Concept of doppler-canceling telemetry system

to remove the doppler shift and to extract the desired information. This system is shown in its conceptual form in Fig. 5, and its operation is described below.

Two signals are used, a clock signal from the satellite and a tracking signal that is transmitted from the ground, received at the satellite, and coherently transmitted back to the ground station. The ratio of the received signal frequency f'' to the transmitted frequency f_0 of the tracking signal is given by

$$\frac{f''_0}{f_0} = \left(\frac{1 - \vec{\beta}_2 \cdot \vec{\epsilon}_{12}}{1 - \vec{\beta}_1 \cdot \vec{\epsilon}_{12}}\right)\left(\frac{1 - \vec{\beta}_3 \cdot \vec{\epsilon}_{23}}{1 - \vec{\beta}_2 \cdot \vec{\epsilon}_{23}}\right) \qquad (3)$$

As discussed in Ref. 10, this expression results from a direct application of the special theory of relativity, and its accuracy is sufficient for the purpose of this experiment. The symbols are explained by Fig. 5.

The clock signal is transmitted from the satellite at a frequency f_0 that is proper to the clock in the satellite. This signal is received by the ground station at a frequency f'_0. The relationship between f_0 and f'_0 is given by

$$\frac{f'_0}{f_0} = \left(\frac{1 + (2\phi_2/c^2) - \beta_2^2}{1 + (2\phi_3/c^2) - \beta_3^2}\right)\left(\frac{1 - \vec{\beta}_3 \cdot \vec{\epsilon}_{23}}{1 - \vec{\beta}_2 \cdot \vec{\epsilon}_{23}}\right) \qquad (4)$$

This expression results directly from the principle of equivalence. It also results from the general theory of relativity when terms in v^2/c^2 and ϕ/c^2 are taken to first order.

When applied to the simple case where the radial accelerations are small and when the

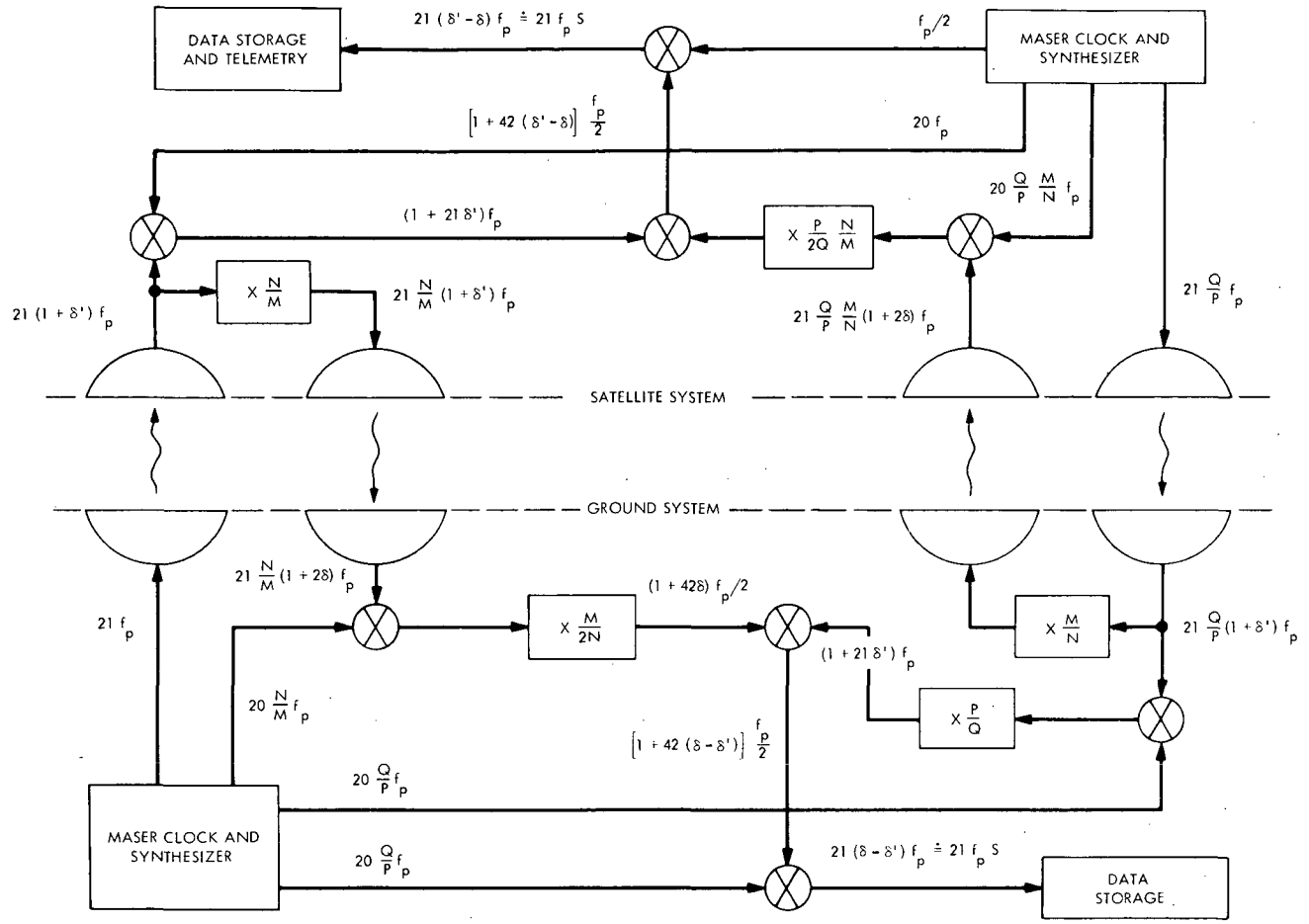

Fig. 6. Schematic block diagram of a symmetrical doppler-canceling telemetry system (Data are taken both in the satellite and on the ground.)

propagation path to and from the satellite is the same, Eqs. (3) and (4) will give us an expression for S. For this case, where $\overrightarrow{\epsilon_{23}} = -\overrightarrow{\epsilon_{12}}$ and $\overrightarrow{\beta_1} = \overrightarrow{\beta_3}$ and δ_s and δ_e are defined as $\overrightarrow{\beta_2} \cdot \overrightarrow{\epsilon_{12}}$ and $\overrightarrow{\beta_1} \cdot \overrightarrow{\epsilon_{12}}$, respectively, we obtain

$$\frac{\Delta f_{out}}{f_0} = \frac{f_0'}{f_0} - 1 - \frac{1}{2}\left(\frac{f_0''}{f_0} - 1\right) = S\left[1 - (\delta_s - \delta_e)\right]$$

$$+ \delta_e(\delta_s - \delta_e) \times \left[1 - (\delta_s - \delta_e)\right] \qquad (5)$$

The first term is the shift S multiplied by a small doppler correction; the second is a residual doppler effect resulting from the ground-station velocity.

The effects of changes in radial velocity of the satellite and the change in position of the ground station due to the earth's rotation depend on the choice of orbit and the location of the ground station. The correction terms that result from these effects can be computed from knowledge of the orbit and the station location.

The telemetry system described above cancels the first-order doppler by dividing the frequency shift in the tracking (go-return) signal by two and subtracts this average shift from the frequency of the one-way clock signal. Since asymmetrical propagation can occur in the up-down paths, the doppler correction of the frequency of the clock signal may be in error. To avoid this problem, it is very desirable to operate the telemetry system in a symmetrical manner, taking the redshift data both on the ground and in the satellite. This is accomplished by the addition of a transponder on the ground that coherently retransmits the clock signal from the satellite. In this way, the satellite can obtain information for doppler cancellation and correct the received frequency of the ground-station signal. This signal is controlled by the ground-based clock. The symmetrical system is shown schematically in Fig. 6. All frequencies are derived from the "proper" frequency f_p, which in this illustration is taken as 100 MHz. Doppler shifts are denoted by δ and relativistic-plus-doppler shifts by δ'.

The up-link to the satellite transponder is at 2100 MHz, and the down-link is at 2100 × N/M = 2280.5 MHz (N = 240, M = 221). The satellite clock signal down-link is at 2100 Q/P = 2290 MHz (Q = 241, P = 221), and the ground-station transponder frequency is at 2100 (Q/P) (M/N) = 2108.7 MHz. These carrier frequencies should be sufficiently close together to avoid dispersion problems in the atmosphere and ionosphere.

This system will allow continuous tracking of the maser clocks by a continuous monitoring of the phase of the two signals transmitted from each of the ground and satellite clocks. Data will be recorded both in the satellite and on the ground and will be compared to the known orbital parameters of the satellite. To make a redshift comparison compatible with the clock stability of 7 parts in 10^{15}, the following requirements on orbit information must be met:

Radial distance	$\Delta r \sim 240$ m
GM	known to 1 part in 10^5
Vector velocity of satellite	$\Delta v \sim 60$ cm/s
Radial acceleration	$\ddot{r} \sim 10^{-4}$ m/s^2

Note that much of the tracking information is available from the doppler measurements made by the system itself and that the limitations to the accuracy of the redshift determination are not likely to result from the tracking system but will depend on the stability of the clock.

III. Corrections to the Redshift

The data obtained will contain contributions from other gravitational effects. These have been estimated in Ref. 10. The significant ones reported here apply to the elliptic orbit described earlier, with the ground station at the equator:

(1)	Quadrupole moment of the earth	
	(a) Correction to the ground-station redshift	$= 3.76 \times 10^{-13}$
	(b) Correction to the satellite redshift at the perigee of the $\epsilon = 0.52$ orbit	$= 9.0 \times 10^{-14}$
(2)	Gravitational effect of the sun	
	(a) Correction to the ground-station redshift	$= 1.81 \times 10^{-17}$
	(b) Correction to the satellite redshift	$= 1.83 \times 10^{-15}$
(3)	Gravitational effect of the moon	
	(a) Correction to the ground-station redshift	$= 3.91 \times 10^{-17}$
	(b) Correction to the satellite redshift	$= 3.28 \times 10^{-15}$
(4)	Effect of earth tides	
	Correction to the ground-station redshift	$= 1 \times 10^{-15}$

Corrections for these effects can be computed from information relating to the geopotential of the earth and earth-body tides. This information is available to far greater accuracy than we need in Gaposchkin and Lambeck (Ref. 11) and Köhnlein (Ref. 12).

IV. Hydrogen-Maser Clock System

The atomic hydrogen maser has been under continuous development since its invention in 1960 by Goldenberg et al. (Ref. 13) and Kleppner et al. (Ref. 14). At present, when used to control the phase of a crystal oscillator, it provides the highest stability of any known system. The characteristics of this system are compared to typical characteristics of other oscillators in Fig. 7 (Vessot, Ref. 15). Note that statistical descriptions of the Rb-gas-cell-controlled crystal oscillators and of the crystal oscillator have been obtained by removing linear drift of frequency.

The high stability of the maser results from the storage-bulb technique that is used to confine ground-state hydrogen atoms in the upper hyperfine level, allowing them to interact with RF resonance radiation within a cavity for intervals of 1 s or longer. During this time, the atoms are coherently stimulated and deliver their energy to the cavity, sustaining the level of RF field if a sufficient flux of atoms enters the bulb.

The device is a self-oscillator at 1.4 GHz with a linewidth given by πT_T^{-1}, where T_T is total effective storage time of the bulb. Normally, the oscillator Q is in the order of 10^9.

Figure 8 is a schematic diagram of the maser and shows the energy levels of atomic hydrogen as a function of magnetic field strength. A cutaway view of the compact maser for space applications is shown in Fig. 9. In brief, the maser operates as follows. Molecular hydrogen is fed to an RF discharge dissociator, and the dissociated molecules are collimated into a beam of hydrogen atoms directed into a vacuum system along the axis of a hexapole magnet. Atoms in the $F = 1$, $M_F = 0$, and 1 states are focused into the storage bulb through a small, well-collimated hole. Atoms

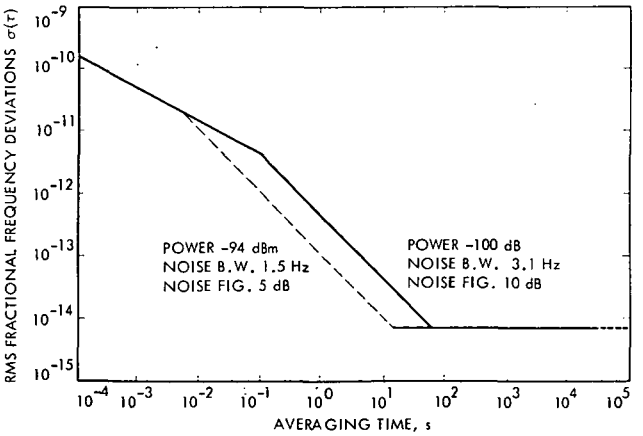

Fig. 7. Stability of hydrogen maser as a function of averaging time

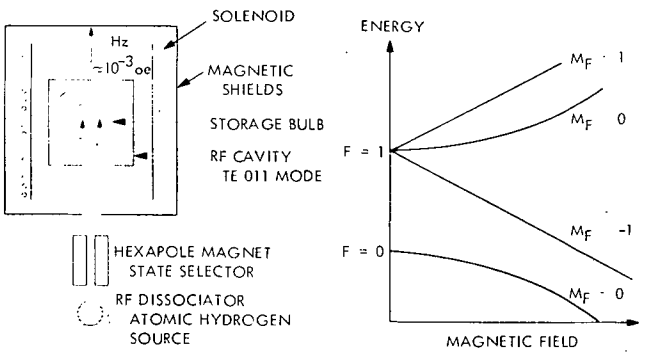

Fig. 8. Schematic diagram of maser and ground-state energy levels of atomic hydrogen

in the other two states are deflected away from the beam axis. The storage bulb confines the atom in an unperturbed way in the in-phase region of the RF magnetic field of a circular E-mode resonant cavity. Upper state, $M_F = 0$, atoms are stimulated to radiate their energy during their stay in the bulb and leave the bulb eventually to be scavenged by the ion pump. When the power available from the atoms in the bulb exceeds the cavity losses and the power coupled out, the maser oscillates.

Normally the output power is about -97 dBm and the signal is used to control the phase of a crystal oscillator. In this way, signal outputs at useful frequencies can be generated. More detailed descriptions of the maser and its associated electronics are available in the listed references.

The stability of the maser is limited by thermal noise whose frequency components lie within the linewidth of the oscillator and by additive noise that competes with the output signal in the bandwidth of the phase-lock system. The expression relating the maser stability to the noise within the linewidth of the oscillator and within the bandwidth of the receiver is given by Cutler and Searle (Ref. 16):

$$\sigma(\tau) = \left[\frac{kT}{2P}\left(\frac{F\omega_B Q_e}{\omega_0^2 \tau^2 Q_c} + \frac{1}{Q_c^2 \tau}\right)\right]^{1/2} \qquad (6)$$

Here, $\sigma(\tau)$ is the fractional rms frequency deviation averaged over a time interval τ, kT is the thermal noise power per unit bandwidth, ω_B is the receiver half-bandwidth (single tuned bandpass), P is the power delivered to the cavity by the atoms, Q_e is the atomic line Q, and Q_c and Q_e are the loaded cavity and external cavity Q, respectively.

The ultimate limit to the maser stability for long time intervals ($\tau > 10^4$ s) is imposed by variations in the resonance frequency of the cavity that are usually of thermal origin. The cavity mistuning "pulls" the output frequency by the ratio of the cavity Q to the line Q times the amount of the mistuning. Normally this ratio is about 10^{-5}, so a 10 Hz change in the cavity causes a 10^{-4} Hz change in the output (or 7 parts in 10^{14}). The

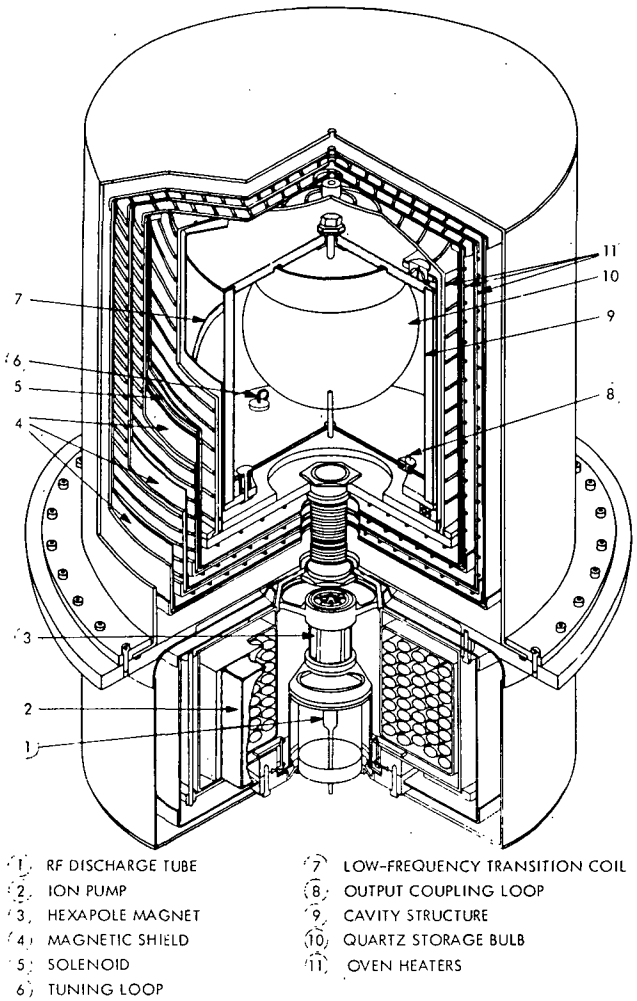

Fig. 9. Cutaway view of NASA maser

cavity frequency variations have been found to have a f^{-1} spectral density, evident from the flattening out of the $\sigma(\tau)$ plot of Fig. 7 (Ref. 17).

It is possible to improve long-term stability at the expense of short-term stability by increasing the storage time of the bulb. This is accompanied by a reduction in the output power from the maser and a corresponding worsening in the short-term stability that goes as $P^{-1/2}$. The tradeoff of short- versus long-term stability is shown in Fig. 10 for several values of the total bulb relaxation rate γ, which is the reciprocal of the effective bulb-storage time.

Several processes limit the storage time in the maser bulb (see References). Recent studies at Harvard and at the Smithsonian Astrophysical Observatory (SAO) on specially prepared polytetrafluorethylene (PTFE-Teflon) surfaces inside the storage bulbs have shown that 10^5 or more collisions with the bulb surface can occur before the atom loses phase with the RF field in the cavity. With bulb sizes now in use, this means that storage times approaching 10 s should be possible; and with the usual type of cavity and thermal controls, values of the rms frequency stability will approach 1 part in 10^{15} for averaging times of 10^3 s.

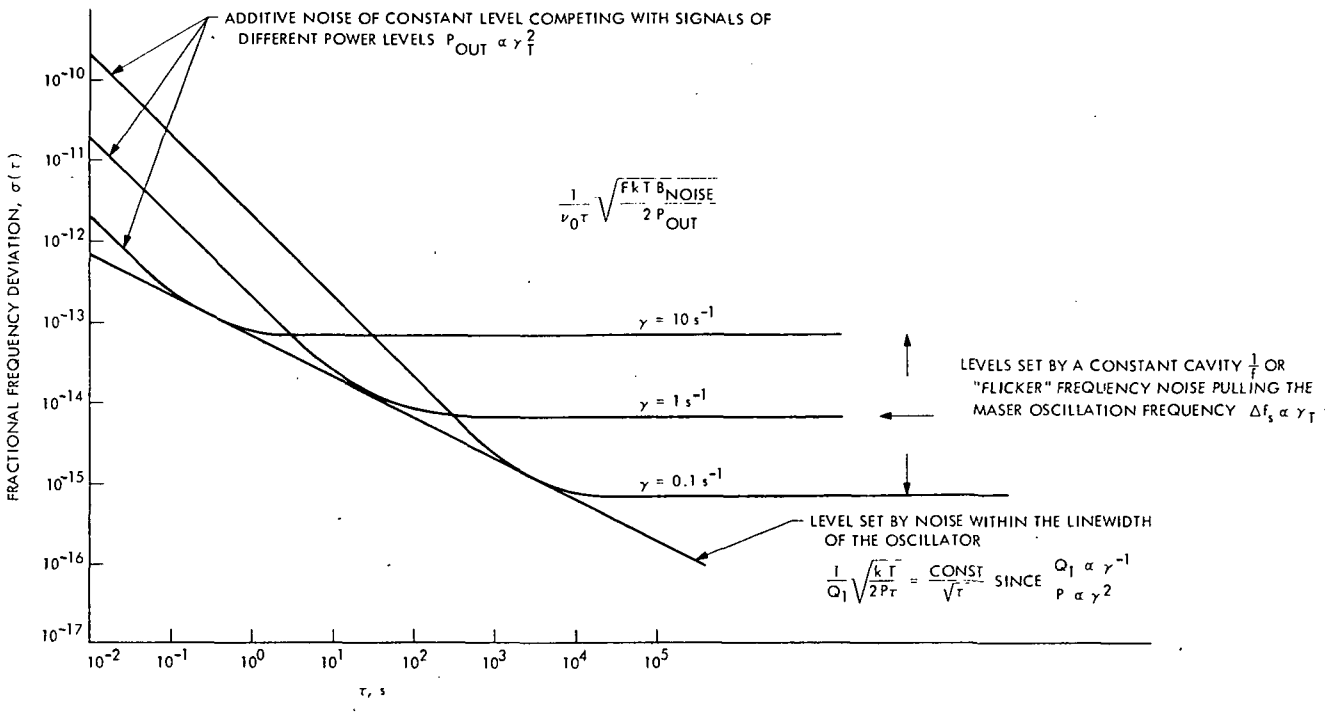

Fig. 10. Maser stability showing influence of total bulb relaxation rate at long and short averaging times

Experiments to verify this expectation are in progress at SAO.

The accuracy of the output frequency from the hydrogen maser is limited by the ability to determine (1) the magnetic field in the bulb, (2) the second-order doppler shift of the atoms in the bulb (which is related to the bulb temperature), (3) the amount of systematic residual mistuning, and (4) the systematic average phase shift per collision of the stored atoms with the walls of the bulb (wall shift). These effects are discussed in detail in Refs. 18, 19, and 20 and will be reviewed only briefly here.

A. Magnetic Field

The average field in the bulb is determined by observing the quenching of the maser output when a resonance transition is caused between the F = 1 magnetic sublevels. These transitions have a frequency dependence of 1.4 MHz/gauss, and using this resonance, the field can be measured to better than $\pm 3 \times 10^{-6}$ gauss. Since the field dependence of the $0 \rightarrow 0$ transition is described by $\Delta\nu_M = 2750 \langle H^2 \rangle_b$, the mean square value of the field over the bulb volume is required. Because gradients in the magnetic field can be observed through the effect of magnetic quenching of the output signal, we can trim the magnetic field, using separate coils in the solenoid so that $\langle H \rangle_b^2 - \langle H^2 \rangle_b$ is very small. An upper bond on the estimate of inaccuracy due to this is a few parts in 10^{14}.

B. Second-Order Doppler

The second-order doppler frequency shift is due to the thermal motion of the atoms in the storage bulb. Since each atom in the bulb makes a large number of collisions, the atoms are in thermal equilibrium with the bulb. The expression describing the shift is

$$\Delta\nu_T = -\nu_0 \frac{3kT}{2mc^2} = -1.9557\ T$$

where ν_0 = 1.4204 GHz, k is Boltzmann's constant, T is in kelvins, c is the velocity of light, and m is the mass of the hydrogen atom. Measurement of the bulb temperature to an accuracy of ±0.25°K at 320°K allows a determination of $\Delta\nu_T/\nu_0$ to about 3 parts in 10^{14}.

C. Cavity Mistuning

Cavity mistuning, as described earlier, will "pull" the output frequency, and a systematically mistuned cavity can be a source of inaccuracy in the output frequency of the maser. A part of the NASA contract that lead to the development of the maser shown in Fig. 9 consisted of the invention and development of an automatic cavity tuning servo system.

The exact expression for the effect of cavity mistuning (Ref. 21) is

$$\Delta\nu_s = \left(\frac{\Delta\nu_{cavity}}{\nu_0} Q_c - BT^{1/2}\right)\frac{1}{\pi}\nu_T \qquad (7)$$

where B is a constant that depends on the bulb and the cavity and on the cavity-bulb geometry, T is

in kelvins, and γ_T is the total relaxation rate of the atoms in the bulb.

The $BT^{1/2}$ term results from shifts in frequency due to hydrogen-hydrogen collisions. This effect is described by Bender (Ref. 22). Crampton et al. (Ref. 21) have shown that the shift is proportional to the linewidth, and by use of the spin-exchange quenching tuning method described below, the shift is eliminated.

Spin-exchange collisions occur among the atoms in the storage bulb and produce pressure-dependent relaxation among the energy levels in the hydrogen atom. This relaxation process, negligible under normal operating conditions, can be used to modulate the total relaxation rate γ_T. If the quantity in parentheses in Eq. (7) is not zero, there will be a modulation in $\Delta\nu_s$ whose magnitude and phase are in proportion to the magnitude and sign of the bracketed quantity. The automatic cavity tuning servo consists of a synchronous detection system to observe the variations in the output frequency due to $\Delta\nu_s$ and to correct the cavity resonance frequency so that $\Delta\nu_s$ is nulled.

The cavity itself is made of CER-VIT and is compensated, by use of re-entrant posts of an alloy with a high-expansion coefficient, to remove the variations in dielectric loading of the fused silica bulb due to the temperature dependence of its dielectric constant. The temperature coefficient of the cavity resonance frequency has been reduced to 100 Hz/°C. With thermal control within limits of $\pm 1 \times 10^{-2}$°C, the resultant output-frequency variations due to the cavity can be maintained below 1 part in 10^{14}.

The fractional frequency stability between two masers operating with automatic tuning systems has been measured to be 2×10^{-14} for averaging times of 4×10^4 (1/2 day) (Ref. 23). Thus, for a single maser, the stability can be estimated to be $2/\sqrt{2} \times 10^{-14}$, or 7 parts in 10^{15} for the above averaging time.

The accuracy of the automatic-tuning technique depends on the type of tuning reference oscillator used and on the time allowed for the servo to operate. When a second hydrogen maser is employed as a tuning reference, less than 1 h is necessary for an accuracy of about 1 part in 10^{13} to be accomplished. Since no systematic effects on the accuracy of the maser output frequency have thus far been attributable to the tuning procedure, the accuracy of the tuning should approach the stability of the tuning, although this remains to be proved experimentally.

D. Wallshift

The systematic average phase shift per wall collision has been the chief limitation in the intrinsic accuracy of the hydrogen maser. Variations in the wallshift determined at several laboratories have led to differences of some 5 parts in 10^{12} in the maser output frequency. Since the wallshift depends on the collision rate of the atoms in the bulb, the texture of the Teflon wall surface is an important consideration in a determination of the surface-to-volume ratio of the bulb. It is difficult to reproduce the same texture of the Teflon from one bulb to another. During the last year, there has been considerable activity investigating the properties of Teflon surfaces. Zitzewitz at Harvard (Ref. 24) found that the phase shift per collision for FEP Teflon* could be made to cross through zero from negative to positive at about 110°C, a function of increasing wall-coating temperature. Vessot and Levine (Ref. 25) at SAO found that for high-molecular-weight PTFE surfaces sintered and rapidly quenched, a zero wallshift temperature of 83°C could be obtained that was independent of the surface-to-volume ratio of the bulb. Brenner (Ref. 26) suggested using a deformable bulb to vary, by a known amount, the surface-to-volume ratio of the bulb, thus allowing a determination of the wall shift of the coating in a particular bulb. This method was successfully demonstrated by Debely (Ref. 27), using a cylindrical bulb whose conical end, made of thin flexible Teflon and stretched inside or outside the cylinder, would determine two easily calculable bulb volumes with the same surface.

Since the zero wallshift temperature is independent of the collision rate, knowledge of the collision rate is no longer required if the correct temperature can be determined. Recently, we suggested that the flexible bulb also be used to vary the collision rate in order to determine the temperature at which there is no collision-rate dependence on the wallshift. We have described a servosystem that accomplishes this automatically (Vessot and Levine, Ref. 28).

Recent measurements by SAO and the National Bureau of Standards of PTFE surfaces applied in a reasonably standardized way have given agreement to 5 parts in 10^{13} in the maser frequency (Ref. 29).

E. Summary of Present Maser Capability

The intrinsic accuracy of the maser can be estimated from the rms of the several accuracy limitations:

$$\Delta\nu_{temp}/\nu_0 \simeq 3 \times 10^{-14}$$

$$\Delta\nu_{mag}/\nu_0 \simeq 3 \times 10^{-14}$$

$$\Delta\nu_{cav}/\nu_0 \simeq 1 \times 10^{-13}$$

$$\Delta\nu_{wall}/\nu_0 \simeq 5 \times 10^{-13}$$

$$\text{Accuracy } \Delta\nu_{rms}/\nu_0 \simeq 5.1 \times 10^{-13}$$

The precision of resettability can be estimated from the rms of the parameters that vary with time:

$$\Delta\nu_{temp}/\nu_0 \simeq 3 \times 10^{-14}$$

$$\Delta\nu_{mag}/\nu_0 \simeq 3 \times 10^{-14}$$

$$\Delta\nu_{cav}/\nu_0 \simeq 1 \times 10^{-13}$$

$$\text{Resettability precision } \Delta\nu_{rms}/\nu_0 \simeq 1.1 \times 10^{-13}$$

*Hexafluoropropylene-polytetrafluoroethylene copolymer.

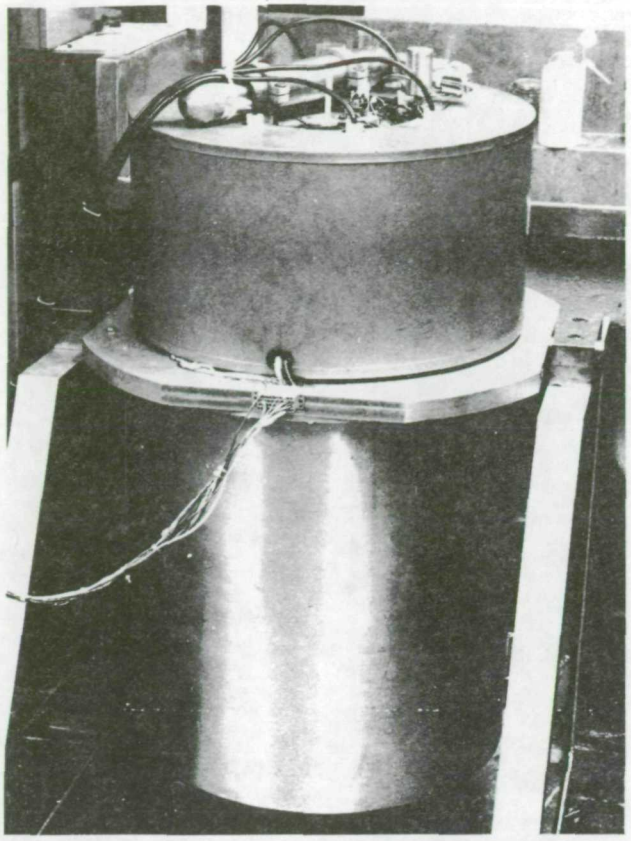

Fig. 11. Photograph of NASA maser developed for satellite use

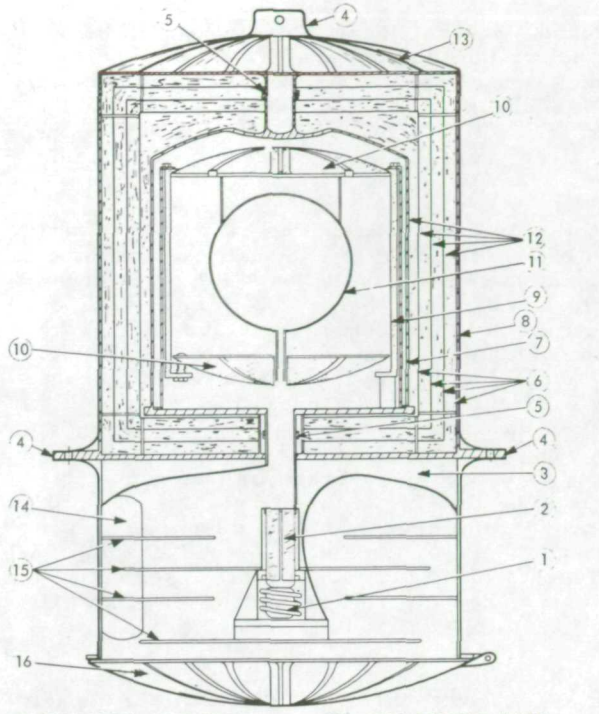

Fig. 12. Lightweight maser based on existing design concepts

The fractional frequency stability of the maser is 7×10^{-15} for averaging time intervals from 100 to 4×10^4 s.

We see that for an unmodulated gravitation experiment, for example a circular orbit, the accuracy of the measurement will depend on the magnitude of the shift (see Fig. 1) and the precision of resettability of the clock. Prior to launch, the satellite clock and ground clock would have been compared. For those clocks not included in this preflight calibration the experiment accuracy is limited by the accuracy of the clocks.

The advantage of using an eccentric orbit results from the excellent stability of the maser and the fact that the measurement can be repeated many times, as long as the satellite is operating. We must, however, be certain that there are no systematic frequency shifts that are synchronized with the orbital period.

V. Maser Configurations, Weight, and Power Estimates

Since 1960, a continuous development of hydrogen masers has been under way with NASA's support. In 1966, NASA supported the development of a small, relatively lightweight maser system for use in spacecraft. The maser oscillator of this system is shown in Fig. 11; the automatic tuner system, phase-lock synthesizer, thermal controls, pressure controls, and RF dissociator have been successfully operated in breadboard form. The cavity and bulb assembly was vibration tested in the sine sweep mode; it successfully survived such tests in all three axes. The complete structure shown in Fig. 11 weighs about 112 kg and requires about 30 W to operate; it is about 81 cm high and 48 cm in diameter.

The vacuum of space can profitably be used in place of the ion pump to scavenge the expended hydrogen. A considerable reduction in weight and power will result from use of multilayer, reflecting insulation under vacuum to replace the microballoon foam insulation currently used to surround the bell jar and ovens. The total weight of the maser can be reduced to about 34 kg, and its power to about 10 W. A sketch of this lightweight maser is shown in Fig. 12. The design concepts of this maser are similar to those of the self-contained unit. Some changes in operation are required, however. Before launch, the maser will be operated by use of a titanium sublimation pump located inside the hatch cover. This system will enable ground comparisons and preflight testing to be conducted.

During launch, the maser will be shut down; later, in orbit, it will be restarted and the cavity

retuned. Several hours of operation will be possible before the titanium evaporated just before launch is used up, and this will allow preliminary system checks. The hatch will be opened to the void of space as soon as the satellite outgassing in the direction of the pump reaches an acceptably low level.

Contamination streaming back into the maser will be kept to a low level by baffles, and the contamination entering the bulb, if it has not been adsorbed on the metal baffles, is very unlikely to attach itself to the Teflon-coated interior of the bulb, which will be maintained at 83°C. In view of the even slight possibility of wallshift changes due to contamination, a test of the continued accuracy of the maser can be made by comparing the average frequency over several orbits early in the experiment with the average frequency at a later time. The stability of the maser, over 4×10^4 s averaging time intervals, would be negligibly affected by bulb-contamination processes that slowly and monotonically could shift the maser output frequency. The data from redshift modulation will continue to be available.

Other, more compact, maser configurations are possible with the use of dielectric or capacitive loading of the RF cavity to reduce its size. Experiments are in progress at SAO* on a spherical, fused-silica, dielectrically loaded cavity 20.3 cm in diameter with an inside diameter of 12.7 cm. The features of spherical geometry and the integral bulb make a very rugged, compact unit. The original proposal to NASA for a satellite-borne maser (Ref. 30) included this cavity. Development and procurement of this cavity proceeded until 1966, when the emphasis on light-weight and low-power consumption was changed to that of pressing for the greatest possible precision of resettability and stability. The cavity was taken over by the USAECOM and successfully used in a maser (Ref. 31). The recent improvements on wall coatings and the desire for a compact lightweight device suitable for a wide range of vehicles bring this design back into prominence. Figure 13 shows the maser with a spherical cavity.

VI. Conclusion

The proposed gravitational redshift experiment described in this paper makes use of technology currently available. Since 1964, when the original proposal was submitted to NASA, the hydrogen-maser clock has been under continuous development for its use in spacecraft, and the feasibility of a lightweight, low-power device has been demonstrated.

Plans for the experiment have evolved considerably. In 1968, the George C. Marshall Space Flight Center completed a Preliminary Program-Development Plan for a Hydrogen-Maser Relativity Satellite, which envisioned a 2700-lb (approximately 1000 kg) satellite containing two masers requiring a total of 1200 W. This satellite would be launched by a Titan IIIC booster into a synchronous, circular orbit. Its objective would be the measurement of the redshift with an accuracy of about 500 parts per million.

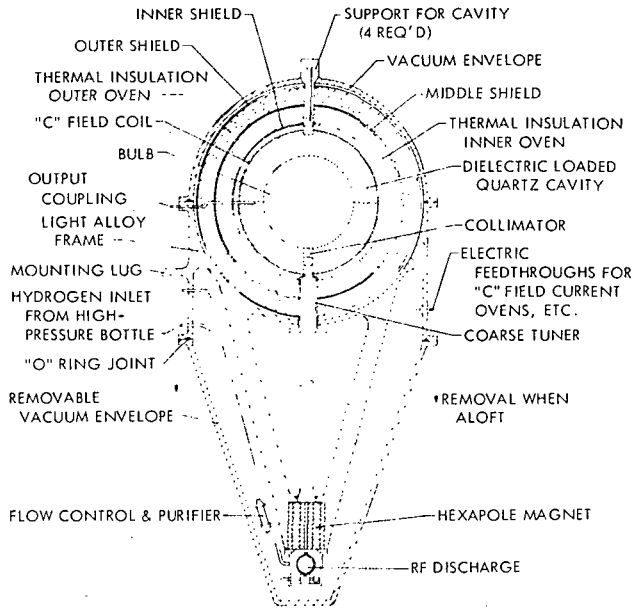

Fig. 13. Hydrogen maser using a dielectrically loaded spherical cavity

Since 1968, the precision and stability of the maser clock have been substantially improved, largely as a result of continuing NASA support for maser development. Also, the use of an eccentric orbit, where the satellite scans back and forth through large differences in the earth's gravitational potential, has made it possible to utilize the maser's excellent frequency stability to good advantage. The present concept of the satellite clock experiment will give much better accuracy at substantially lower cost. A total satellite weight of 500 lb (187 kg), consisting of the maser, its electronics, a transmitter-transponder, batteries, and solar panels, is now possible. The thrust-augmented Thor-Delta vehicle can launch this payload into an eccentric orbit.

The previously mentioned limits to eccentricity, imposed by the desire to keep the satellite constantly in sight of the ground station, can be relaxed, thus giving a larger gravitational modulation. Since a satellite with a 24-h period in a highly eccentric orbit cannot be observed both at perigee and at apogee from a single ground station, a different period should be used, allowing a ground station to track all phases of the orbit over a period of time, though not continuously. A further advantage to this highly eccentric orbit is that more than one ground station can independently participate in the experiment. The limit on eccentricity is probably imposed by the requirement that the satellite be in sight of a particular station long enough to allow 1 h or longer of phase tracking of the doppler-corrected carrier. At the 2.5-GHz carrier frequency, assuming about 10° of phase resolution, the system should allow each measurement to be made to the limits of the clock stability. At present, there are several tracking stations already equipped with hydrogen masers that, with a modest amount of additional equipment, can be used to track the satellite maser signals. Studies

*Supported in part by contract DAAB07-70-C-A-A108 from the U.S. Army Electronics Command, Ft. Monmouth, New Jersey.

on weight, power, orbits, and booster capability are continuing.

We believe that an accurate test of the equivalence principle for clocks in space is a necessary phase of the continuing space program and that this test, successfully performed, will not only advance our knowledge of science but also open new fields of technology that will be of value to our exploration of the universe.

References

1. Einstein, A., Jahrb. Radioakt. u. Elektronik, 4, 411, 1907.
2. Roll, P. G., Krotkov, R., and Dicke, R. H., Ann. Phys., 26, 442, 1964.
3. Ramsey, N. F., Molecular Beams, Oxford Univ. Press, 1956.
4. Winterberg, F., Astronautica Acta, 2, 25, 1956.
5. Singer, S. F., Phys. Rev., 104, 11, 1956.
6. Hoffman, B., Phys. Rev., 106, 358, 1957.
7. Refsdal, S., Phys. Rev., 124, 996, 1961.
8. Pound, R. V., and Rebka, G. A., Jr., Phys. Rev. Letters, 4, 337, 1960.
9. Pound, R. V., and Snider, J. L., Phys. Rev., 140, B788, 1965.
10. Kleppner, D., Vessot, R. F. C., and Ramsey, N. F., Astrophys. Space Sci., 6, 13, 1970.
11. Gaposchkin, E. M., and Lambeck, K., Smithsonian Astrophys. Obs. Spec. Rep. No. 315, 1970.
12. Köhnlein, W., Smithsonian Astrophys. Obs. Spec. Rep. No. 198, 1966.
13. Kleppner, D., Goldenberg, H. M., and Ramsey, N. F., Phys. Rev., 126, 603, 1962.
14. Goldenberg, H. M., Kleppner, D., and Ramsey, N. F., Phys. Rev. Letters, 5, 361, 1960.
15. Vessot, R. F. C., Hewlett-Packard Journal, p. 15, Oct. 1968.
16. Cutler, L. S., and Searle, C. L., Proc. IEEE, 54, 136, 1966.
17. Barnes, J. A., et al., NBS Tech. Note 394, Washington, D. C., 1970.
18. Vessot, R. F. C., and Levine, M. W., "Proceedings of 24th Annual Symposium on Frequency Control," U.S. Army Electronics Command, Ft. Monmouth, N.J., Apr. 27-29, 1970.
19. Vessot, R. F. C., et al., IEEE Trans. Instr. Meas., IM-15, 165, 1966.
20. Vessot, R. F. C., et al., "Proceedings of International Conference on Precision Measurement and Fundamental Constants," National Bureau of Standards, Gaithersberg, Md., Aug. 3-7, 1970.
21. Crampton, S. B., Kleppner, D., and Ramsey, N. F., Phys. Rev. Letters, 11, 338, 1963.
22. Bender, P. L., Phys. Rev., 132, 2154, 1964.
23. Risley, A. S., et al., "Conference on Precision Electromagnetic Measurements," National Bureau of Standards, Boulder, Colo., June 1970.
24. Zitzewitz, P. W., Uzgiris, E. E., and Ramsey, N. F., Rev. Sci. Instr., 41, 81, 1970.
25. Vessot, R. F. C., and Levine, M. W., Meteorologia, (in press).
26. Brenner, D., Bull. Amer. Phys. Soc., 14, 943, 1969.
27. Debely, P., Rev. Sci. Instr., 41, 1290, 1970.
28. Vessot, R. F. C., and Levine, M. W., NASA Disclosure HQN-10654, 1970.
29. Hellwig, H., Vessot, R., Levine, M., Zitzewitz, P., Allan, D., and Glaze, D., IEEE Trans. Instr. Meas., IM-19, Nov. 1970.
30. Vessot, R. F. C., Kleppner, D., and Ramsey, N. F., "Atomic Hydrogen Maser for Space Vehicle Applications," Varian Associates Proposal BP 812-64-09, Oct. 30, 1964.
31. Hellwig, H., and Pannaci, E., J. Appl. Phys., 39, No. 12, 5496, 1968.

Recent Developments Affecting the Hydrogen Maser as a Frequency Standard *

R. F. C. Vessot and M. W. Levine

Smithsonian Astrophysical Observatory and Harvard College Observatory, Cambridge, Mass. 02138

and

P. W. Zitzewitz, P. Debely,*** and N. F. Ramsey**

Lyman Physics Laboratory, Harvard University, Cambridge, Mass. 02138

The processes limiting the accuracy and stability of hydrogen-maser frequency-standard systems are described. Recent developments of the maser systems in the following areas are discussed:

(1) The temperature dependence of wall shifts.
(2) The use of the zero wall-shift temperature to eliminate the wall shift.
(3) The deformable storage bulb technique for varying the wall-collision rate.
(4) The large-bulb maser.
(5) Electronic phase-lock systems and cavity-tuning servos.

Key words: Accurate frequency standards; accurate time standards; frequency stability; maser oscillators; oscillator phase locks; quantum electronics.

1. Introduction

1.1. Description of the Maser

The atomic hydrogen maser was invented in 1960 by Goldenberg, Kleppner, and Ramsey [1]. Since this time, the maser has been under continual development as a frequency standard. At present, when used to control a crystal oscillator with a phase-lock system, it has been found to exceed that of all other known systems for sampling periods ranging up to at least 10^4 s.

Figure 1a shows a schematic diagram of the maser; figure 1b, the energy levels of atomic hydrogen; and figure 1c, a cutaway drawing of a compact maser oscillator packaged in a cylindrical form 20 inch in diameter and 32 inch in length. The hydrogen maser is the first successful maser to use a confining technique to keep a constantly replenished group of state-selected atoms in a region of rf field. The stored atoms, interacting with their rf magnetic field at their resonance frequency, are stimulated to emit continuous radiation. When this radiation is strong enough to sustain a coherent rf magnetic field at a high enough level, the system becomes self-oscillating. In practice, the atoms are stored in a bottle located so that it occupies a volume of rf magnetic field of nearly constant phase and direction in a resonant cavity.

Limitations in the stability and accuracy of the maser arise from several causes. The fundamental stability limitations are imposed by the oscillator line width, thermal noise within the line width, and thermal noise within the bandwidth of the equipment receiving the maser signal. Further stability limitations arise from systematic effects that perturb the oscillator frequency.

Accuracy limitations arise from incomplete knowledge of the magnitude of four contributions to frequency shift: (1) the magnetic field offset $\Delta\nu_m$, (2) the second-order Doppler shift $\Delta\nu_T$, (3) the effect of cavity mistunings $\Delta\nu_s$, and (4) the effect of atomic-hydrogen collisions with the walls of the storage bottle (wall shift) $\Delta\nu_w$. These shifts, when added to the unperturbed hydrogen hyperfine frequency separation ν_0, give $\nu_{\text{out}}=\nu_0+\Delta\nu_m+\Delta\nu_T+\Delta\nu_s+\Delta\nu_w$, the maser output frequency.

At present, the most uncertain correction is the wall-shift effect.

1.2. Stability Limitations

Stability is restricted by thermal noise. The expression giving the effect of noise-frequency components within the line width of the oscillator and in the bandwidth of the receiver is given by Cutler and Searle [2]:

$$\sigma(\tau)=\left[\frac{kT}{2P}\left(\frac{F\omega_B Q_e}{\omega_0^2\tau^2 Q_{e,l}}+\frac{1}{Q_l^2\tau}\right)\right]^{1/2}. \qquad (1)$$

* This work was supported in part by the National Aeronautics and Space Administration, the National Bureau of Standards, the National Science Foundation, and the Office of Naval Research.

** Currently at the University of Western Ontario, London, Ontario.
*** Currently at the Laboratoires Suisses de Recherches Horlogères, Neuchatel, Switzerland.

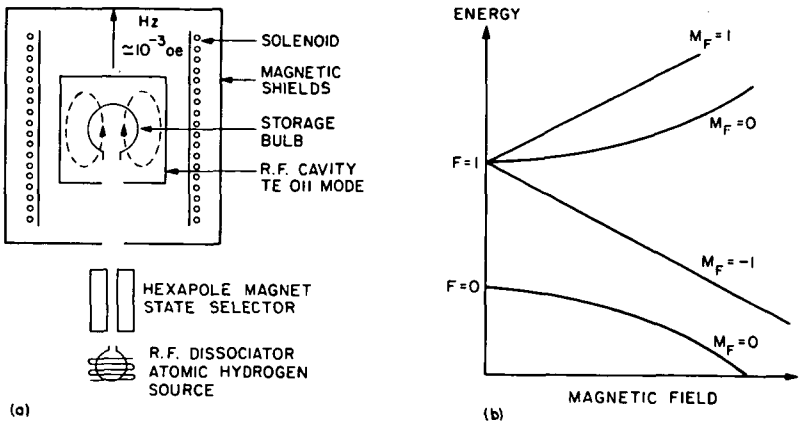

FIGURE 1. *(a) Schematic diagram of the hydrogen maser; (b) energy-level diagram of atomic hydrogen.*

Here, $\sigma(\tau)$ is the fractional rms frequency deviation averaged over a time interval τ; kT is the thermal noise power per unit bandwidth; ω_B is the receiver half-bandwidth (single-tuned band-pass characteristic); P is the power delivered by the atoms to the cavity; Q_l is the atomic line Q given by $Q_l = \omega_0/2\gamma_{2T}$; $Q_{c,l}$ is the loaded cavity Q; and Q_e is the external cavity Q.

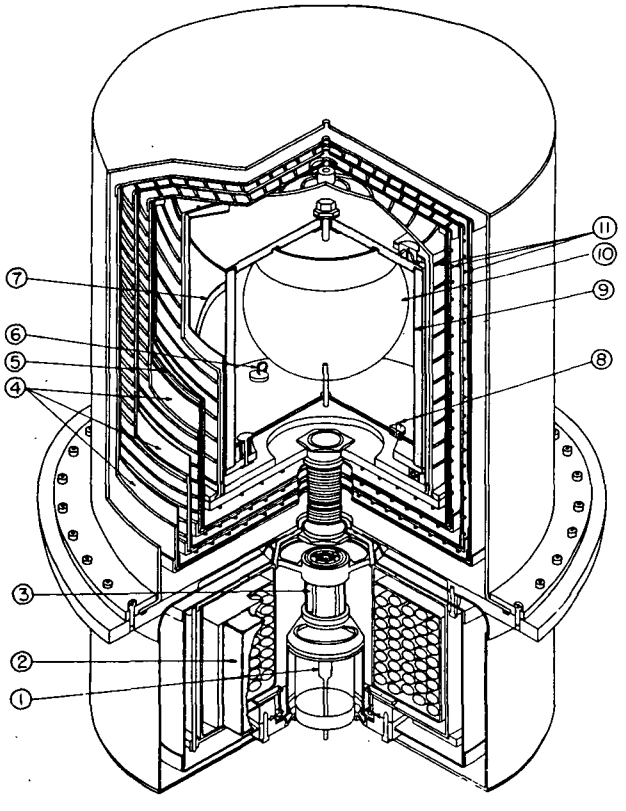

FIGURE 1c. *Hydrogen maser.*
Item 1, rf discharge tube; item 2, ion pump; item 3, hexapole magnet; item 4, magnetic shield; item 5, solenoid; item 6, tuning loop; item 7, low-frequency transition coil; item 8, output coupling loop; item 9, cavity structure; item 10, quartz storage bulb; item 11, oven heaters.

Generally, for $\tau < 30$ s, the first term in eq (1) dominates and the stability function $\sigma(\tau)$ goes as τ^{-1}. At longer periods, the effect due to the second term, resulting from thermal noise within the oscillator line, should dominate. The $\tau^{-1/2}$ behavior thus predicted has not yet been observed because it has been obscured by systematic effects that have leveled off $\sigma(\tau)$ at about 7×10^{-15}. Figure 2 shows the two-sample variance [3] as a function of averaging time τ for the maser. The lower curve shows the theoretical behavior (as described in eq 1) that applies to the maser and to the system used to obtain the data.

The single most important aspect of the storage-bulb maser technique is the ability to store an aggregate of atoms with an average velocity very close to zero in the standing wave of a cavity so that they can interact for an extended period of time, $\Delta\tau$, with the in-phase components of the rf magnetic field in the cavity. The narrow resonance line width $\Delta\nu$ results from the Heisenberg uncertainty principle, $\Delta\nu\Delta\tau \simeq 1$. In the oscillating maser, the narrow resonance line width is electrically equivalent to an oscillator having very high Q; this Q, designated Q_l in eq (1), is proportional to the storage time $\Delta\tau$. The net effective storage time, equal to the reciprocal

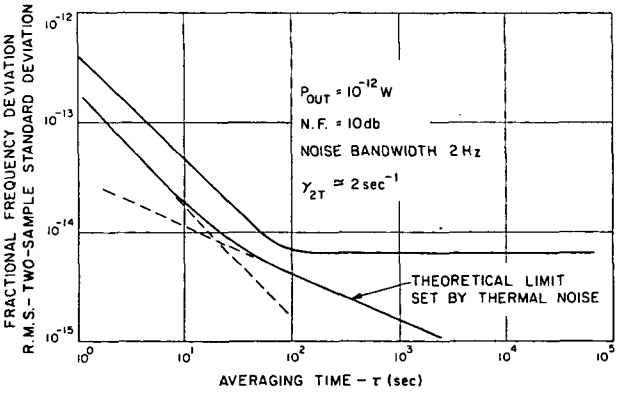

FIGURE 2. *Fractional frequency stability as a function of averaging time.*

of the net relaxation time γ_{2T}, results from a series of relaxation processes that go on in the storage bulb:

$$\gamma_{2T}=\gamma_b+\gamma_{2w}+\gamma_{2se}+\gamma_{2m}, \quad (2)$$

where $\gamma_b=\bar{v}A_aK/4V_b$ is the escape rate of the atoms from the bulb. Here $\bar{v}$ is the average velocity of the atoms, V_b is the bulb volume, A_a is the aperture area, and K is the collimator kappa factor for the entrance-exit hole [4]. Also, $\gamma_{2w}=(\bar{v}/\lambda)w_{2r}$ is the wall-collision relaxation rate, λ is the mean distance between collisions ($=4/3R$ in the case of a spherical bulb), and w_{2r} is the probability of a dephasing collision at the bulb wall. Chemical recombination of hydrogen or chemical interaction with the wall destroys the phase coherence of the atomic oscillating dipole moment with the rf magnetic field and is a dephasing collision.

The spin-exchange dephasing collision rate is $\gamma_{2se}=n\bar{v}_r\sigma$. It depends on the *relative* atomic velocity $\bar{v}_r$, the spin-exchange cross section σ, and the density n of the atoms in the bulb. The term γ_{2m} is the dephasing effect of the dc magnetic-field gradients in the bulb. The oscillation frequency of the coupled electron and proton magnetic-dipole moments has, in the "field independent" transition, a second-order magnetic-field dependence $\Delta\nu_m=2750\bar{H}^2$, where H is the magnetic field. The atom will gain or lose phase with the rf field as it moves in the bulb if the dc magnetic field varies from place to place within the bulb.

Magnetic gradients can also cause transitions among the $F=1$ magnetic sublevels at magnetic fields where the collision rate of the atoms is near the transition frequency of the sublevels.

The strongest limitation on the long-term stability encountered thus far is the effect of cavity mistuning. Since the maser is an active oscillator, the cavity resonance frequency affects the output frequency in proportion to the ratio of the cavity Q to the line Q. This "pulling" effect is described approximately by the expression

$$\Delta\nu_{\text{out}}\approx\Delta\nu_{\text{cavity}}(Q_c/Q_l). \quad (3)$$

In practice, there is a lower limit on the cavity Q set by the requirement that the maser oscillate. An oscillation parameter q, given by Klepper et el. [4], relates the cavity-bulb geometry, the cavity Q, and other constants. The expression for q is

$$q=\frac{\sigma\bar{v}_r\hbar\gamma_{2T}V_c}{8\pi\mu_0^2\gamma_b\eta V_b}\frac{1}{Q}\frac{I_{\text{tot}}}{I},$$

where

σ is the spin-exchange cross section for hydrogen,
$\bar{v}_r$ is the average relative velocity of the atoms,
$\hbar$ is Planck's constant divided by 2π,
μ_0 is the Bohr magneton,
V_c and V_b are the cavity volume and bulb volume, respectively,
Q is the loaded cavity quality factor,
η is $\langle H_z\rangle_{\text{bulb}}^2/\langle H^2\rangle_{\text{cavity}}$, and
I_{tot}/I is the ratio of the total atomic flux to the flux in the desired state.

Here, H_z is the Z component of the rf magnetic field.

For oscillation, the value of q must be less than 0.172.

The threshold flux for oscillation, neglecting spin-exchange processes, is

$$I_{\text{th}}=\hbar V_c\gamma_{2T}^2/4\pi\mu_0^2Q\eta.$$

The power delivered by the beam to the cavity[1] is

$$P=\tfrac{1}{2}(\hbar\omega)I_{\text{th}}[-2q^2(I/I_{\text{th}})^2+(1-3q)(I/I_{\text{th}})-1]. \quad (4a)$$

The maximum power is

$$P_{\max}=(\omega\hbar^2V_c\gamma_{2T}^2/64\pi\mu_0^2Q\eta)[1-(6/q)+(1/q^2)]. \quad (4b)$$

The flux at maximum power is

$$I_{\max}P=(\hbar V_c/4\pi\mu_0^2Q\eta)\gamma_{2T}^2[(1-3q)/4q^2]. \quad (4c)$$

Normally, the loaded cavity Q is about 35,000 and the line Q is about 1.5×10^9, making the ratio Q_c/Q_l about 2×10^{-5}. Thus, a shift of the cavity frequency of about 100 Hz will cause a change of 2×10^{-3} Hz in the output or a fractional frequency shift of about 1.5×10^{-12}.

There are several possible approaches for reducing the effect of cavity "pulling." One is to stabilize the cavity by improving the mechanical and thermal properties of the cavity. Another is to employ a cavity-tuning servosystem using a stable reference oscillator. This servo constantly maintains the cavity near its proper frequency by modulating the line Q and correlating the shifts in frequency with the modulation. The cavity is kept tuned by maintaining the condition that no correlation exist between the modulation and the frequency shifts.

A third approach, involving a fundamental feature of the hydrogen maser, is to extend further the storage time of the atoms in the bulb. At this point, it should be recognized that in the self-oscillating maser, the reduction of the atomic line width is accompanied by a reduction in output power. This results from the γ_{2T}^2 term in the quantity I_{th} in eq (4). The stability at short time intervals is controlled by the first term in eq (1), which gives the τ^{-1} behavior. The power depends on γ_{2T}^2, and the line width on γ_{2T}^{-1}. With $Q_l=\omega/2\gamma_{2T}$, the product of the first term in the brackets and $kT/2P$ is adversely affected and the second term is unaffected. The line width reduction helps directly in the cavity-pulling expression. The effect of varying γ_{2T} on the long- and short-term stability is shown in figure 3. For this family of curves, the maser receiver noise figure and bandwidth are kept constant, the cavity bulb geometry and Q are kept constant, and only γ_{2T} is varied. The contributions from a cavity-mistuning perturbation having a particular $1/f$ or "flicker" frequency spectral density are shown by the horizontal lines for $\sigma(\tau)$ [2], the contributions from additive white phase noise are shown by the τ^{-1} slope in the lines, and the constant limit set by thermal noise within the line is shown by a line with slope $\tau^{-1/2}$.

[1] If the wall-relaxation is due to recombination of atoms.

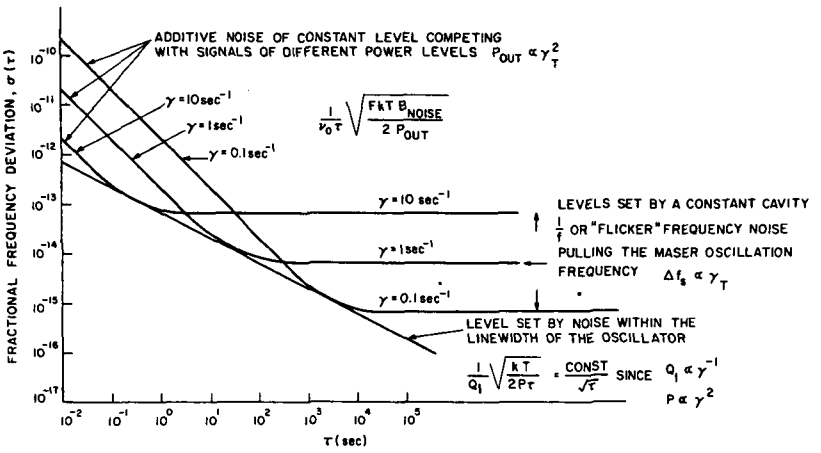

FIGURE 3. *Effect of varying the relaxation rate γ_{2T} in the maser:* $\gamma_1 > \gamma_2 > \gamma_3$.

1.3. Accuracy Limitations

The following four effects cause a bias in the frequency of the maser oscillator. They are systematic shifts, as distinguished from the random effects described above.

A. The magnetic-field behavior of the $F=1$, $m_F=0 \rightarrow F=0$, $m_F=0$ transition shown in figure 1 is described by

$$\Delta\nu_m = 2750\langle H^2\rangle_b,$$

where $\Delta\nu_m$ is in hertz when H is in oersteds.

The squared magnetic field $\langle H^2\rangle_b$ is averaged over the volume of the bulb. To establish the value of $\Delta\nu_m$, the average value of H is determined by externally causing $\Delta m_F = \pm 1$ transitions among the $F=1$ state sublevels and observing the frequency ν_Z at which the maser output is quenched. The average field H in the bulb is obtained by the expression $\langle H\rangle_b = \nu_Z/1.4\times10^6$. Since ν_Z is easily measurable to better than 5 Hz, at the normal operating value of 10^{-3} Oe, the value of $\langle H\rangle_b$ is known to better than $\pm 3\times10^{-6}$ Oe and $\Delta\nu_m$ can be determined to 1 part in 10^{14}. If gradients are present in the bulb, it is not appropriate to use $\langle H\rangle_b^2$ in place of $\langle H^2\rangle_b$. However, the effect of magnetic gradients can be determined and minimized by observing the quenching of the maser through the γ_m term previously discussed. The error in $\Delta\nu_m$ resulting from taking $\langle H\rangle_b^2$ for $\langle H^2\rangle_b$ is about 1 part in 10^{14}, giving an overall error in $\Delta\nu_m$ of a few parts in 10^{14}.

B. The second-order Doppler frequency shift results from the thermal motion of the atoms within the bulb. Since the atoms on the average spend about 0.5 s in the bulb and make in the order of 10^4 collisions with the walls, the temperature of the bulb is taken as the temperature of the atoms. The second-order Doppler shift is given by

$$\Delta\nu_T = -\nu_D(3kT/2mc^2) = -1.9557\times10^{-4}T.$$

Here, k is Boltzmann's constant, T is in Kelvins, c is the velocity of light, and m is the mass of the hydrogen atom. Since we can measure the temperature to better than 0.5 K, the probable error in the second-order Doppler shift is in the order of 5 parts in 10^{14}.

C. The effect of cavity mistuning on the output frequency results from the pulling effect described earlier. There is also a systematic shift due to atom-atom collisions [5]. One can make use of the spin-exchange interatomic collisions to modulate the line Q of the maser for tuning purposes, as described earlier. When this is done, the output frequency is shifted by the pulling process and a systematic shift due to interatomic collisions. Both these processes are proportional to the line width and are described by the expression for the mistuning shift:

$$\Delta\nu_s = \left(\frac{\Delta\nu_{cavity}}{\nu_0}Q_c - \frac{13\sqrt{2}}{32}\frac{\bar{v}\hbar a_0^2 V_c}{Q_c\mu_0^2\eta V_b}\right)\frac{\gamma_{2T}}{\pi},$$

which is a more exact version of eq (3).

If we modulate γ_{2T} by varying the flux into the bulb, we can make the quantity in the brackets zero by adjusting $\Delta\nu_{cavity}$. The density-independent output frequency ($\Delta\nu_s = 0$) resulting from this tuning process in the maser effectively removes the collision shift [6].

The effect of the cavity shift on the accuracy of the maser frequency depends on the type of tuning system used. If the device is constantly being tuned by a servodevice, the value of $\Delta\nu_s$ will have a zero mean value and the value of the stability function $\sigma(\tau)$ will probably vary as $\tau^{-1/2}$ for large values of τ.

If the system is tuned and left alone, the accuracy of the output frequency will depend on the precision of the tuning and the stability of the cavity resonance frequency.

D. The strongest limitation on the accuracy of the maser is due to the fact that the atom, upon collision with the walls, suffers an average phase shift per collision. The collision process can be briefly described by a Van der Waal's potential function with the usual r^{-6} dipole-dipole attractive term and a r^{-12} term due to exchange forces. During its approach to the wall, the atom is polarized and experiences a r^{-6} type of potential, gaining energy until it en-

counters the r^{-12} repulsion due to close-range electron-exchange forces. It is therefore polarized during the time it is in the r^{-6} potential, resulting in a Stark-effect shift in the energy levels and a reduction in the ground-state hyperfine separation. The oscillating atomic dipole is thus retarded in phase with respect to the rf field in the cavity during the r^{-6} portion of its travel. During the repulsive portion of the collision, the electron cloud surrounding the proton can be visualized as being compressed, and during the time the r^{-12} forces are acting, the interaction energy between the proton and the electron is stronger, resulting in an increase in hyperfine separation. The oscillating atomic moment is thus advanced in phase during this part of the collision. It has been found [7] that the either positive or negative phase shift can predominate and that it is possible to establish conditions where an average zero phase shift per collision can be obtained.

The wall shift $\Delta\nu_w$ is usually determined by coating a number of bulbs of different sizes that provide a range of wall-collision rates that is as large as possible. The maser output frequency is then plotted as a function of collision rate. The value obtained on extrapolating to zero collision rate and correcting for magnetic and Doppler effects is taken as the unperturbed hydrogen frequency. The wall shift is related to the phase shift per collision as follows:

$$\Delta\nu_w = (\nu_c/2\pi)\bar{\phi}(T),$$

where ν_c, the average collision rate, equals $3\bar{v}/4R$ for a spherical bulb of radius R. The average phase shift per collision $\bar{\phi}(T)$ is a function of temperature, and $\bar{v} = (8kT/\pi m)^{1/2}$ is the average velocity.

Comparison of wall shifts is most often made by means of the quantity

$$K(T) = \Delta\nu_w D = 3\bar{v}\bar{\phi}(T)/4\pi,$$

where D is the bulb diameter.

2. Wall-Coating Materials and Techniques

The chief limitation in the accuracy of the maser as a frequency standard has been due to the wall shift. Accurate measurement of the wall shift is not easy and has depended on the ability of the experimenter to coat many bulbs in a reproducible manner. The value of the wall shift thus obtained can be applied with confidence only to the bulbs actually measured. Variations between laboratories in the measurement of this parameter have led to differences of some 5 parts in 10^{12} in the maser frequency.

In most cases, the material that has been used for coating the bulbs has been the FEP-120 Teflon dispersion made by duPont. This is a polytetrafluorethylene-hexafluoropropylene copolymer supplied in an aqueous dispersion; it is coated on the inside of the bulb, allowed to dry, and then sintered or fused to form a coating. Various coating processes have been used. However, all are essentially the same and involve burning off the wetting agent by heating in air and then heating to a temperature where the coating is fused to form a slick, clear coating. Adhesion to the inside of the bulb can be improved by roughing the fused silica surface with glass shot and abrasive grit until a ground-glass appearance is obtained.

Early measurements of the FEP material were made by Vanier and Vessot [8]. The wall shift that they gave for this material and that pertaining to the particular set of bulbs used in the measurement was until recently generally accepted as an intrinsic property of the material. This conclusion was wrong, since differences in the surface texture of the material can cause variations in the wall shift from one bulb to another.

Recently, there has been considerable activity in the study of the wall shift, using various types of Teflon bulb coatings. Zitzewitz [9] at Harvard found that Teflon showed a temperature-dependent shift that went from negative to positive, as shown in figure 4. Here, the data are given in terms of phase shift per collision versus temperature. The breaks in the curve, identified by α, β, and γ, are due to transitions in the internal short-range ordering of the molecules analogous to those in glass. Data are shown for two types of Teflon, the FEP copolymer and polytetrafluoroethylene homopolymer (PTFE duPont Teflon 42). The zero phase shift per collision temperature is about 107 °C.

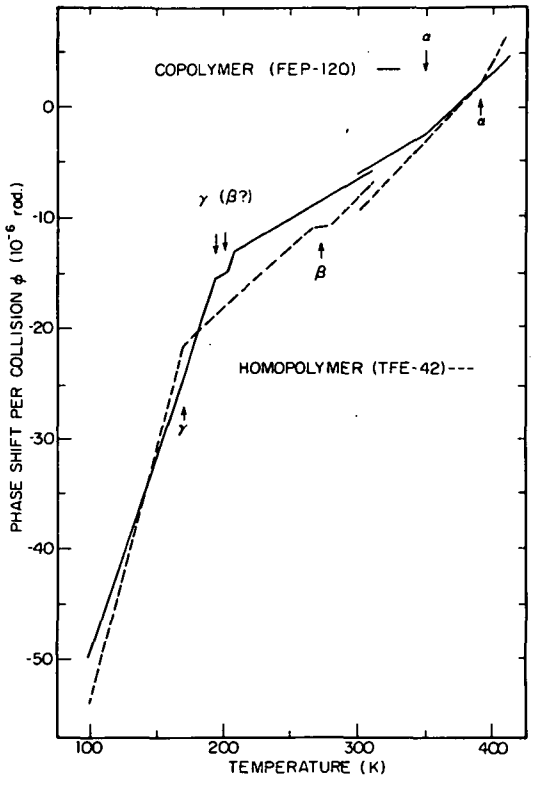

FIGURE 4. *Temperature dependence of phase shift per collision for PTFE and FEP Teflon.*

At the Smithsonian Astrophysical Observatory (SAO), studies on PTFE Teflon have been made by Vessot and Levine [10] using Teflon 42 under various conditions of curing. In these experiments, bulbs having integral collimators and smooth interior surfaces were coated with a single layer of Teflon dispersion. The dispersion consisted of 50 percent Teflon 42, 40 percent water, and 10 percent Triton x-100 (a wetting agent made by Rohm and Haas). The coatings were drained and dried for several hours by a slight flow of dry nitrogen introduced into the bulb through the collimator. The bulbs were sintered for 30 min at 360 °C in a horizontal air-flow oven with a constant flow of dry oxygen entering the bulb. The bulbs were then removed from the oven and quickly cooled in a stream of room-temperature air. It was found that the zero wall-shift temperature was reduced to 83 °C and that the wall-relaxation rate appeared to be very low. Very good reproducibility of phase shift per collision as a function of temperature was obtained for several bulbs.

The temperature slope of the phase shift per collision for the quickly cooled (quenched) PTFE was found to be 0.15 ± 0.004 μrad/°C. When the bulb was annealed in oxygen at a rate of 0.05 °C/min from 340 to 295 °C, the temperature slope decreased to 0.09 ± 0.01 μrad/°C and the intercept temperature went up to 142 °C. Zitzewitz gives values of 0.1294 and 0.1248 for the slope and a zero wall-shift temperature of 107 °C. For a recent experiment, he reports confirmation of the lower (83 °C) temperature at which the phase shift per collision is zero for a quenched PTFE-coated bulb.

With the same PTFE sample as that used by the SAO and Harvard groups, Hellwig at the National Bureau of Standards (NBS) made wall-shift measurements. His data taken at 24 °C gave a value of the wall-shift parameter K very close to the SAO value at the same temperature:

$$K_{\mathrm{NBS}} = 0.528 \text{ Hz cm}$$
$$K_{\mathrm{SAO}} = 0.522 \text{ Hz cm} \qquad \text{at } 24\ ^\circ\mathrm{C}.$$

To relate the values of the unperturbed hydrogen frequency among the laboratories at Harvard, SAO, and NBS and to give this frequency in terms of the ^{133}Cs hyperfine frequency that serves as the definition of the second, the SAO group undertook to make a traveling maser frequency-standard experiment. This work, reported by Hellwig et al. [11], gives the following new value for the unperturbed hydrogen hyperfine separation frequency in terms of the NBS cesium standard:

$$\nu_0 = 1\ 420\ 405\ 751.768 \pm 0.003 \text{ Hz}.$$

This value is in disagreement with that obtained by Vessot et al. [12] in 1965, who gave

$$\nu_0 = 1\ 420\ 405\ 751.7864 \pm 0.0017 \text{ Hz}.$$

The reasons for the difference are difficult to assess. Retrospective corrections for possible wall-shift errors in hydrogen and for possible errors in the frequency of the cesium devices have failed to close the gap between the two numbers and their error estimates.

In the present determination of the value of ν_0, the agreement in the unperturbed hydrogen frequency among all three laboratories is within ±0.002 Hz, or about ±1.4 parts in 10^{12}.

In summary, the PTFE wall-coating material appears to offer several advantages in performance over the FEP preparation:

A. The molecular weight of PTFE is larger by a factor of about 10 than that of FEP. The number of Teflon molecular-chain end groups for a given volume of material is thus reduced. The presence of atoms other than fluorine on the walls will cause different values of average phase shift per collision.

B. The relaxation rate associated with hydrogen collisions appears to be lower for PTFE than for FEP, especially between 50 and 100 °C. From preliminary measurements of relaxation rate, it appears possible to extend the storage time to about 5 s. This would substantially reduce the linewidth of the maser. The substance can be made highly crystalline, a property that reduces surface porosity and should further extend the storage time of the maser.

C. Structure does not change near the temperature at which the phase shift per collision is zero.

D. From recent data determined by different experimenters, wall-shift measurements appear more reproducible with PTFE than with FEP.

3. Elimination of the Wall Shift

The existence of a reasonably low operating temperature at which the wall shift goes to zero and at which the wall-relaxation rate is small makes possible a new method of measuring the wall shift.

Since the wall shift can be independent of the

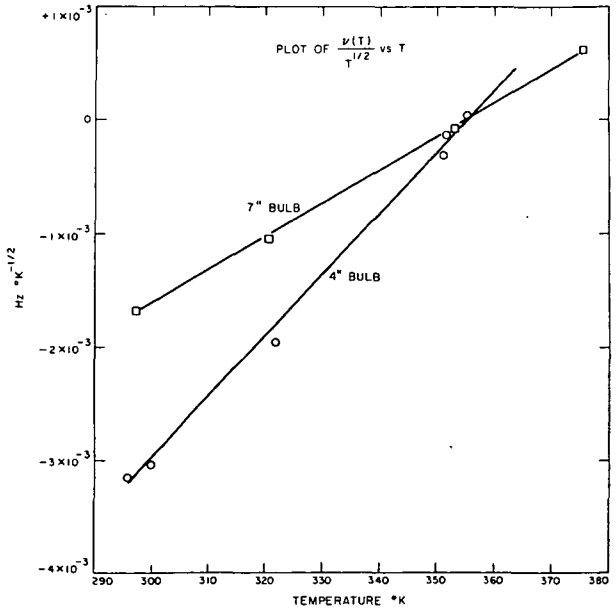

FIGURE 5. *Plot of* $\nu(T)/T^{1/2}$ *vs* T.

collision rate only when the average phase shift per collision is zero, it is not necessary to know the collision rate to obtain the zero shift temperature. One need only operate a maser with bulbs having different collision rates and determine the temperature at which the output frequency is the same. By obtaining the output frequency at this temperature the only further requirement for eliminating the wall shift is that the wall-coating material be the same for all bulbs.

Figure 5 shows wall-shift data taken at SAO [10] with a 4 in-diam bulb and a 7 in-diam bulb and plotted in terms of $\Delta\nu_w/T^{1/2}$. The division by $T^{1/2}$ removes the effect of the temperature dependence of the velocity of the atoms and makes the data linear and the intercept easier to compute. The intercept of the two resulting straight lines is well defined and gives a value of the unperturbed hydrogen frequency with an error $(0.2\pm1.1)\times10^{-3}$ Hz when related to the value obtained in the Harvard-NBS-SAO comparison reported earlier [11].

4. The Flexible Bulb

To overcome the uncertainties associated with the use of several separate bulbs to determine the wall shift, Brenner [13] suggested the use of a single flexible storage bulb that would allow the collision rate to be changed by a known amount without changing the nature of the surface. Recently, Debely [14] at Harvard conducted experiments on a maser using an open-end cylinder with a flexible cone at the other end that could be pushed into or pulled out of the cylinder to change the storage volume. This storage vessel is shown in figure 6. The movable part was made of a thin film of the FEP-120 copolymer that was also used to coat the bulb and the collimator. The ratio of maximum to minimum volume in this experiment was 1.299 ± 0.004. By tuning the maser in each of the positions, Debely obtained the wall shift of a reference maser, with an uncertainty of ±0.0023 Hz. In his design, he took pains to see that the annular joints of the Teflon coating of the bulb to the movable cone did not move or expose a different surface when the cone was moved.

The flexible-bulb technique can be used to establish the temperature at which the phase shift per collision is zero. This removes the uncertainty in the constancy of the wall shift with time and also overcomes the problem of using separate bulbs. By systematically changing the volume of the bulb (retuning the maser cavity at each position) and comparing the output frequency in each position against a stable frequency reference, one can adjust the temperature so that no change is observed in the output frequency. This procedure could be made automatic [15] by using servotechniques to maintain the proper temperature and promises to help greatly in ridding the maser of its most serious limitation on accuracy.

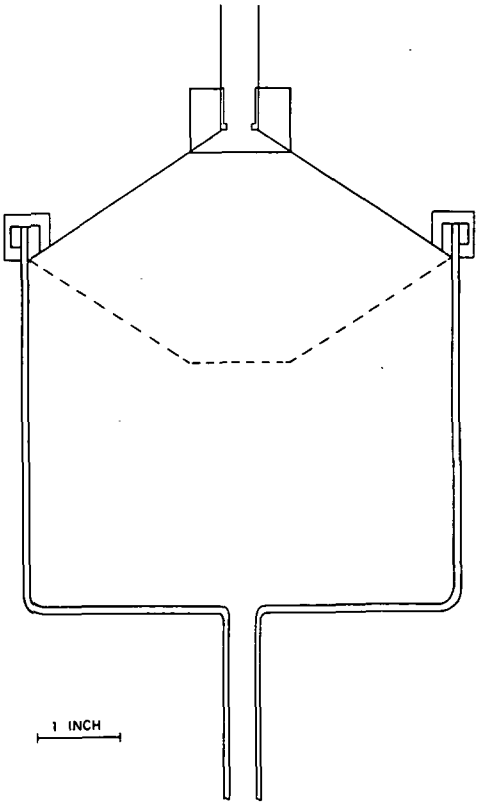

FIGURE 6. *Variable-collision-rate storage bulb.*

5. Multiple-Region Maser With Reduced Wall Shift

Since the wall-shift and relaxation rates in the maser depend on the collision rate of the atoms in the storage vessel, an important advantage can be gained by simply enlarging the storage bulb. However, limitations on bulb diameter of the self-oscillating maser are imposed by the cavity Q and the filling factor combination V_b/V_c that appears in the oscillating parameter q (see eq 4). A new concept of the maser was introduced in 1968 by Uzgiris and Ramsey [16] to overcome this limitation. A schematic of the new maser is shown in figure 7. The storage vessel consists of a 60 in Teflon-coated storage bulb connected to two rf interaction regions, each consisting of an rf cavity and a bulb, as in the usual maser. One cavity picks up the radiation from the atoms in its bulb, and this signal is amplified and sent to the other cavity to prestimulate the atoms in the other bulb. Since free molecule flow prevails in the three connected bulbs, the atoms can be put into a radiant state to emit at an enhanced rate in the low-level cavity. The loop is thus closed and the system will oscillate. The role of the amplifier is to make up for the lack of cavity Q and of the filling factor in the expression for q. The voltage gain R in the amplifier is given by the ratio of the rf magnetic field in the stimulating cavity to the rf field in the detecting cavity. The value of q for this maser is simply the value given earlier for the usual maser multiplied by $(1/R)(V_B/V_D)$, where V_B is the large

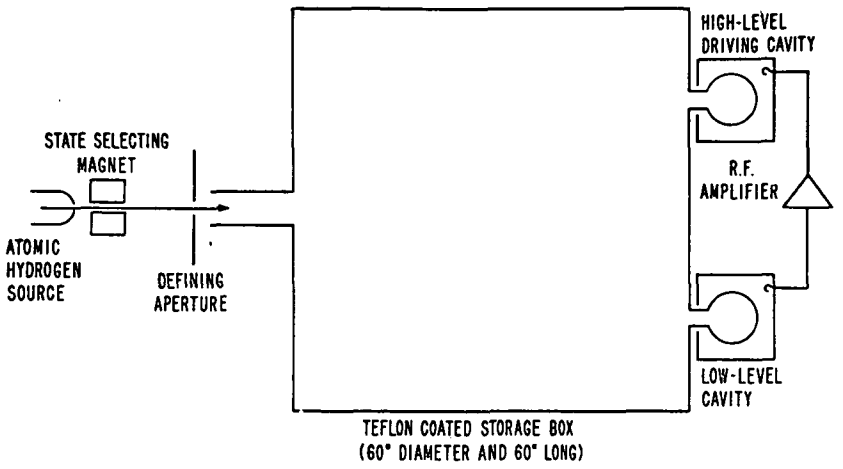

FIGURE 7. *Schematic of multiple-region hydrogen maser.*

bulb volume and V_D is the high-level cavity-bulb volume. The threshold flux I_{th} in this case is the usual value times a factor $1/R(V_B/V_D)^2$. Uzgiris calculates that the minimum gain required is about 70 dB and found that about 80 dB is required to make the maser oscillate.

The cavity pulling effect is complicated by the fact that both cavity resonant frequencies and the phase of the amplifier response must be included in the pulling expression along with a very small flow-dependent term that is not line width dependent. Except that the small effect of this term (in the order of 1 part in 10^{13}) must be accounted for, the tuning procedure is similar to that ordinarily used. The ratio of high-flux line-width to low-flux line width is about 1.7, as in conventional masers.

With the bulb geometry used in the experiment, the confinement time is calculated to be 10 s ($\gamma_b = 0.1$). At low-flux operation, a value of γ_{2T} of about 0.33 s^{-1} was observed, and the data indicate an excess relaxation rate of about 0.2 s^{-1} over the sum of the spin-exchange and bulb escape rates. This excess is most likely due to wall relaxation and is estimated to correspond to a probability of 10^{-4} per collision.

The results on the wall shift confirm the prediction that it would be 10 times lower than that encountered in the usual maser operating with the same wall materials and at the same temperature. A value of the shift of $(-2.3\pm0.8)\times10^{-3}$ Hz was obtained. At present, the multiple-region maser with a large storage vessel is being modified to incorporate the deformable bulb technique discussed in section 4 for measuring the wall shift of the maser coating that is actually in use. With this modification, the large-bulb maser should combine the advantage of a much smaller wall shift with the deformable technique for measuring that small shift.

6. Wall Relaxation

The storage-bulb technique depends on the ability of the bulb surface material to bounce the hydrogen atom without causing it to lose phase with the rf magnetic field in the cavity. Processes that lose the atom through chemical reactions or that change its atomic state and, thus, cause a loss of magnetization (T_1 processes), and collision processes that cause the oscillating atom to lose phase coherence with the rf field (T_2 processes) both contribute to the overall limitation on the storage time.

Early work by Berg [17] at Harvard gave values of the wall-relaxation probability w_r of about 1×10^{-5} per collision for FEP Teflon. Most of the masers constructed since then have used the FEP copolymer; and later measurements of the relaxation on this material [18] give values of w_r of about 1×10^{-4} per collision. The relaxation process has been found to be due mostly to recombination of the atomic hydrogen.

In recent work on PTFE, the value of relaxation probability per collision is approximately 1×10^{-5}, and the slow annealing process described earlier has yielded bulbs that give even more optimistic data. The difficulty in these recent results lies in the estimation of the bulb storage time, γ_b. Most of these bulbs have storage times $\sim$0.7 s ($\gamma_b\simeq1.4$ s^{-1}). The wall-relaxation rates have been estimated by measuring the exponential decay γ_{2T} of pulsed radiation after shutting off the atomic-hydrogen source and calculating $\gamma_w = \gamma_{2T} - \gamma_b$. For a 7 in bulb, values of $\gamma_w = 0.1\pm0.1$ s^{-1} have been obtained. The sensitivity of the measurement can be improved by using bulbs with very long storage times, thus making wall relaxation the dominant effect. Work along these lines is in progress at SAO to determine if the annealed surfaces offer any improvement in the relaxation rate.

If the present data on PTFE are correct, it should be possible to extend the storage time by a factor of 3 to 5 beyond the limits obtained by using FEP Teflon. Values of $\gamma_{2T} = 0.25$ s^{-1} or less should be possible in 7 in-diam bulbs. The benefits of this type of Teflon on the large bulb maser would also be very significant.

7. Electronic Systems

7.1. Cavity-Tuning Systems

a. Maser Cavity Resonator

The hydrogen masers constructed to date have all used a resonator operating in the cylindrical TE_{011} mode. This mode is convenient because, since only azimuthal wall currents flow, electrical contact between the cylinder and the end plates is not required.

Silver-coated CER-VIT[2] is used for cavity construction at SAO [19], while solid aluminum is preferred by the Goddard Space Flight Center [20]. The CER-VIT cavities are tuned by means of a voltage-variable capacitor mounted within the cavity and coupled to the rf magnetic field by a small loop. The aluminum cavities are thermally tuned; the relatively high temperature coefficient of expansion is used to advantage to permit tuning by small adjustments of cavity temperature.

b. Cavity Tuning

The oscillation frequency of the maser is pulled by tuning the resonator, as shown by eq (3).

There are essentially two problems associated with cavity pulling: (1) the cavity must be set to the correct frequency at the initiation of maser operation, and (2) the cavity must be held at this frequency indefinitely in the presence of environmental perturbations. The first problem is related to accuracy; the second, to stability. The setting of the cavity frequency can be accomplished by manual tuning techniques or by either of the two automatic tuners described in the next section. A series of careful experiments indicates that error in maser frequency attributable to cavity tuning is $\pm 7\times10^{-13}$ in a 90 percent confidence interval [11].

Once the maser is initially tuned, there remains the problem of maintaining this condition. One approach is to build the resonator out of materials of ultra-low thermal expansion, such as CER-VIT, which has a coefficient of expansion less than 5×10^{-8}/°C, and adequately control the temperature. Alternatively, the cavity can be servoed to resonance by continuous operation of an automatic tuning system.

c. Automatic Tuning Systems and Techniques

The hydrogen maser is tuned by modulating the line Q and adjusting the cavity resonator so that there are no correlated frequency shifts. Several automatic systems for timing masers have been devised; two of these are described below:

A. *Random-walk tuning* [20]. The masers used in this system are equipped with beam shutters so that the hydrogen flux and therefore the line Q can be modulated mechanically.

The maser frequency is compared to the reference oscillator, a stable crystal oscillator; a comparator circuit determines if the maser frequency was measured either high or low with respect to the reference. The comparator generates a "plus" pulse if the maser is higher in frequency than the reference and a "minus" pulse if it is lower. The plus and minus pulses are added algebraically in a reversible counter. When the comparator pulses accumulate to either a positive or a negative preset limit, a pulse of the appropriate sign is generated. These pulses are accumulated in a cavity-register circuit. A digital-to-analog converter translates the binary number stored in the cavity register to a cavity-control voltage that is used to servo the cavity to the correct frequency.

This random-walk automatic tuner, when used with an extremely low-noise crystal reference oscillator ($\sigma(\tau)=4\times10^{-13}$), will correct an initial maser-frequency error of 3×10^{-12} to approximately 2×10^{-13} in 20 h. The ultimate tuning error is claimed to be in the order of 5×10^{-14}.

B. *Fast automatic tuning* [19, 21]. The fast automatic tuner modulates the line Q by changing the rf power level into the hydrogen dissociator. The flux level must be modulated as rapidly as possible to minimize the phase-noise contribution from the reference oscillator.

The effect of linear frequency drift in the reference can be eliminated by using an algorithm devised by L. S. Cutler (private communication, 1968). The period of the beat between the maser and the reference is measured an odd number of times, alternately at low and at high flux. The measurements at low flux are assigned a negative sign; those at high flux, a positive sign. The first and the last measurements are divided by 2, and all the measurements are then summed algebraically. This residue,

$$N_R=-\tfrac{1}{2}(a_1+a_n)+\sum_{k=2}^{n-1}(-1)^k a_k,$$

is a measure of the cavity detuning and is independent of linear frequency drifts in the reference oscillator.

In practice, each beat measurement is approximately 6.6 s, and a complete cycle consists of 21 measurements, 11 at low flux and 10 at high flux. The period measurements are taken on a reversible counter, counting down for the low-flux measurements and up for the high-flux. The addition of one-half the 1st and 21st measurements is accomplished automatically by dividing the clock rate by 2 for these two measurements. The binary number in the counter at the end of the cycle (the residue) is translated by a digital-to-analog converter into a voltage that is used to correct the cavity frequency.

The precision of this tuning procedure is approximately $\pm7\times10^{-13}$ after 2 to 3 h of operation. Normally, the maser is initially tuned and then left unperturbed except for periodic tuning checks. Continuous automatic tuning is usually not desired, because of the average reduction in line Q required by the modulation process. A further difficulty in continuous tuning can arise from the changes in maser output-signal level with flux modulation. Un-

[2] Owens-Illinois trade name for a partly vitrified glass with a low expansion coefficient.

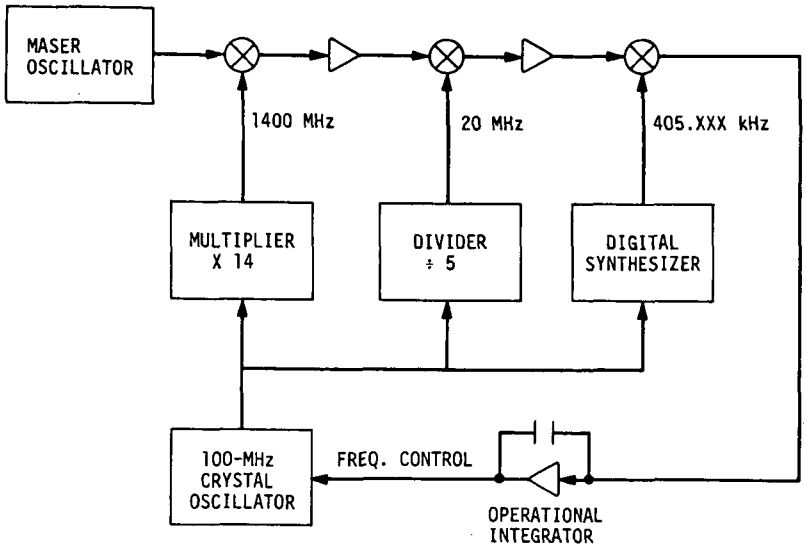

FIGURE 8. *Phase-lock system.*

less extraordinary precautions are taken in the design of the phase-lock circuitry, significant phase shifts will accompany amplitude changes. These phase shifts will not affect the automatic tuner, because they occur between operating cycles of the autotuner; but they will degrade the performance of external clocks.

Long-term frequency-stability data between two masers each operating with autotuning servos have been taken [22]. A value of $\sigma(\tau) = 2 \times 10^{-14}$ for $\tau =$ 12 h has been obtained.

7.2. Phase-Lock Systems

a. Description

The hydrogen maser is an active oscillator with an output of approximately −96 dBm at 1420.4 MHz. A crystal oscillator is phase-locked to the maser signal by a simple dual-conversion system, shown in figure 8. To provide standard frequencies at useful levels, the synthesizer is used to set the time scale.

The output of the maser at 1420.4 MHz is heterodyned in a low-noise balanced mixer with the output of the frequency multiplier at 1400 MHz. The 20.4-MHz output of the first mixer is amplified and heterodyned in the second mixer with a 20-MHz signal derived from the crystal oscillator. The resulting 405-kHz signal is amplified and used as one input to the phase detector. The reference signal is provided by the digital frequency synthesizer, which is referenced to the quartz oscillator. The dc output of the phase detector is used to phase-lock the quartz-crystal oscillator through a high-gain operational integrator. Double integration is incorporated into the phase-lock loop so that the phase-tracking error is very nearly zero. The time constant of the integrator is selected such that the closed-loop response has a bandwidth of about 20 Hz and is critically damped.

b. Recent Developments

Before 1968, the frequency of the crystal oscillator shown in figure 8 was usually 1 or 5 MHz. Recently, a high-quality 100-MHz quartz-crystal oscillator has been substituted for the lower frequency slave oscillator.

The use of the 100-MHz oscillator offers two important advantages. First, the additive phase noise at 1400 MHz is reduced by approximately 26 dB for the same oscillator-drive level. This permits the use of a much wider phase-lock-loop bandwidth and improves the overall signal-to-noise ratio. Typically, the 10- to 20-Hz bandwidth used with the 5-MHz slave oscillator can be increased to 100 to 150 Hz for the 100-MHz quartz oscillator. Second, the multiplication ratio to 1400 MHz is reduced from 280 to 14; this is of particular importance because the multiplier chain is a source of phase noise.

Usually, the phase noise is very small at 1400 MHz since at this frequency the local oscillator is most directly compared with the maser. The phase of the crystal oscillator, however, is steered to make up for phase changes in the multiplier, and if the output of the crystal oscillator is used, phase noise will be observed. Generally, the spectral density of the output-frequency fluctuations exhibits a flicker of frequency $(1/f)$ behavior. It has been observed that for a typical ×280 multiplier driven by a 5-MHz oscillator, the $\sigma(\tau)$ function is unaffected at 1 s, but in the range from 1 to 100 s, there is degradation of stability. The high-frequency crystal oscillator substantially improves the performance in this range, and the value of σ (100 s) is limited by the cavity stability.

8. Conclusion

Present stability performance of the maser frequency-standard system exceeds that of all other

known frequency standards; however, the accuracy of the device has justifiably been open to question, mostly owing to problems involving the wall shift. The improvements that can be brought about as a result of recent developments when engineered into operational devices will make a great deal of difference in the acceptability of the hydrogen maser as both an accurate and a stable frequency standard.

9. References

[1] Goldenberg, H. M., Kleppner, D., and Ramsey, N. F., Phys. Rev. Letters **5**, 361 (1960); Kleppner, D., Goldenberg, H. M., and Ramsey, N. F., Phys. Rev. **126**, 603 (1962).

[2] Cutler, L. S., and Searle, C. L., Proc. IEEE **54**, 136 (1966).

[3] Allan, D. W., Proc. IEEE **54**, 221 (1966).

[4] Kleppner, D., Berg, H. C., Crampton, S. B., Ramsey, N. F., Vessot, R. F. C., Peters, H. E., and Vanier, J., Phys. Rev. **138**, A972 (1965).

[5] Bender, P. L., Phys. Rev. **132**, 2154 (1964).

[6] Crampton, S. B., Kleppner, D., and Ramsey, N. F., Phys. Rev. Letters **11**, 338 (1963).

[7] Zitzewitz, P. W., Preliminary Report on the Temperature Dependence of the Wall Shift of the Hydrogen Maser for FEP and TFE Teflon, Harvard University, October 2 (1969).

[8] Vanier, J., and Vessot, R. F. C., Metrologia, **6**, 116 (1970).

[9] Zitzewitz, P. W., Ph. D. Thesis, Harvard University (1970).

[10] Vessot, R. F. C., and Levine, M. W., Metrologia, in press.

[11] Hellwig, H., Vessot, R. F. C., Levine, M. W., Zitzewitz, P. W., Allan, D. W., and Glaze, D. J., IEEE Trans. Instr. Meas., **IM-19** (November 1970).

[12] Vessot, R., Peters, H., Vanier, J., Beehler, R., Halford, D., Harrach, R., Allan, D., Glaze, D., Snyder, C., Barnes, J., Cutler, L., and Bodily, L., IEEE Trans. Instr. Meas. **IM-15**, 165 (1966).

[13] Brenner, D., Bull. Am. Phys. Soc. **14**, 943 (1969).

[14] Debely, P. E., Rev. Sci. Instr., in press.

[15] Smithsonian Astrophysical Observatory, New Technology Disclosure, NASA Contract NSR 09-015-098, June 1 (1970).

[16] Uzgiris, E. E., and Ramsey, N. F., Phys. Rev. **A1**, 429 (1970).

[17] Berg, H. C., Phys. Rev. **137**, 1621 (1965).

[18] Vanier, J., and Vessot, R. F. C., IEEE Trans. Instr. Meas. **IM-13**, 185 (1964).

[19] Levine, M. W., and Vessot, R. F. C., Radio Sci., **5**, 1287 (1970).

[20] Peters, H. E., McGunigal, T. E., and Johnson, E. H., Proceedings of the 22nd Annual Symposium on Frequency Control, U.S. Army Electronics Command, Ft. Monmouth, N.J., April (1968).

[21] Hellwig, H., and Pannaci, E., Proc. IEEE (Letters) **55**, 551 (1969).

[22] Risley, A. S., Allan, D. W., Peters, H. E., Johnson, E. H., Vessot, R. F. C., Levine, M. W., Gray, J. E., Shoaf, J. H., Machlan, H. E., and Glaze, D. J., Conference on Precision Electromagnetic Measurements, Boulder, Colo., June (1970).

From PRECISION MEASUREMENT AND FUNDAMENTAL CONSTANTS, Proceedings of the International Conference held at the National Bureau of Standards, Gaithersburg, Maryland, August 3-7, 1970, edited by D. N. Langenberg and B. N. Taylor. (NBS Special Publication 343). Order by SD Catalog No. C13.10:343 from the Superintendent of Documents, Government Printing Office. Washington. D.C. 20402. Price is $6.00 per copy; add one-fourth additional for foreign mailing. Make check or money order payable to the Superintendent of Documents.

Characterization of Frequency Stability

JAMES A. BARNES, SENIOR MEMBER, IEEE, ANDREW R. CHI, SENIOR MEMBER, IEEE, LEONARD S. CUTLER, MEMBER, IEEE, DANIEL J. HEALEY, MEMBER, IEEE, DAVID B. LEESON, SENIOR MEMBER, IEEE, THOMAS E. McGUNIGAL, MEMBER, IEEE, JAMES A. MULLEN, JR., SENIOR MEMBER, IEEE, WARREN L. SMITH, SENIOR MEMBER, IEEE, RICHARD L. SYDNOR, MEMBER, IEEE, ROBERT F. C. VESSOT, AND GERNOT M. R. WINKLER, MEMBER, IEEE

Abstract—Consider a signal generator whose instantaneous output voltage $V(t)$ may be written as

$$V(t) = [V_0 + \epsilon(t)] \sin [2\pi\nu_0 t + \varphi(t)]$$

where V_0 and ν_0 are the nominal amplitude and frequency, respectively, of the output. Provided that $\epsilon(t)$ and $\dot{\varphi}(t) = (d\varphi/(dt)$ are sufficiently small for all time t, one may define the fractional instantaneous frequency deviation from nominal by the relation

$$y(t) \equiv \frac{\dot{\varphi}(t)}{2\pi\nu_0}.$$

A proposed definition for the measure of frequency stability is the spectral density $S_y(f)$ of the function $y(t)$ where the spectrum is considered to be one sided on a per hertz basis.

An alternative definition for the measure of stability is the infinite time average of the sample variance of two adjacent averages of $y(t)$; that is, if

$$\bar{y}_k = \frac{1}{\tau} \int_{t_k}^{t_k+\tau} y(t)\, dt$$

where τ is the averaging period, $t_{k+1} = t_k + T, k = 0, 1, 2 \cdots, t_0$ is arbitrary, and T is the time interval between the beginnings of two successive measurements of average frequency; then the second measure of stability is

$$\sigma_y^2(\tau) \equiv \left\langle \frac{(\bar{y}_{k+1} - \bar{y}_k)^2}{2} \right\rangle$$

where $\langle\ \rangle$ denotes infinite time average and where $T = \tau$.

In practice, data records are of finite length and the infinite time averages implied in the definitions are normally not available; thus estimates for the two measures must be used. Estimates of $S_y(f)$ would be obtained from suitable averages either in the time domain or the frequency domain. An obvious estimate for $\sigma_y^2(\tau)$ is

$$\sigma_y^2(\tau) \approx \frac{1}{m} \sum_{k=1}^{m} \frac{(\bar{y}_{k+1} - \bar{y}_k)^2}{2}.$$

Parameters of the measuring system and estimating procedure are of critical importance in the specification of frequency stability. In practice, one should experimentally establish confidence limits for an estimate of frequency stability by repeated trials.

Manuscript received December 1, 1970. The authors of this paper are members of the Subcommittee on Frequency Stability of the Technical Committee on Frequency and Time of the IEEE Group on Instrumentation and Measurement.

J. A. Barnes is with the Time and Frequency Division, Institute for Basic Standards, NBS, Boulder, Colo. 80302.

A. R. Chi is with the Head Timing Systems Section, NASA Goddard Space Flight Center, Greenbelt, Md. 20771.

L. S. Cutler is with the Physical Research Laboratory, Hewlett-Packard Company, Palo Alto, Calif. 94304.

D. J. Healey is with the Aerospace Division, Westinghouse Electric Corporation, Baltimore, Md. 21203.

D. B. Leeson is with California Microwave, Inc., Sunnyvale, Calif. 94086.

T. E. McGunigal is with the RF and Quantum Techniques Section, NASA Goddard Space Flight Center, Greenbelt, Md. 21715.

J. A. Mullen is with the Research Division, Raytheon Company, Waltham, Mass. 02154.

W. L. Smith is with Bell Telephone Laboratories, Allentown, Pa. 18108.

R. L. Sydnor is with the Telecommunications Department, Jet Propulsion Laboratory, Pasadena, Calif. 91103.

G. M. R. Winkler is with the Time Service Division, U. S. Naval Observatory, Washington, D. C. 20390.

R. F. C. Vessot is with the Smithsonian Astrophysical Observatory, Cambridge, Mass. 02138.

Glossary of Symbols

$B_1(N, r, \mu)$, $B_2(r, \mu)$	Bias function for variances based on finite samples of a process with a power-law spectral density. (See [13].)
C_α	A real constant defined by (70).
c_0, c_1	Real constants.
$c(t)$	A real, deterministic function of time.
$D_x^2(\tau)$	Expected value of the squared second difference of $x(t)$ with lag time τ. See (80).
$f \equiv \omega/2\pi$	Fourier frequency variable.
f_h	High-frequency cutoff of an idealized infinitely sharp cutoff low-pass filter.
f_l	Low-frequency cutoff of an idealized infinitely sharp cutoff, high-pass filter.
$g(t)$	A real function of time.
h_α	Positive real coefficient of f^α in a power series expansion of the spectral density of the function $y(t)$.
i, j, k, m, n	Integers, often a dummy index of summation.
M	Positive integer giving the number of cycles averaged.
N	Positive integer giving the number of data points used in obtaining a sample variance.
$n(t)$	A nondeterministic function of time.
$R_y(\tau)$	Autocovariance function of $y(t)$. See (58).
r	Positive real number defined by $r \equiv T/\tau$.

S An intermediate term used in deriving (23). The definition of S is given by (64).

$S_g(f)$ One-sided (power) spectral density on a per hertz basis of the pure real function $g(t)$. The dimensions of $S_g(f)$ are the dimensions of $g^2(t)/f$.

$S_y(f)$ A definition for the measure of frequency stability. One-sided (power) spectral density of $y(t)$ on a per hertz basis. The dimensions of $S_y(f)$ are Hz^{-1}.

T Time interval between the beginnings of two successive measurements of average frequency.

t Time variable.

t_0 An arbitrary fixed instant of time.

t_k The time coordinate of the beginning of the kth measurement of average frequency. By definition, $t_{k+1} = t_k + T$, $k = 0, 1, 2 \cdots$.

u Dummy variable of integration; $u \equiv \pi f \tau$.

$V(t)$ Instantaneous output voltage of signal generator. See (2).

V_0 Nominal peak amplitude of signal generator output. See (2).

$V_r(t)$ Instantaneous voltage of reference signal. See (40).

V_{0r} Peak amplitude of reference signal. See (40).

$v(t)$ Voltage output of ideal product detector.

$v'(t)$ Low-pass filtered output of product detector.

$x(t)$ Real function of time related to the phase of the signal $V(t)$ by $x(t) \equiv [\varphi(t)]/(2\pi\nu_0)$.

$\hat{x}(t)$ A predicted value for $x(t)$.

$y(t)$ Fractional frequency offset of $V(t)$ from the nominal frequency. See (7).

$\bar{y}_k$ Average fractional frequency offset during the kth measurement interval. See (9).

$\langle \bar{y} \rangle_N$ The sample average of N successive values of $\bar{y}_k$. See (76).

$z_n(t)$ Nondeterministic (noise) function with (power) spectral density given by (25).

α Exponent of f for a power-law spectral density.

γ Positive real constant.

$\delta_k(r - 1)$ The Kronecker δ function defined by $\delta_k(r - 1) \equiv \begin{cases} 1, & \text{if } r = 1 \\ 0, & \text{otherwise.} \end{cases}$

$\epsilon(t)$ Amplitude fluctuations of signal. See (2).

μ Exponent of τ. See (29).

$\nu(t)$ Instantaneous frequency of $V(t)$. Defined by

$$\nu(t) \equiv \frac{1}{2\pi} \frac{d}{dt} \Phi(t).$$

ν_0 Nominal (constant) frequency of $V(t)$.

$\kappa(t)$ The Fourier transform of $n(t)$.

$\sigma_y^2(N, T, \tau)$ Sample variance of N averages of $y(t)$, each of duration τ, and spaced every T units of time. See (10).

$\langle \sigma_y^2(N, T, \tau) \rangle$ Average value of the sample variance $\sigma_y^2(N, T, \tau)$.

$\sigma_y^2(\tau)$ A second choice of the definition for the measure of frequency stability. Defined by $\sigma_y^2(\tau) \equiv \langle \sigma_y^2(N = 2, T = \tau, \tau) \rangle$.

$\sigma_x^2(\tau)$ Time stability measure defined by $\sigma_x^2(\tau) \equiv \tau^2 \sigma_y^2(\tau)$.

τ Duration of averaging period of $y(t)$ to obtain $\bar{y}_k$. See (9).

$\Phi(t)$ Instantaneous phase of $V(t)$. Defined by $\Phi(t) \equiv 2\pi\nu_0 t + \varphi(t)$.

$\varphi(t)$ Instantaneous phase fluctuations about the ideal phase $2\pi\nu_0 t$. See (2).

$\psi_x^2(T, \tau)$ Mean-square time error for Doppler radar. See (82).

$\omega \equiv 2\pi f$ Angular Fourier frequency variable.

I. Introduction

THE measurement of frequency and fluctuations in frequency has received such great attention for so many years that it is surprising that the concept of frequency stability does not have a universally accepted definition. At least part of the reason has been that some uses are most readily described in the frequency domain and other uses in the time domain, as well as in combinations of the two. This situation is further complicated by the fact that only recently have noise models been presented that both adequately describe performance and allow a translation between the time and frequency domains. Indeed, only recently has it been recognized that there can be a wide discrepancy between commonly used time domain measures themselves. Following the NASA–IEEE Symposium on Short-Term Stability in 1964 and the Special Issue on Frequency Stability in the PROCEEDINGS OF THE IEEE, February 1966, it now seems reasonable to propose a definition of frequency stability. The present paper is presented as technical background for an eventual IEEE standard definition.

This paper attempts to present (as concisely as practical) adequate, self-consistent definitions of frequency stability. Since more than one definition of frequency stability is presented, an important part of this paper

(perhaps the most important part) deals with translations among the suggested definitions of frequency stability. The applicability of these definitions to the more common noise models is demonstrated.

Consistent with an attempt to be concise, the references cited have been selected on the basis of being of most value to the reader rather than on the basis of being exhaustive. An exhaustive reference list covering the subject of frequency stability would itself be a voluminous publication.

Almost any signal generator is influenced to some extent by its environment. Thus observed frequency instabilities may be traced, for example, to changes in ambient temperature, supply voltages, magnetic field, barometric pressure, humidity, physical vibration, or even output loading, to mention the more obvious. While these environmental influences may be extremely important for many applications, the definition of frequency stability presented here is independent of these causal factors. In effect, we cannot hope to present an exhaustive list of environmental factors and a prescription for handling each even though, in some cases, these environmental factors may be by far the most important. Given a particular signal generator in a particular environment, one can obtain its frequency stability with the measures presented below, but one should not then expect an accurate prediction of frequency stability in a new environment.

It is natural to expect any definition of stability to involve various statistical considerations such as stationarity, ergodicity, average, variance, spectral density, etc. There often exist fundamental difficulties in rigorous attempts to bring these concepts into the laboratory. It is worth considering, specifically, the concept of stationarity since it is a concept at the root of many statistical discussions.

A random process is mathematically defined as stationary if every translation of the time coordinate maps the ensemble onto itself. As a necessary condition, if one looks at the ensemble at one instant of time t, the distribution in values within the ensemble is exactly the same as at any other instant of time t'. This is not to imply that the elements of the ensemble are constant in time, but, as one element changes value with time, other elements of the ensemble assume the previous values. Looking at it in another way, by observing the ensemble at some instant of time, one can deduce no information as to when the particular instant was chosen. This same sort of invariance of the *joint* distribution holds for any set of times $t_1, t_2, \cdots, t_n$ and its translation $t_1 + \tau, t_2 + \tau, \cdots, t_n + \tau$.

It is apparent that any ensemble that has a finite past as well as a finite future cannot be stationary, and this neatly excludes the real world and anything of practical interest. The concept of stationarity does violence to concepts of causality since we implicitly feel that current performance (i.e., the applicability of stationary statistics) cannot be logically dependent upon future events (i.e., if the process is terminated some time in the distant future). Also, the verification of stationarity would involve hypothetical measurements that are *not* experimentally feasible, and therefore the concept of stationarity is not directly relevant to experimentation.

Actually the utility of statistics is in the formation of idealized models that *reasonably* describe significant observables of real systems. One may, for example, consider a hypothetical ensemble of noises with certain properties (such as stationarity) as a model for a particular real device. If a model is to be acceptable, it should have at least two properties: first, the model should be tractable; that is, one should be able to easily arrive at estimates for the elements of the models; and second, the model should be consistent with *observables* derived from the real device that it is simulating.

Notice that one does not need to know that the device was selected from a stationary ensemble, but only that the observables derived from the device are *consistent* with, say, elements of a hypothetically stationary ensemble. Notice also that the actual model used may depend upon how clever the experimenter–theorist is in generating models.

It is worth noting, however, that while some texts on statistics give "tests for stationarity," these tests are almost always inadequate. Typically, these tests determine only if there is a substantial fraction of the noise power in Fourier frequencies whose periods are of the same order as the data length or longer. While this may be very important, it is *not* logically essential to the concept of stationarity. If a nonstationary model actually becomes common, it will almost surely be because it is useful or convenient and not because the process is "actually nonstationary." Indeed, the phrase "actually nonstationary" appears to have no meaning in an operational sense. In short, stationarity (or nonstationarity) is a property of models, *not* a property of data [1].

Fortunately, many statistical models exist that adequately describe most present-day signal generators; many of these models are considered below. It is obvious that one cannot guarantee that all signal generators are adequately described by these models, but the authors do feel they are adequate for the description of most signal generators presently encountered.

II. Statement of the Problem

To be useful, a measure of frequency stability must allow one to predict performance of signal generators used in a wide variety of situations as well as allow one to make meaningful relative comparisons among signal generators. One must be able to predict performance in devices that may most easily be described either in the time domain, or in the frequency domain, or in a combination of the two. This prediction of performance may involve actual distribution functions, and thus

second moment measures (such as power spectra and variances) are not totally adequate.

Two common types of equipment used to evaluate the performance of a frequency source are (analog) spectrum analyzers (frequency domain) and digital electronic counters (time domain). On occasion the digital counter data are converted to power spectra by computers. One must realize that any piece of equipment simultaneously has certain aspects most easily described in the time domain and other aspects most easily described in the frequency domain. For example, an electronic counter has a high-frequency limitation, an experimental spectra are determined with finite time averages.

Research has established that ordinary oscillators demonstrate noise, which appears to be a superposition of causally generated signals and random nondeterministic noises. The random noises include thermal noise, shot noise, noises of undetermined origin (such as flicker noise), and integrals of these noises.

One might well expect that for the more general cases one would need to use a nonstationary model (not stationary even in the wide sense, i.e., the covariance sense). Nonstationarity would, however, introduce significant difficulties in the passage between the frequency and time domains. It is interesting to note that, so far, experimenters have seldom found a nonstationary (covariance) model useful in describing actual oscillators.

In what follows, an attempt has been made to separate general statements that hold for any noise or perturbation from the statements that apply only to specific models. It is important that these distinctions be kept in mind.

III. Background and Definitions

To discuss the concept of frequency stability immediately implies that frequency can change with time and thus one is not considering Fourier frequencies (at least at this point). The conventional definition of instantaneous (angular) frequency is the time rate of change of phase; that is

$$2\pi\nu(t) \equiv \frac{d\Phi(t)}{dt} \equiv \dot{\Phi}(t) \tag{1}$$

where $\Phi(t)$ is the instantaneous phase of the oscillator. This paper uses the convention that time-dependent frequencies of oscillators are denoted by $\nu(t)$ (cycle frequency, hertz), and Fourier frequencies are denoted by ω (angular frequency) or f (cycle frequency, hertz) where $\omega \equiv 2\pi f$. In order for (1) to have meaning, the phase $\Phi(t)$ must be a well-defined function. This restriction immediately eliminates some "nonsinusoidal" signals such as a pure random uncorrelated ("white") noise. For most real signal generators, the concept of phase is reasonably amenable to an operational definition and this restriction is not serious.

Of great importance to this paper is the concept of spectral density, $S_g(f)$. The notation $S_g(f)$ is to represent the one-sided spectral density of the (pure real) function $g(t)$ on a per hertz basis; that is, the total "power" or mean-square value of $g(t)$ is given by

$$\int_0^\infty S_g(f)\, df.$$

Since the spectral density is such an important concept to what follows, it is worthwhile to present some important references on spectrum estimation. There are many references on the estimation of spectra from data records, but worthy of special note are [2]–[5].

IV. Definition of Measures of Frequency Stability (Second-Moment Type)

A. General

Consider a signal generator whose instantaneous output voltage $V(t)$ may be written as

$$V(t) = [V_0 + \epsilon(t)] \sin [2\pi\nu_0 t + \varphi(t)] \tag{2}$$

where V_0 and ν_0 are the nominal amplitude and frequency, respectively, of the output and it is assumed that

$$\left|\frac{\epsilon(t)}{V_0}\right| \ll 1 \tag{3}$$

and

$$\left|\frac{\dot{\varphi}(t)}{2\pi\nu_0}\right| \ll 1 \tag{4}$$

for substantially all time t. Making use of (1) and (2) one sees that

$$\Phi(t) = 2\pi\nu_0 t + \varphi(t) \tag{5}$$

and

$$\nu(t) = \nu_0 + \frac{1}{2\pi}\dot{\varphi}(t). \tag{6}$$

Equations (3) and (4) are essential in order that $\varphi(t)$ may be defined conveniently and unambiguously (see measurement section).

Since (4) must be valid even to speak of an instantaneous frequency, there is no real need to distinguish stability measures from instability measures. That is, any fractional frequency stability measure will be far from unity, and the chance of confusion is slight. It is true that in a very strict sense people usually measure instability and speak of stability. Because the chances of confusion are so slight, the authors have chosen to continue in the custom of measuring "instability" and speaking of stability (a number always much less than unity).

Of significant interest to many people is the radio frequency (RF) spectral density $S_V(f)$. This is of direct concern in spectroscopy and radar. However, this is *not* a good primary measure of frequency stability for two reasons. First, fluctuations in the amplitude $\epsilon(t)$ contribute directly to $S_V(f)$; and second, for many cases when

$\epsilon(t)$ is insignificant, the RF spectrum $S_V(f)$ is not uniquely related to the frequency fluctuations [6].

B. General: First Definition of the Measure of Frequency Stability—Frequency Domain

By definition, let

$$y(t) \equiv \frac{\dot{\varphi}(t)}{2\pi\nu_0}, \tag{7}$$

where $\varphi(t)$ and ν_0 are as in (2). Thus $y(t)$ is the instantaneous fractional frequency deviation from the nominal frequency ν_0. A proposed definition of frequency stability is the spectral density $S_y(f)$ of the instantaneous fractional frequency fluctuations $y(t)$. The function $S_y(f)$ has the dimensions of Hz^{-1}.

One can show [7] that if $S_\varphi(f)$ is the spectral density of the phase fluctuations, then

$$S_y(f) = \left(\frac{1}{2\pi\nu_0}\right)^2 S_{\dot{\varphi}}(f) = \left(\frac{1}{\nu_0}\right)^2 f^2 S_\varphi(f). \tag{8}$$

Thus a knowledge of the spectral density of the phase fluctuations $S_\varphi(f)$ allows a knowledge of the spectral density of the frequency fluctuations $S_y(f)$, the first definition of frequency stability. Of course, $S_y(f)$ cannot be *perfectly* measured—this is the case for any physical quantity; useful estimates of $S_y(f)$ are, however, easily obtainable.

C. General: Second Definition of the Measure of Frequency Stability—Time Domain

The second definition is based on the sample variance of the fractional frequency fluctuations. In order to present this measure of frequency stability, define $\bar{y}_k$ by the relation

$$\bar{y}_k \equiv \frac{1}{\tau}\int_{t_k}^{t_k+\tau} y(t)\,dt = \frac{\varphi(t_k+\tau) - \varphi(t_k)}{2\pi\nu_0\tau}, \tag{9}$$

where $t_{k+1} = t_k + T$, $k = 0, 1, 2, \cdots$, T is the repetition interval for measurements of duration τ, and t_0 is arbitrary. Conventional frequency counters measure the number of cycles in a period τ; that is, they measure $\nu_0\tau(1 + \bar{y}_k)$. When τ is 1 s they count the number of $\nu_0(1 + \bar{y}_k)$. The second measure of frequency stability, then, is defined in analogy to the sample variance by the relation

$$\langle\sigma_y^2(N, T, \tau)\rangle \equiv \left\langle \frac{1}{N-1}\sum_{n=1}^{N}\left(\bar{y}_n - \frac{1}{N}\sum_{k=1}^{N}\bar{y}_k\right)^2\right\rangle, \tag{10}$$

where $\langle g\rangle$ denotes the infinite time average of g. This measure of frequency stability is dimensionless.

In many situations it would be wrong to assume that (10) converges to a meaningful limit as $N \to \infty$. First, of course, one cannot practically let N approach infinity and, second, it is known that some actual noise processes contain substantial fractions of the total noise power in the Fourier frequency range below one cycle per year. In order to improve comparability of data, it is important to specify particular N and T. For the preferred definition we recommend choosing $N = 2$ and $T = \tau$ (i.e., no dead time between measurements). Writing $\langle\sigma_y^2(N=2, T=\tau, \tau)\rangle$ as $\sigma_y^2(\tau)$, the Allan variance [8], the proposed measure of frequency stability in the time domain may be written as

$$\sigma_y^2(\tau) = \left\langle \frac{(\bar{y}_{k+1} - \bar{y}_k)^2}{2}\right\rangle \tag{11}$$

for $T = \tau$.

Of course, the experimental estimate of $\sigma_y^2(\tau)$ must be obtained from finite samples of data, and one can never obtain perfect confidence in the estimate; the true time average is not realizable in a real situation. One estimates $\sigma_y^2(\tau)$ from a finite number (say, m) of values of $\sigma_y^2(2, \tau, \tau)$ and averages to obtain an estimate of $\sigma_y^2(\tau)$. Appendix I shows that the ensemble average of $\sigma_y^2(2, \tau, \tau)$ is convergent (i.e., as $m \to \infty$) even for noise processes that do not have convergent $\langle\sigma_y^2(N, \tau, \tau)\rangle$ as $N \to \infty$. Therefore, $\sigma_y^2(\tau)$ has greater utility as an idealization than does $\langle\sigma_y^2(\infty, \tau, \tau)\rangle$ even though both involve assumptions of infinite averages. In effect, increasing N causes $\sigma_y^2(N, T, \tau)$ to become more sensitive to the low-frequency components of $S_y(f)$. In practice, one must distinguish between an experimental estimate of a quantity (say, of $\sigma_y^2(\tau)$) and its idealized value. It is reasonable to believe that extensions to the concept of statistical ("quality") control [9] may prove useful here. One should, of course, specify the actual number m of independent samples used for an estimate of $\sigma_y^2(\tau)$.

In summary, therefore, $S_y(f)$ is the proposed measure of (instantaneous) frequency stability in the (Fourier) frequency domain and $\sigma_y^2(\tau)$ is the proposed measure of frequency stability in the time domain.

D. Distributions

It is natural that people first become involved with second moment measures of statistical quantities and only later with actual distributions. This is certainly true with frequency stability. While one can specify the argument of a distribution function to be, say $(\bar{y}_{k+1} - \bar{y}_k)$, it makes sense to postpone such a specfication until a real use has materialized for a particular distribution function. This paper does not attempt to specify a preferred distribution function for frequency fluctuations.

E. Treatment of Systematic Variations

1) General: The definition of frequency stability $\sigma_y^2(\tau)$ in the time domain is useful for many situations. However, some oscillators, for example, exhibit an aging or almost linear drift of frequency with time. For some applications, this trend may be calculated and should be removed [8] before estimating $\sigma_y^2(\tau)$.

In general, a systematic trend is perfectly deterministic (i.e., predictable) while the noise is nondeterministic. Consider a function $g(t)$, which may be written in the form

$$g(t) = c(t) + n(t) \tag{12}$$

where $c(t)$ is some deterministic function of time and $n(t)$, the noise, is a nondeterministic function of time. We will define $c(t)$ to be the *systematic trend* to the function $g(t)$. A problem of significance here is to determine when and in what sense $c(t)$ is measurable.

2) Specific Case—Linear Drift: As an example, if we consider a typical quartz crystal oscillator whose fractional frequency deviation is $y(t)$, we may let

$$g(t) = \frac{d}{dt} y(t). \tag{13}$$

With these conditions, $c(t)$ is the drift rate of the oscillator (e.g., 10^{-10}/day) and $n(t)$ is related to the frequency "noise" of the oscillator by a time derivative. One sees that the time average of $g(t)$ becomes

$$\frac{1}{T}\int_{t_0}^{t_0+T} g(t)\,dt = c_1 + \frac{1}{T}\int_{t_0}^{t_0+T} n(t)\,dt \tag{14}$$

where $c(t) = c_1$ is assumed to be the constant drift rate of the oscillator. In order for c_1 to be an observable, it is natural to expect the average of the noise term to vanish, that is, converge to zero.

It is instructive to assume [8], [10] that in addition to a linear drift, the oscillator is perturbed by a flicker noise, i.e.,

$$S_y(f) = \begin{cases} h_{-1}f^{-1}, & 0 < f \le f_h \\ 0, & f > f_h \end{cases} \tag{15}$$

where h_{-1} is a constant (see Section V-A-2) and thus,

$$S_n(f) = \begin{cases} (2\pi)^2 h_{-1} f, & 0 \le f \le f_h \\ 0, & f > f_h \end{cases} \tag{16}$$

for the oscillator we are considering. With these assumptions, it is seen that

$$\lim_{T\to\infty} \frac{1}{T}\int_{t_0}^{t_0+T} n(t)\,dt = \kappa(0) = 0 \tag{17}$$

and that

$$\lim_{T\to\infty} \left\{ \text{variance} \left[\frac{1}{T}\int_{t_k}^{t_k+T} n(t)\,dt \right] \right\} = 0 \tag{18}$$

where $\kappa(f)$ is the fourier transform of $n(t)$. Since $S_n(0) = 0$, $\kappa(0)$ must also vanish both in probability and in mean square. Thus, not only does $n(t)$ average to zero, but one may obtain arbitrarily good confidence on the result by longer averages.

Having shown that one can reliably estimate the drift rate c_1 of this (common) oscillator, it is instructive to attempt to fit a straight line to the frequency aging. That is, let

$$g(t) = y(t) \tag{19}$$

and thus

$$g(t) = c_0 + c_1(t - t_0) + n'(t) \tag{20}$$

where c_0 is the frequency intercept at $t = t_0$ and c_1 is the drift rate previously determined. A problem arises here because

$$S_{n'}(f) = S_y(f) \tag{21}$$

and

$$\lim_{T\to\infty} \left\{ \text{variance} \left[\frac{1}{T}\int_{t_k}^{t_k+T} n'(t)\,dt \right] \right\} = \infty \tag{22}$$

for the noise model we have assumed. This follows from the fact that the (infinite N) variance of a flicker noise process is infinite [7], [8], [10]. Thus, c_0 cannot be measured with any realistic precision, at least, in an absolute sense.

We may interpret these results as follows. After experimenting with the oscillator for a period of time one can fit an empirical equation to $y(t)$ of the form

$$y(t) = c_0 + tc_1 + n'(t),$$

where $n'(t)$ is nondeterministic. At some later time it is possible to reevaluate the coefficients c_0 and c_1. According to what has been said, the drift rate c_1 should be reproducible to within the confidence estimates of the experiment regardless of when it is reevaluated. For c_0, however, this is not true. In fact, the more one attempts to evaluate c_0, the larger the fluctuations are in the result.

Depending on the spectral density of the noise term, it may be possible to predict future measurements of c_0 and to place realistic confidence limits on the prediction [11]. For the case considered here, however, these confidence limits tend to infinity when the prediction interval is increased. Thus, in a certain sense, c_0 is "measurable" but it is not in statistical control (to use the language of the quality control engineer [9]).

V. Translations Among Frequency Stability Measures

A. Frequency Domain to Time Domain

1) General: It is of value to define $r = T/\tau$; that is, r is the ratio of the time interval between successive measurements to the duration of the averaging period. Cutler has shown (see Appendix I) that

$$\langle \sigma_y^2(N, T, \tau) \rangle = \frac{N}{(N-1)} \int_0^\infty df\, S_y(f) \frac{[\sin^2(\pi f \tau)]}{(\pi f \tau)^2} \left\{ 1 - \frac{\sin^2(\pi r f N \tau)}{N^2 \sin^2(\pi r f \tau)} \right\}. \tag{23}$$

Equation (23) in principle allows one to calculate the time-domain stability $\langle \sigma_y^2(N, T, \tau) \rangle$ from the frequency-domain stability $S_y(f)$.

2) Specific Model: A model that has been found useful [8], [10]–[13] consists of a set of five independent noise processes $z_n(t)$, $n = -2, -1, 0, 1, 2$, such that

$$y(t) = z_{-2}(t) + z_{-1}(t) + z_0(t) + z_1(t) + z_2(t) \quad (24)$$

and the spectral density of z_n is given by

$$S_{z_n}(f) = \begin{cases} h_n f^n, & 0 \le f \le f_h \\ 0, & f > f_h, n = -2, -1, 0, 1, 2, \end{cases} \quad (25)$$

where the h_n are constants. Thus, $S_y(f)$ becomes

$$S_y(f) = h_{-2}f^{-2} + h_{-1}f^{-1} + h_0 + h_1 f + h_2 f^2, \quad (26)$$

for $0 \le f \le f_h$ and $S_y(f)$ is assumed to be negligible beyond this range. In effect, each z_n contributes to both $S_y(f)$ and $\langle\sigma_y^2(N, T, \tau)\rangle$ independently of the other z_n. The contributions of the z_n to $\langle\sigma_y^2(N, T, \tau)\rangle$ are tabulated in Appendix II.

Any electronic device has a finite bandwidth and this certainly applies to frequency-measuring equipment also. For fractional frequency fluctuations $y(t)$ whose spectral density varies as

$$S_y(f) \sim f^\alpha, \qquad \alpha \ge -1 \quad (27)$$

for the higher Fourier components, one sees (from Appendix I) that $\langle\sigma_y^2(N, T, \tau)\rangle$ may depend on the exact shape of the frequency cutoff. This is true because a substantial fraction of the noise "power" may be in these higher Fourier components. As a simplifying assumption, this paper assumes a sharp cutoff in noise "power" at the frequency f_h for the noise models. It is apparent from the tables of Appendix II that the time domain measure of frequency stability may depend on f_h in a very important way, and, in some practical cases, the actual shape of the frequency cutoff may be very important [7]. On the other hand, there are many practical measurements where the value of f_h has little or no effect. Good practice, however, dictates that the system noise bandwidth f_h should be specified with any results.

In actual practice, the model of (24)–(26) seems to fit almost all real frequency sources. Typically, only two or three of the h-coefficients are actually significant for a real device and the others can be neglected. Because of its applicability, this model is used in much of what follows. Since the z_n are assumed to be independent noises, it is normally sufficient to compute the effects for a general z_n and recognize that the superposition can be accomplished by simple additions for their contributions to $S_y(f)$ or $\langle\sigma_y^2(N, T, \tau)\rangle$.

B. Time Domain to Frequency Domain

1) General: For general $\langle\sigma_y^2(N, T, \tau)\rangle$ no simple prescription is available for translation into the frequency domain. For this reason, one might prefer $S_y(f)$ as a general measure of frequency stability. This is especially true for theoretical work.

2) Specific Model: Equations (24)–(26) form a realistic model that fits the random nondeterministic noises found on most signal generators. Obviously, if this is a good model, then the tables in Appendix II may be used (in reverse) to translate into the frequency domain.

Allan [8] and Vessot [12] showed that if

$$S_y(f) = \begin{cases} h_\alpha f^\alpha, & 0 \le f \le f_h \\ 0, & f > f_h \end{cases} \quad (28)$$

where α is a constant, then

$$\langle\sigma_y^2(N, T, \tau)\rangle \sim |\tau|^\mu, \qquad 2\pi\tau f_h \gg 1 \quad (29)$$

for N and $r = T/\tau$ held constant. The constant μ is related to α by the mapping shown[1] in Fig. 1. If (28) and (29) hold over a reasonable range for a signal generator, then (28) can be substituted into (23) and evaluated to determine the constant h_α from measurements of $\langle\sigma_y^2(N, T, \tau)\rangle$. It should be noted that the model of (28) and (29) may be easily extended to a superposition of similar noises as in (26).

C. Translations Among the Time-Domain Measures

1) General: Since $\langle\sigma_y^2(N, T, \tau)\rangle$ is a function of N, T, and τ (for some types of noise f_h is also important), it is very desirable to be able to translate among different sets of N, T, and τ (f_h held constant). This is, however, not possible in general.

2) Specific Model: It is useful to restrict consideration to a case described by (28) and (29). Superpositions of independent noises with different power-law types of spectral densities (i.e., different α) can also be treated by this technique, e.g., (26). One may define two "bias functions," B_1 and B_2 by the relations [13]

$$B_1(N, r, \mu) \equiv \frac{\langle\sigma_y^2(N, T, \tau)\rangle}{\langle\sigma_y^2(2, T, \tau)\rangle} \quad (30)$$

and

$$B_2(r, \mu) \equiv \frac{\langle\sigma_y^2(2, T, \tau)\rangle}{\langle\sigma_y^2(2, \tau, \tau)\rangle} \quad (31)$$

where $r \equiv T/\tau$ and μ is related to α by the mapping of Fig. 1. In words, B_1 is the ratio of the average variance for N samples to the average variance for two samples (everything else held constant), while B_2 is the ratio of the average variance with dead time between measurements ($r \ne 1$) to that of no dead time ($r = 1$ and with $N = 2$ and τ held constant). These functions are tabulated in [13]. Figs. 2 and 3 show a computer plot of $B_1(N, r = 1, \mu)$ and $B_2(r, \mu)$.

Suppose one has an experimental estimate of $\langle\sigma_y^2(N_1, T_1, \tau_1)\rangle$ and its spectral type is known, i.e., (28) and (29) form a good model and μ is known. Suppose also that one wishes to know the variance at some other set of measurement parameters N_2, T_2, τ_2. An unbiased estimate of $\langle\sigma_y^2(N_2, T_2, \tau_2)\rangle$ may be calculated by

[1] It should be noted that in Allan [8], the exponent α corresponds to the spectrum of *phase* fluctuations while variances are taken over average *frequency* fluctuations. In the present paper, α is identical to the exponent $\alpha + 2$ in [8].

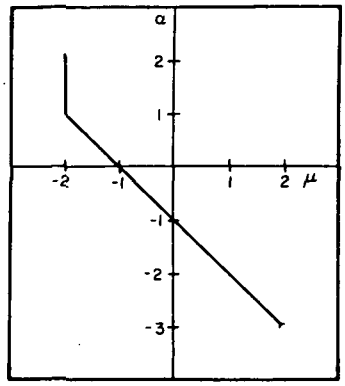

Fig. 1. $\mu - \alpha$ mapping.

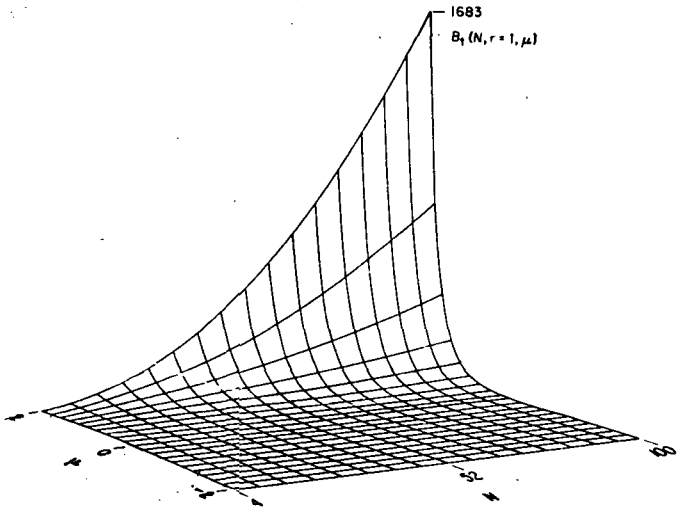

Fig. 2. Function $B_1(N, r = 1, \mu)$.

$$\langle \sigma_y^2(N_2, T_2, \tau_2) \rangle = \left(\frac{\tau_2}{\tau_1}\right)^{\mu} \cdot \left[\frac{B_1(N_2, r_2, \mu) B_2(r_2, \mu)}{B_1(N_1, r_1, \mu) B_2(r_1, \mu)}\right] \langle \sigma_y^2(N_1, T_1, \tau_1) \rangle, \quad (32)$$

where $r_1 = T_1/\tau_1$ and $r_2 = T_2/\tau_2$.

3) General: While it is true that the concept of the bias functions B_1 and B_2 could be extended to other processes besides those with the power-law types of spectral densities, this generalization has not been done. Indeed, spectra of the form given in (28) [or superpositions of such spectra as in (26)] seem to be the most common types of nondeterministic noises encountered in signal generators and associated equipment. For other types of fluctuations (such as causally generated perturbations), translations must be handled on an individual basis.

VI. Applications of Stability Measures

Obviously, if one of the stability measures is exactly the important parameter in the use of a signal generator, the stability measure's application is trivial. Some nontrivial applications arise when one is interested in a different parameter, such as in the use of an oscillator in Doppler radar measurements or in clocks.

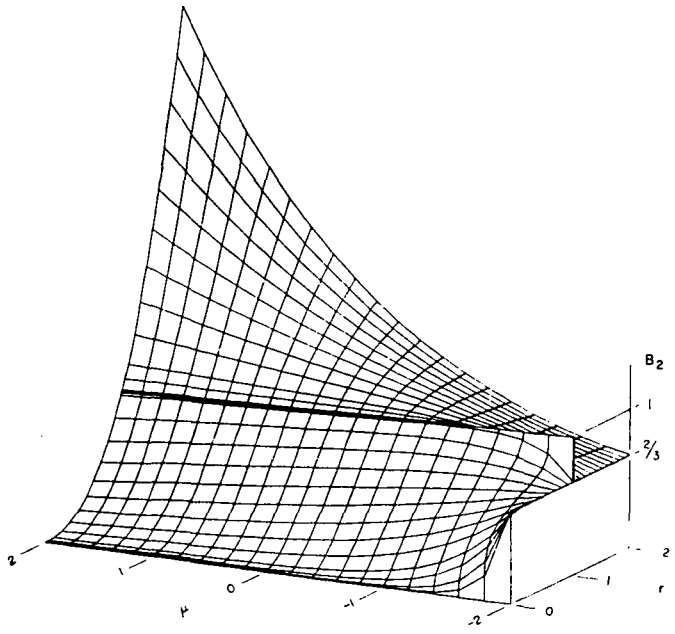

Fig. 3. Bias function $B_2(r, \mu)$.

A. Doppler Radar

1) General: From its transmitted signal, a Doppler radar receives from a moving target a frequency-shifted return signal in the presence of other large signals. These large signals can include clutter (ground return) and transmitter leakage into the receiver (spillover). Instabilities of radar signals result in noise energy on the clutter return, on spillover, and on local oscillators in the equipment.

The limitations of subclutter visibility (SCV) rejections due to the radar signals themselves are related to the RF power spectral density $S_V(f)$. The quantity typically referred to is the carrier-to-noise ratio and can be mathematically approximated by the quantity

$$\frac{S_V(f)}{\int_0^{\infty} S_V(f')df'}.$$

The effects of coherence of target return and other radar parameters are amply considered in the literature [14]–[17].

2) Special Case: Because FM effects generally predominate over AM effects, this carrier-to-noise ratio is approximately given by [6]

$$\frac{S_V(f)}{\int_0^{\infty} S_V(f')\, df'} \approx \tfrac{1}{2} S_\varphi(|f - \nu_0|), \quad (33)$$

for many signal sources provided $|f - \nu_0|$ is sufficiently greater than zero. (The factor of $\frac{1}{2}$ arises from the fact that $S_\varphi(f)$ is a one-sided spectrum.) Thus, if $f - \nu_0$ is

a frequency separation from the carrier, the carrier-to-noise ratio at that point is approximately

$$\tfrac{1}{2}S_\varphi(|f-\nu_0|) = \frac{1}{2}\left(\frac{\nu_0}{f-\nu_0}\right)^2 S_\nu(|f-\nu_0|). \tag{34}$$

B. Clock Errors

1) General: A clock is a device that counts the cycles of a periodic phenomenon. Thus, the reading error $x(t)$ of a clock run from the signal given by (2) is

$$x(t) = \frac{\varphi(t)}{2\pi\nu_0} \tag{35}$$

and the dimensions of $x(t)$ are seconds.

If this clock is a secondary standard, then one could have available some past history of $x(t)$, the time error relative to the standard clock. It often occurs that one is interested in predicting the clock error $x(t)$ for some future date, say $t_0 + \tau$, where t_0 is the present date. Obviously, this is a problem in pure prediction and can be handled by conventional methods [3].

2) Special Case: Although one could handle the prediction of clock errors by the rigorous methods of prediction theory, it is more common to use simpler prediction methods [10], [11]. In particular, one often predicts a clock error for the future by adding to the present error a correction that is derived from the current rate of gain (or loss) of time. That is, the predicted error $\hat{x}(t_0 + \tau)$ is related to the past history of $x(t)$ by

$$\hat{x}(t_0 + \tau) = x(t_0) + T\left[\frac{x(t_0) - x(t_0 - T)}{T}\right]. \tag{36}$$

It is typical to let $T = \tau$.

Thus, the mean-square error of prediction for $T = \tau$ becomes

$$\langle[x(t_0+\tau) - \hat{x}(t_0+\tau)]^2\rangle = \langle[x(t_0+\tau) - 2x(t_0) + x(t_0-\tau)]^2\rangle, \tag{37}$$

which, with the aid of (11), can be written in the form

$$\langle[x(t_0+\tau) - \hat{x}(t_0+\tau)]^2\rangle = 2\tau^2\sigma_y^2(\tau). \tag{38}$$

One can define a *time* stability measure $\sigma_x^2(\tau)$ by

$$\sigma_x^2(\tau) \equiv \tau^2\sigma_y^2(\tau). \tag{39}$$

Clearly, however, the actual errors of prediction of clock readings are dependent on the prediction algorithm used and the utility of such a definition as $\sigma_x^2(\tau)$ is not great. Caution should be used in employing this definition.

VII. Measurement Techniques for Frequency Stability

A. Heterodyne Techniques (General)

It is possible for oscillators to be very stable and values of $\sigma_y(\tau)$ can be as small as 10^{-14} in some state-of-the-art equipment. Thus, one often needs measuring techniques capable of resolving very small fluctuations in $y(t)$. One of the most common techniques is a heterodyne or beat frequency technique. In this method, the signal from the oscillator to be tested is mixed with a reference signal of almost the same frequency as the test oscillator in order that one is left with a lower average frequency for analysis without reducing the frequency (or phase) fluctuations themselves. Following Vessot *et al.* [18], consider an ideal reference oscillator whose output signal is

$$V_r(t) = V_{0r}\sin 2\pi\nu_0 t \tag{40}$$

and a second oscillator whose output voltage $V(t)$ is given by (2): $V(t) = [V_0 + \epsilon(t)]\sin[2\pi\nu_0 t + \varphi(t)]$. Let these two signals be mixed in a product detector; that is, the output of the product detector $v(t)$ is equal to the product $\gamma V(t) \times V_r(t)$, where γ is a constant (see Fig. 4).

Let $v(t)$, in turn, be processed by a sharp low-pass filter with cutoff frequency f_h' such that

$$0 < f_h < f_h' < \nu_0. \tag{41}$$

One may write

$$\begin{aligned}\gamma V(t)\cdot V_r(t) &= \gamma V_{0r}(V_0+\epsilon)[\sin 2\pi\nu_0 t][\sin(2\pi\nu_0 t+\varphi)] \\ &= v(t) = \gamma\frac{(V_{0r}V_0)}{2}\left(1+\frac{\epsilon}{V_0}\right)[\cos\varphi - \cos(4\pi\nu_0 t+\varphi)].\end{aligned} \tag{42}$$

Assume that $\cos[\varphi(t)]$ has essentially no power in Fourier frequencies f in the region $f \geq f_h'$. The effect of the low-pass filter then is to remove the second term on the extreme right of (42); that is

$$v'(t) = \gamma\frac{V_{0r}V_0}{2}\left(1+\frac{\epsilon}{V_0}\right)\cos\varphi(t). \tag{43}$$

This separation of terms by the filter is correct only if $|[\dot{\varphi}(t)/2\pi\nu_0]| \ll 1$ for all t (4).

The following two cases are of interest.

Case I: The relative phase of the oscillators is adjusted so that $|\varphi(t)| \ll 1$ (in-phase condition) during the period of measurement. Under these conditions

$$v'(t) \approx \frac{\gamma}{2}V_{0r}V_0 + \frac{\gamma}{2}V_{0r}\epsilon(t), \tag{44}$$

since $\cos\varphi(t) \approx 1$. That is to say one detects the amplitude noise $\epsilon(t)$ of the signal.

Case II: The relative phase of the oscillators is adjusted to be in approximate quadrature; that is

$$\varphi'(t) = \varphi(t) + \frac{\pi}{2} \tag{45}$$

where $|\varphi'(t)| \ll 1$. Under these conditions,

$$\cos\varphi(t) = \sin\varphi'(t) \approx \varphi'(t) \tag{46}$$

and

$$v'(t) = \frac{\gamma}{2}V_{0r}V_0\varphi'(t) + \frac{\gamma}{2}V_{0r}\varphi'(t)\epsilon(t). \tag{47}$$

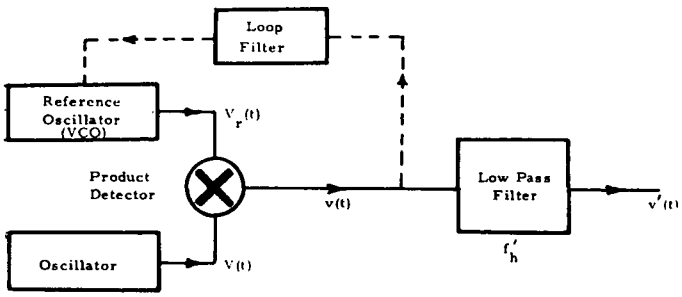

Fig. 4. Heterodyne scheme.

If it is true that $|[\epsilon(t)/V_0]| \ll 1$ for all t (3), then (47) becomes

$$v'(t) \approx \frac{\gamma}{2} V_{0r} V_0 \varphi'(t); \tag{48}$$

that is, $v'(t)$ is proportional to the phase fluctuations. Thus, in order to observe $\varphi'(t)$ by this method, (3) and (4) must be valid. For different average phase values, mixtures of amplitude and phase noise are observed.

In order to maintain the two signals in quadrature for long observational periods, the reference oscillator can be a voltage-controlled oscillator (VCO) and one may feed back the phase error voltage as defined in (48) to control the frequency of the VCO [19]. In this condition of the phase-locked oscillator, the voltage $v'(t)$ is the analog of the *phase* fluctuations for Fourier frequencies above the loop cutoff frequency of the locked loop. For Fourier frequencies below the loop cutoff frequency of the loop, $v'(t)$ is the analog of *frequency* fluctuations. In practice, one should measure the complete servo-loop response.

B. Period Measurement

Assume one has an oscillator whose voltage output may be represented by (2). If $|[\epsilon(t)/V_0]| \ll 1$ for all t and the total phase

$$\Phi(t) = 2\pi\nu_0 t + \varphi(t) \tag{5}$$

is a monotonic function of time (that is, $|[\dot{\varphi}(t)/2\pi\nu_0]| \leq 1$), then the time t between successive positive going zero crossings of $V(t)$ is related to the average frequency during the interval τ. Specifically

$$\frac{1}{\tau} = \nu_0(1 + \bar{y}_n). \tag{49}$$

If one lets τ be the time between a positive going zero crossing of $V(t)$ and the Mth successive positive going zero crossing, then

$$\frac{M}{\tau} = \nu_0(1 + \bar{y}_n). \tag{50}$$

If the variations $\Delta\tau$ of the period are small compared to the average period τ_0, Cutler and Searle [7] have shown that one may make a reasonable approximation to $\langle\sigma_y^2(N, T, \tau_0)\rangle$ using period measurements.

C. Period Measurement With Heterodyning

Suppose that $\varphi(t)$ is a monotonic function of time. The output of the filter of Section VII-A (43) becomes

$$v'(t) \approx \gamma \frac{V_{0r} V_0}{2} \cos\varphi(t) \tag{51}$$

if $|[\epsilon(t)/V_0]| \ll 1$. Then one may measure the period τ of two successive positive zero crossings of $v'(t)$. Thus

$$\frac{1}{\tau} = \nu_0 |\bar{y}_n| \tag{52}$$

and for the Mth positive crossover

$$\frac{M}{\tau} = \nu_0 |\bar{y}_n|. \tag{53}$$

The magnitude bars appear because $\cos\varphi(t)$ is an even function of $\varphi(t)$. It is impossible to determine by this method alone whether φ is increasing with time or decreasing with time. Since $\bar{y}_n$ may be very small ($\sim 10^{-11}$ or 10^{-12} for very good oscillators), τ may be quite long and thus measurable with a good relative precision.

If the phase $\varphi(t)$ is not monotonic, the true $\bar{y}_n$ may be near zero but one could still have many zeros of $\cos\varphi(t)$ and thus (52) and (53) would not be valid.

D. Frequency Counters

Assume the phase (either Φ or φ) is a montonic function of time. If one counts the number M of positive going zero crossings in a period of time τ, then the average frequency of the signal is M/τ. If we assume that the signal is $V(t)$ as defined in (2), then

$$\frac{M}{\tau} = \nu_0(1 + \bar{y}_n). \tag{54}$$

If we assume that the signal is $v'(t)$ as defined in (48), then

$$\frac{M}{\tau} = \nu_0 |\bar{y}_n|. \tag{55}$$

Again, one measures only positive frequencies.

E. Frequency Discriminators

A frequency discriminator is a device that converts frequency fluctuations into an analog voltage by means of a dispersive element. For example, by slightly detuning a resonant circuit from the signal $V(t)$ the frequency fluctuations $(1/2\pi)]\dot{\varphi}(t)$ are converted to amplitude fluctuations of the output signal. Provided the input amplitude fluctuations $[\epsilon(t)]/V_0$ are insignificant, the output amplitude fluctuations can be a good measure of the frequency fluctuations. Obviously, more sophisticated frequency discriminators exist (e.g., the cesium beam).

From the analog voltage one may use analog spectrum analyzers to determine $S_y(f)$, the frequency stability. By converting to digital data, other analyses are possible on a computer.

F. Common Hazards

1) Errors Caused by Signal-Processing Equipment: The intent of most frequency stability measurements is to evaluate the source and not the measuring equipment. Thus, one must know the performance of the measuring system. Of obvious importance are such aspects of the measuring equipment as noise level, dynamic range, resolution (dead time), and frequency range.

It has been pointed out that the noise bandwidth f_h is very essential for the mathematical convergence of certain expressions. Insofar as one wants to measure the signal *source*, one must know that the measuring system is not limiting the frequency response. At the very least, one must recognize that the frequency limit of the measuring system may be a very important, implicit parameter for either $\sigma_y^2(t)$ or $S_y(f)$. Indeed, one must account for any deviations of the measuring system form ideality such as a "nonflat" frequency response of the spectrum analyzer itself.

Almost any electronic circuit that processes a signal will, to some extent, convert amplitude fluctuations at the input terminals into phase fluctuations at the output. Thus, AM noise at the input will cause a time-varying phase (or FM noise) at the output. This can impose important constraints on limiters and automatic gain control (AGC) circuits when good frequency stability is needed. Similarly, this imposes constraints on equipment used for frequency stability measurements.

2) Analog Spectrum Analyzers (Frequency Domain): Typical analog spectrum analyzers are very similar in design to radio receivers of the superheterodyne type, and thus certain design features are quite similar. For example, image rejection (related to predetection bandwidth) is very important. Similarly, the actual shape of the analyzer's frequency window is important since this affects spectral resolution. As with receivers, dynamic range can be critical for the analysis of weak signals in the presence of substantial power in relatively narrow bandwidths (e.g., 60 Hz).

The slewing rate of the analyzer must be consistent with the analyzer's frequency window and the post-detection bandwidth. If one has a frequency window of 1 Hz, one cannot reliably estimate the intensity of a bright line unless the slewing rate is much slower than 1 Hz/s. Additional post-detection filtering will further reduce the maximum usable slewing rate.

3) Spectral Density Estimation from Time Domain Data: It is beyond the scope of this paper to present a comprehensive list of hazards for spectral density estimation; one should consult the literature [2]–[5]. There are a few points, however, which are worthy of special notice: a) data aliasing (similar to predetection bandwidth problems); b) spectral resolution; and c) confidence of the estimate.

4) Variances of Frequency Fluctuations $\sigma_y^2(\tau)$: It is not uncommon to have discrete frequency modulation of a source such as that associated with the power supply frequencies. The existence of discrete frequencies in $S_y(f)$ can cause $\sigma_y^2(\tau)$ to be a very rapidly changing function of τ. An interesting situation results when τ is an exact multiple of the period of the modulation frequency (e.g., one makes $\tau = 1$ s and there exists 60-Hz frequency modulation on the signal). In this situation, $\sigma_y^2(\tau = 1\text{ s})$ can be very optimistic relative to values with slightly different values of τ.

One also must be concerned with the convergence properties of $\sigma_y^2(\tau)$ since not all noise processes will have finite limits to the estimates of $\sigma_y^2(\tau)$ (see Appendix I). One must be as critically aware of any "dead time" in the measurement process as of the system bandwidth.

5) Signal Source and Loading: In measuring frequency stability one should specify the exact location in the circuit from which the signal is obtained and the nature of the load used. It is obvious that the transfer characteristics of the device being specified will depend on the load and that the measured frequency stability might be affected. If the load itself is not constant during the measurements, one expects large effects on frequency stability.

6) Confidence of the Estimate: As with any measurement in science, one wants to know the confidence to assign to numerical results. Thus, when one measures $S_y(f)$ or $\sigma_y^2(\tau)$, it is important to know the accuracies of these estimates.

a) The Allan Variance: It is apparent that a single sample variance $\sigma_y^2(4, \tau, \tau)$ does not have good confidence, but, by averaging many independent samples, one can improve the accuracy of the estimate greatly. There is a key point in this statement, "independent samples." For this argument to be true, it is important that one sample variance be independent of the next. Since $\sigma_y^2(2, \tau, \tau)$ is related to the first difference of the frequency (11), it is sufficient that the noise perturbing $y(t)$ have "independent increments," i.e., that $y(t)$ be a random walk. In other words, it is sufficient that $S_y(f) \sim f^{-2}$ for low frequencies. One can show that for noise processes that are more divergent at low frequencies than f^{-2}, it is difficult (or impossible) to gain good confidence on estimates of $\sigma_y^2(\tau)$. For noise processes that are less divergent than f^{-2}, no problem exists.

It is worth noting that if we were interested in $\sigma_y^2(N = \infty, \tau, \tau)$, then the limit noise would become $S_y(f) \sim f^0$ instead of f^{-2} as it is for $\sigma_y^2(2, \tau, \tau)$. Since most real signal generators possess low-frequency divergent noises, $\langle\sigma_y^2(2, \tau, \tau)\rangle$ is more useful than $\sigma_y^2(N = \infty, \tau, \tau)$.

Although the sample variances $\sigma_y^2(2, \tau, \tau)$ will not be normally distributed, the variance of the average of m

independent (nonoverlapping) samples of $\sigma_y^2(2, \tau, \tau)$ (i.e., the variance of the Allan variance) will decrease as $1/m$ provided the conditions on low-frequency divergence are met. For sufficiently large m, the distribution of the m sample averages of $\sigma_y^2(2, \tau, \tau)$ will tend toward normal (central limit theorem). It is thus possible to estimate confidence intervals based on the normal distribution.

As always, one may be interested in τ values approaching the limits of available data. Clearly, when one is interested in τ values of the order of a year, one is severely limited in the size of m, the number of samples of $\sigma_y^2(2, \tau, \tau)$. Unfortunately, there seems to be no substitute for many samples and one extends τ at the expense of confidence in the results. "Truth in packaging" dictates that the sample size m be stated with the results.

b) Spectral Density: As before, one is referred to the literature for discussions of spectrum estimation [2]–[5]. It is worth pointing out, however, that for $S_y(f)$ there are basically two different types of averaging that can be employed: sample averaging of independent estimates of $S_y(f)$, and frequency averaging where the resolution bandwidth is made much greater than the reciprocal data length.

VIII. Conclusions

A good measure of frequency stability is the spectral density $S_y(f)$ of fractional frequency fluctuations $y(t)$. An alternative is the expected variance of N sample averages of $y(t)$ taken over a duration τ. With the beginning of successive sample periods spaced every T units of time, the variance is denoted by $\sigma_y^2(N, T, \tau)$. The stability measure, then, is the expected value of many measurements of $\sigma_y^2(N, T, \tau)$ with $N = 2$ and $T = \tau$; that is, $\sigma_y^2(\tau)$. For all real experiments one has a finite bandwidth. In general, the time domain measure of frequency stability $\sigma_y^2(\tau)$ is dependent on the noise bandwidth of the system. Thus, there are four important parameters to the time domain measure of frequency stability.

- N Number of sample averages ($N = 2$ for preferred measure).
- T Repetition time for successive sample averages ($T = \tau$ for preferred measure).
- τ Duration of each sample average.
- f_h System noise bandwidth.

Translations among the various stability measures for common noise types are possible, but there are significant reasons for choosing $N = 2$ and $T = \tau$ for the preferred measure of frequency stability in the time domain. This measure, the Allan variance, ($N = 2$) has been referenced by [12], [20]–[22] and more.

Although $S_y(f)$ appears to be a function of the single variable f, actual experimental estimation procedures for the spectral density involve a great many parameters. Indeed, its experimental estimation can be at least as involved as the estimation of $\sigma_y^2(\tau)$.

Appendix I

We want to derive (23) in the text. Starting from (10) we have

$$\begin{aligned}
&\langle \sigma_y^2(N, T, \tau) \rangle \\
&\equiv \left\langle \frac{1}{N-1} \sum_{n=1}^{N} \left(\bar{y}_n - \frac{1}{N} \sum_{k=1}^{N} \bar{y}_k \right)^2 \right\rangle \\
&= \frac{1}{N-1} \left\{ \sum_{n=1}^{N} \langle \bar{y}_n^2 \rangle - \frac{1}{N} \sum_{i=1}^{N} \sum_{j=1}^{N} \langle \bar{y}_i \bar{y}_j \rangle \right\} \\
&= \frac{1}{(N-1)\tau^2} \left\{ \sum_{n=1}^{N} \int_{t_n}^{t_n+\tau} dt'' \int_{t_n}^{t_n+\tau} dt' \, \langle y(t')y(t'') \rangle \right. \\
&\quad \left. - \frac{1}{N} \sum_{i=1}^{N} \sum_{j=1}^{N} \int_{t_i}^{t_i+\tau} dt'' \int_{t_j}^{t_j+\tau} dt' \, \langle y(t')y(t'') \rangle \right\} \qquad (56)
\end{aligned}$$

where (9) has been used. Now

$$\langle y(t')y(t'') \rangle = R_y(t' - t'') \qquad (57)$$

where $R_y(\tau)$ is the autocorrelation function of $y(t)$ and is the Fourier transform of $S_y(f)$, the power spectral density of $y(t)$. Equation (57) is true provided that $y(t)$ is stationary (at least in the wide or covariance sense), and that the average exists. If we assume the power spectral density of $y(t)$, $S_y(f)$ has low and high frequency cutoffs f_l and f_h (if necessary) so that

$$\int_0^\infty S_y(f) \, df$$

exists, then if y is a random variable, the average does exist and we may safely assume stationarity.

In practice, the high-frequency cutoff f_h is always present either in the device being measured or in the measuring equipment itself. When the high-frequency cutoff is necessary for convergence of integrals of $S_y(f)$ (or is too low in frequency), the stability measure will depend on f_h. The latter case can occur when the measuring equipment is too narrow-band. In fact, a useful type of spectral analysis may be done by varying f_h purposefully [18].

The low-frequency cutoff f_l may be taken to be much smaller than the reciprocal of the longest time of interest. The results of calculations as well as measurements will be meaningful if they are independent of f_l as f_l approaches zero. The range of exponents in power law spectral densities for which this is true will be discussed and are given in Fig. 1.

To continue, the derivation requires the Fourier transform relationships between the autocorrelation function and the power spectral density

$$\begin{aligned}
S_y(f) &= 4 \int_0^\infty R_y(\tau) \cos 2\pi f \tau \, d\tau \\
R_y(\tau) &= \int_0^\infty S_y(f) \cos 2\pi f \tau \, df. \qquad (58)
\end{aligned}$$

Using (58) and (57) in (56) gives

$$\langle\sigma_y^2(N, T, \tau)\rangle = \frac{1}{(N-1)\tau^2}\left\{\sum_{n=1}^{N}\int_0^\infty df\, S_y(f)\int_{t_n}^{t_n+\tau} dt'' \cdot\int_{t_n}^{t_n+\tau} dt' \cos 2\pi f(t'-t'') - \frac{1}{N}\sum_{i=1}^{N}\sum_{j=1}^{N}\int_0^\infty df\, S_y(f) \cdot\int_{t_i}^{t_i+\tau} dt''\int_{t_j}^{t_j+\tau} dt' \cos 2\pi f(t'-t'')\right\}$$

$$= \frac{1}{(N-1)\tau^2}\left\{\sum_{n=1}^{N}\left[\int_0^\infty df\, S_y(f)\frac{\sin^2\pi f\tau}{(\pi f)^2}\right] - \frac{1}{N}\sum_{i=1}^{N}\sum_{j=1}^{N}\left[\int_0^\infty df\,\frac{S_y(f)}{(2\pi f)^2}(2\cos 2\pi fT(j-i) - \cos 2\pi f[T(j-i)+\tau] - \cos 2\pi f[T(j-i)-\tau])\right]\right\}. \tag{59}$$

(The interchanges in order of integration are permissible here since the integrals are uniformly convergent with the given restrictions on $S_y(f)$.) The first summation in the curly brackets is independent of the summation index n and thus gives just

$$N\int_0^\infty df\, S_y(f)\frac{\sin^2\pi f\tau}{(\pi f)^2}. \tag{60}$$

The kernel in the second term in the curly brackets may be further simplified

$$2\cos 2\pi fT(j-i) - \cos 2\pi f(T(j-i)+\tau) - \cos 2\pi f(T(j-i)-\tau) = 4\sin^2\pi f\tau\cos 2\pi fT(j-i). \tag{61}$$

The second term is then

$$-\frac{1}{N}\left(\int_0^\infty df\,\frac{S_y(f)}{(\pi f)^2}\sin^2\pi f\tau\sum_{i=1}^{N}\sum_{j=1}^{N}\cos 2\pi fT(j-i)\right). \tag{62}$$

(The interchange of summation and integration is justified.) We must now do the double sum. Let

$$j - i = k$$
$$2\pi fT = x. \tag{63}$$

Changing summation indices from i and j to i and k gives for the sum

$$S \equiv \sum_{i=1}^{N}\sum_{j=1}^{N}\cos x(j-i) = \sum_{i=1}^{N}\sum_{k=1-i}^{N-i}\cos kx. \tag{64}$$

The region of summation over the discrete variables i and k is shown in Fig. 5 for $N = 4$.

The summand is independent of i so that one may interchange the order of summation and sum over i first. The summand is even in k and the contributions for $k < 0$ are equal to those for $k > 0$, and so we may pull out the term for $k = 0$ separately and write

$$S = 2\left(\sum_{k=1}^{N-1}\cos kx\sum_{i=1}^{N-k}1\right) + \sum_{i+1}^{N}1 = 2\left(\sum_{k=1}^{N-1}(N-k)\cos kx\right) + N. \tag{65}$$

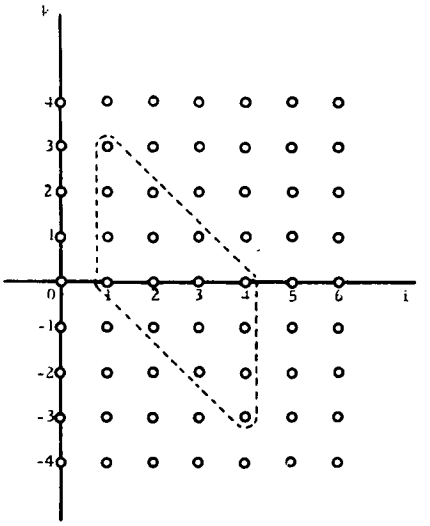

Fig. 5. Region of summation for i and k for $N = 4$.

This may be written as

$$S = N + 2\,\mathrm{Re}\left[N - \frac{1}{i}\frac{d}{dx}\right]\sum_{k=1}^{N-1}e^{ikx} \tag{66}$$

where Re[U] means the real part of U and d/dx is the differential operator. The series is a simple geometric series and may be summed easily, giving

$$S = N + 2\,\mathrm{Re}\left\{\left[N - \frac{1}{i}\frac{d}{dx}\right]\frac{e^{ix} - e^{iNx}}{1-e^{ix}}\right\} = N + 2\,\mathrm{Re}\left\{\frac{1 - e^{iNx} - N(1-e^{ix})}{4\sin^2 x/2}\right\} = \frac{\sin^2 Nx/2}{\sin^2 x/2}. \tag{67}$$

Combining everything we get, after some rearrangement,

$$\langle\sigma_y^2(N, T, \tau)\rangle = \frac{N}{N-1}\int_0^\infty df\, S_y(f)\frac{\sin^2\pi f\tau}{(\pi f\tau)^2}\left[1 - \frac{\sin^2\pi rfN\tau}{N^2\sin^2\pi rf\tau}\right] \tag{68}$$

where $r = T/\tau$. This is the result given in (23).

We can determine a number of things very easily from this equation. First let us change variables. Let $\pi f\tau = u$, then

$$\langle\sigma_y^2(N, T, \tau)\rangle = \frac{N}{(N-1)\pi\tau}\int_0^\infty du\, S_y\left(\frac{u}{\pi\tau}\right)\frac{\sin^2 u}{u^2}\left\{1 - \frac{\sin^2 Nru}{N^2\sin^2 ru}\right\}. \tag{69}$$

The kernel behaves like u^2 as $u \to 0$ and like u^{-2} as $u \to \infty$. Therefore $\langle\sigma_y^2(N, T, \tau)\rangle$ is convergent for power law spectral densities, $S_y(f) = h_\alpha f^\alpha$, without any low- or high-frequency cutoffs for $-3 < \alpha < 1$. Using (69) for power law spectral densities we find

$$\langle\sigma_y^2(N, T, \tau)\rangle = \tau^{-\alpha-1}h_\alpha C_\alpha, \qquad -3 < \alpha < 1$$
$$= \tau^\mu h_\alpha C_\alpha, \qquad \mu \equiv -\alpha - 1$$

and

$$C_\alpha \equiv \frac{N}{(N-1)\pi^{\alpha+1}} \int_0^\infty du\, u^\alpha \frac{\sin^2 u}{u^2} \left\{1 - \frac{\sin^2 Nru}{N^2 \sin^2 ru}\right\}. \tag{70}$$

This is the basis for the plot in Fig. 1 in the text of μ versus α. For $\alpha \geq 1$ we must include the high-frequency cutoff f_h.

For $N = 2$ and $r = 1$ the results are particularly simple. We have

$$\langle \sigma_y^2(2, \tau, \tau) \rangle = \tau^{-\alpha-1} h_\alpha \frac{2}{\pi^{\alpha+1}} \int_0^\infty du\, u^{\alpha-2} \sin^4 u \tag{71}$$

for power law spectral densities. For $N = 2$ and general r we get

$$\langle \sigma_y^2(2, T, \tau) \rangle$$

$$= \frac{1}{2\pi\tau} \int_0^\infty du\, S_y\left(\frac{u}{\pi\tau}\right) \cdot \frac{1 - \cos 2u - \cos 2ru + \frac{\cos 2u(r+1)}{2} + \frac{\cos 2u(r-1)}{2}}{u^2}$$

$$= \frac{2}{\pi\tau} \int_0^\infty du\, S_y\left(\frac{u}{\pi\tau}\right) \frac{\sin^2 u \sin^2 ru}{u^2}. \tag{72}$$

The first form in (72) is particularly simple and is also useful for $r = 1$ in place of (71).

Let us discuss the case for $\alpha \geq 1$ in a little more detail. As mentioned above we must include the high-frequency cutoff f_h for convergence. The general behavior can be seen most easily from (68). After placing the factor τ^{-2} outside the integral and combining the factor f^{-2} with $S_y(f)$ we find that the remaining part of the kernel consists of some constants and some oscillatory terms. If $2\pi f_h \tau \gg 1$ it is apparent that the rapidly oscillating terms contribute very little to the integral. Most of the contribution comes from the integral over the constant term causing the major portion of the τ dependence to be the τ^{-2} factor outside the integral. This is the reason for the vertical slope at $\mu = -2$ in the μ versus α plot in Fig. 1 in the text.

One other point deserves some mention. The constant term of the kernel discussed in the preceding paragraph is different for $r = 1$ from the value for $r \neq 1$. This is readily seen from (72) for $N = 2$; for $r = 1$ the constant term is 3/2 while for $r \neq 1$ it is 1. This is the reason for $\delta_k(r-1)$, which appears in some of the results of Appendix II. In practice, $\delta_k(r-1)$ does not have zero width but is smeared out over a width of approximately $(2\pi f_h \tau)^{-1}$. If there must be dead time $r \neq 1$, it is wise to choose $(r-1) \gg (2\pi f_h \tau)^{-1}$ or $(r-1) \ll (2\pi f_h \tau)^{-1}$ but with $2\pi f_h \tau \gg 1$. In the latter case, one may assume $r \approx 1$.

Appendix II

Let $y(t)$ be a sample function of a random noise process with a spectral density $S_y(f)$. The function $y(t)$ is assumed to be pure real and $S_y(f)$ is a one-sided spectral density relative to a cycle frequency (i.e., the dimensions of $S_y(f)$ are that of y^2 per hertz). (For additional information see Appendix I, [7], [8], [18].)

Let $x(t)$ be defined by the equation

$$\dot{x}(t) \equiv \frac{dx}{dt} \equiv y(t). \tag{73}$$

Define the following. t_0 is arbitrary instant of time and

$$t_{n+1} \equiv t_n + T, \qquad n = 0, 1, 2, \cdots, \tag{74}$$

$$\bar{y}_n \equiv \frac{1}{\tau} \int_{t_n}^{t_n+\tau} y(t)\, dt = \frac{x(t_n + \tau) - x(t_n)}{\tau} \tag{75}$$

$$\langle \bar{y} \rangle_N \equiv \frac{1}{N} \sum_{n=1}^{N} \bar{y}_n, \tag{76}$$

and let f_h be a high-frequency cutoff (infinitely sharp) with $2\pi f_h \tau \gg 1$.

Definition:

$$\langle \sigma_y^2(N, T, \tau) \rangle \equiv \left\langle \frac{1}{N-1} \sum_{n=1}^{N} (\bar{y}_n - \langle \bar{y} \rangle_N)^2 \right\rangle. \tag{77}$$

Special Case:

$$\langle \sigma_y^2(2, T, \tau) \rangle = \left\langle \frac{(\bar{y}_2 - \bar{y}_1)^2}{2} \right\rangle. \tag{78}$$

Special Case:

$$\sigma_y^2(\tau) \equiv \langle \sigma_y^2(2, \tau, \tau) \rangle = \left\langle \frac{[x(t_0 + 2\tau) - 2x(t_0 + \tau) + x(t_0)]^2}{2\tau^2} \right\rangle. \tag{79}$$

Definition:

$$D_x^2(\tau) \equiv \langle [x(t_0 + 2\tau) - 2x(t_0 + \tau) + x(t_0)]^2 \rangle. \tag{80}$$

Consequence of Definitions:

$$D_x^2(\tau) = 2\tau^2 \sigma_y^2(\tau) \equiv 2\sigma_x^2(\tau). \tag{81}$$

Definition:

$$\psi_x^2(T, \tau) \equiv \langle [x(t_0 + T + \tau) - x(t_0 + T) - x(t_0 + \tau) + x(t_0)]^2 \rangle. \tag{82}$$

Consequence of Definitions:

$$\psi_x^2(T, \tau) = 2\tau^2 \langle \sigma_y^2(2, T, \tau) \rangle. \tag{83}$$

Special Case:

$$\psi_x^2(\tau, \tau) = D_x^2(\tau). \tag{84}$$

Random Walk y

$$S_y(f) = \frac{h_{-2}}{f^2} \qquad \left(S_x(f) = \frac{h_{-2}}{(2\pi)^2 f^4}\right)$$

$$r \equiv \frac{T}{\tau}, \qquad 0 \leq f \leq f_h.$$

Quantity	*Relation*	
$\langle\sigma_y^2(N, T, \tau)\rangle$	$h_{-2}\cdot\frac{(2\pi)^2\lvert\tau\rvert}{12}[r(N+1)-1], \quad r \geq 1$	(85)
$\langle\sigma_y^2(N, \tau, \tau)\rangle$	$h_{-2}\cdot\frac{(2\pi)^2\lvert\tau\rvert}{12}\cdot N, \quad r = 1$	(86)
$\sigma_y^2(\tau)$	$h_{-2}\cdot\frac{(2\pi)^2\lvert\tau\rvert}{6}, \quad N = 2, r = 1$	(87)
$D_x^2(\tau) = 2\sigma_x^2(\tau)$	$h_{-2}\cdot\frac{2(2\pi)^2\lvert\tau\rvert^3}{6}$	(88)
$\psi_x^2(T, \tau)$	$h_{-2}\cdot\frac{(2\pi)^2\lvert\tau\rvert^3}{6}(3r-1), \quad r \geq 1$	
	$h_{-2}\cdot\frac{(2\pi)^2\lvert T\rvert^3}{6}\left(\frac{3}{r}-1\right), \quad r \leq 1$.	(89)

Flicker y

$$S_y(f) = \frac{h_{-1}}{f} \qquad \left(S_x(f) = \frac{h_{-1}}{(2\pi)^2 f^3}\right)$$

$$r = T/\tau, \qquad 0 \leq f \leq f_h .$$

Quantity	*Relation*	
$\langle\sigma_y^2(N, T, \tau)\rangle$	$h_{-1}\cdot\frac{1}{N(N-1)}\sum_{n=1}^{N}(N-n)$	
	$\cdot[-2(nr)^2\ln(nr) + (nr+1)^2\ln(nr+1)$	
	$+ (nr-1)^2\ln\lvert nr-1\rvert]$	(90)
$\langle\sigma_y^2(N, \tau, \tau)\rangle$	$h_{-1}\cdot\frac{N\ln N}{N-1}, \quad (r = 1)$	(91)
$\sigma_y^2(\tau)$	$h_{-1}\cdot 2\ln 2, (N = 2, r = 1)$	(92)
$D_x^2(\tau) = 2\sigma_x^2(\tau)$	$h_{-1}\cdot 4\tau^2\ln 2$	(93)
$\psi_x^2(T, \tau)$	$h_{-1}\cdot\tau^2[-2r^2\ln r + (r+1)^2\ln(r+1)$	
	$+ (r-1)^2\ln\lvert r-1\rvert]$	(94)
	$\sim h_{-1}\cdot 2\tau^2(2+\ln r), \quad r \gg 1$	
	$\sim h_{-1}\cdot 2T^2(2-\ln r), \quad r \ll 1$.	(95)

White y (Random Walk x)

$$S_y(f) = h_0 \qquad S_x(f) = \frac{h_0}{(2\pi)^2 f^2}$$

$$r = T/\tau, \qquad 0 \leq f \leq f_h .$$

Quantity	*Relation*	
$\langle\sigma_y^2(N, T, \tau)\rangle$	$\frac{h_0}{2}\cdot\lvert\tau\rvert^{-1}, \quad r \geq 1$	
	$h_0\cdot\frac{1}{6}r(N+1)\lvert\tau\rvert^{-1}, \quad Nr \leq 1$	(96)
$\langle\sigma_y^2(N, \tau, \tau)\rangle$	$\frac{h_0}{2}\cdot\lvert\tau\rvert^{-1}, \quad r = 1$	(97)
$\sigma_y^2(\tau)$	$\frac{h_0}{2}\cdot\lvert\tau\rvert^{-1}, \quad N = 2, r = 1$	(98)
$D_x^2(\tau) = 2\sigma_x^2(\tau)$	$h_0\cdot\lvert\tau\rvert$	(99)
$\psi_x^2(T, \tau)$	$h_0\cdot\lvert\tau\rvert, \quad r \geq 1$	
	$h_0\cdot T, \quad r \leq 1.$	(100)

Flicker x

$$S_y(f) = h_1\lvert f\rvert\left(S_x(f) = \frac{h_1}{(2\pi)^2 f}\right)$$

$$r = T/\tau, \qquad 2\pi f_h\tau \gg 1, \qquad 2\pi f_h T \gg 1, \qquad 0 \leq f \leq f_h .$$

Quantity	*Relation*	
$\langle\sigma_y^2(N, T, \tau)\rangle$	$h_1\cdot\frac{2}{(2\pi\tau)^2}\left\{2 + \ln(2\pi f_h\tau)\right.$	
	$+ \frac{1}{N(N-1)}\sum_{n=1}^{N-1}(N-n)$	
	$\left.\cdot\ln\left[\frac{n^2r^2}{n^2r^2-1}\right]\right\}, \quad r \gg 1$	(101)
$\langle\sigma_y^2(N, \tau, \tau)\rangle$	$h_1\cdot\frac{2(N+1)}{N\tau^2(2\pi)^2}\left[2 + \ln(2\pi f_h\tau) - \frac{\ln N}{N^2-1}\right],$	
	$r = 1$	(102)
$\sigma_y^2(\tau)$	$h_1\cdot\frac{1}{\tau^2(2\pi)^2}\left\{3[2 + \ln(2\pi f_h\tau)] - \ln 2\right\},$	
	$N = 2, r = 1$	(103)
$D_x^2(\tau) = 2\sigma_x^2(\tau)$	$\frac{h_1}{(2\pi)^2}\cdot 2\left\{3[2 + \ln(2\pi f_h\tau)] - \ln 2\right\}$	(104)
$\psi_x^2(T, \tau)$	$h_1\cdot\frac{4}{(2\pi)^2}[2 + \ln(2\pi f_h\tau)], \quad r \gg 1$	
	$h_1\cdot\frac{2}{(2\pi)^2}\left\{3[2 + \ln(2\pi f_h\tau)] - \ln 2\right\},$	
	$r = 1$	(105)
	$h_1\cdot\frac{4}{(2\pi)^2}[2 + \ln(2\pi f_h T)], \quad r \ll 1 .$	

White x

$$S_y(f) = h_2 f^2 \qquad \left(S_x(f) = \frac{h_2}{(2\pi)^2}\right)$$

$$r = T/\tau;\ \delta_k(r-1) = \begin{cases} 1, & \text{if } r = 1 \\ 0, & \text{otherwise} \end{cases}$$

$$2\pi f_h\tau \gg 1, \qquad 0 \leq f \leq f_h .$$

Quantity	*Relation*	
$\langle\sigma_y^2(N, T, \tau)\rangle$	$h_2\cdot\frac{N+\delta_k(r-1)}{N(2\pi)^2}\cdot\frac{2f_h}{\tau^2}$	(106)
$\langle\sigma_y^2(N, \tau, \tau)\rangle$	$h_2\cdot\frac{N+1}{N(2\pi)^2}\cdot\frac{2f_h}{\tau^2}, \quad r = 1$	(107)
$\sigma_y^2(\tau)$	$h_2\cdot\frac{3f_h}{(2\pi)^2\tau^2}, \quad N = 2, r = 1$	(108)
$D_x^2(\tau) = 2\sigma_x^2(\tau)$	$h_2\cdot\frac{6f_h}{(2\pi)^2}$	(109)
$\psi_x^2(T, \tau)$	$h_2\cdot[2 + \delta_k(r-1)]\frac{2f_h}{(2\pi)^2}$	(110)

Acknowledgment

The authors are particularly indebted to D. W. Allan, Dr. D. Halford, Dr. S. Jarvis, and Dr. J. J. Filliben of the National Bureau of Standards. The authors are also indebted to Mrs. Carol Wright for preparing the many revised copies of this paper.

References

[1] E. T. Jaynes, "Information theory and statistical mechanics," *Phys. Rev.*, vol. 108, sec. 15, Oct. 1957, pp. 171–190.
[2] C. Bingham, M. D. Godfrey, and J. W. Tukey, "Modern techniques of power spectrum estimation," *IEEE Trans. Audio Electrocoust.*, vol. AU-15, June 1967, pp. 56–66.
[3] R. B. Blackman, *Linear Data Smoothing and Prediction in Theory and Practice.* Reading, Mass.: Addison-Wesley, 1965.
[4] R. B. Blackman and J. W. Tukey, *The Measurement of Power Spectra.* New York: Dover, 1958.
[5] E. O. Brigham and R. E. Morrow, "The fast Fourier transform," *IEEE Spectrum*, vol. 4, Dec. 1967, pp. 63–70.
[6] E. J. Baghdady, R. D. Lincoln, and B. D. Nelin, "Short-term frequency stability: theory, measurement, and status," *Proc. IEEE–NASA Symp. on Short-Term Frequency Stability* (NASA SP-80), Nov. 1964, pp. 65–87; also in *Proc. IEEE*, vol. 53, July 1965, pp. 704–722 and *Proc. IEEE* (Corresp.), vol 53, Dec. 1965, pp. 2110–2111.
[7] L. Cutler and C. Searle, "Some aspects of the theory and measurement of frequency fluctuations in frequency standards," *Proc. IEEE*, vol. 54, Feb. 1966, pp. 136–154.
[8] D. W. Allan, "Statistics of atomic frequency standards," *Proc. IEEE*, vol. 54, Feb. 1966, pp. 221–230.
[9] N. A. Shewart, *Economic Control of Quality of Manufactured Product.* Princeton, N. J.: Van Nostrand, 1931, p. 146.
[10] J. A. Barnes, "Atomic timekeeping and the statistics of precision signal generators," *Proc. IEEE*, vol. 54, Feb. 1966, pp. 207–220.
[11] J. A. Barnes and D. W. Allan, "An approach to the prediction of coordinated universal time," *Frequency*, vol. 5, Nov.–Dec. 1967, pp. 15–20.
[12] R. F. C. Vessot *et al.*, "An intercomparison of hydrogen and cesium frequency standards," *IEEE Trans. Instrum. Meas.*, vol. IM-15, Dec. 1966, pp. 165–176.
[13] J. A. Barnes, "Tables of bias functions, B_1 and B_2, for variances based on finite samples of processes with power law spectral densities," NBS, Washington, D. C., Tech. Note 375, Jan. 1969.
[14] D. B. Leeson and G. F. Johnson, "Short-term stability for a Doppler radar: requirements, measurements, and techniques," *Proc. IEEE*, vol. 54, Feb. 1966, pp. 244–248.
[15] W. K. Saunders in *Radar Handbook*, M. I. Skolnik, Ed. New York: McGraw Hill, 1970, ch. 16.
[16] R. S. Raven, "Requirements on master oscillators for coherent radar," *Proc. IEEE*, vol. 54, Feb. 1966, pp. 237–243.
[17] D. B. Leeson, "A simple model of feedback oscillator noise spectrum," *Proc. IEEE* (Lett.), vol. 54, Feb. 1966, pp. 329–330.
[18] R. F. C. Vessot, L. Mueller, and J. Vanier, "The specification of oscillator characteristics from measurements made in the frequency domain," *Proc. IEEE*, vol. 54, Feb. 1966, pp. 199–207.
[19] Floyd M. Gardner, *Phaselock Techniques.* New York: Wiley, 1966.
[20] C. Menoud, J. Racine, and P. Kartaschoff, "Atomic hydrogen maser work at L.S.R.H., Neuchatel, Switzerland," *Proc. 21st Ann. Symp. Frequency Control*, Apr. 1967, pp. 543–567.
[21] A. G. Mungall, D. Morris, H. Daams, and R. Bailey, "Atomic hydrogen maser development at the National Research Council of Canada," *Metrologia*, vol. 4, July 1968, pp. 87–94.
[22] R. F. C. Vessot, "Atomic hydrogen masers, an introduction and progress report," *Hewlett-Packard J.*, vol. 20, Oct. 1968, pp. 15–20.

Reprinted by permission from
IEEE TRANSACTIONS ON
INSTRUMENTATION AND MEASUREMENT
Vol. IM-20, No. 2, May 1971